Multi-CubeSat Deployment Strategies: How Different Satellite Deployment Schemes Affect Satellite Separation and Detection for Various Types of Constellations and Missions

THESIS

Scott A. Biehl, Jr., 1st Lt, USAF

AFIT-ENY-MS-16-M-198

DEPARTMENT OF THE AIR FORCE
AIR UNIVERSITY

AIR FORCE INSTITUTE OF TECHNOLOGY

Wright-Patterson Air Force Base, Ohio

AFIT-ENY-MS-16-M-198

Multi-CubeSat Deployment Strategies: How Different Satellite Deployment Schemes Affect Satellite Separation and Detection for Various Types of Constellations and Missions

THESIS

Presented to the Faculty

Department of Aeronautics and Astronautics

Graduate School of Engineering and Management

Air Force Institute of Technology

Air University

Air Education and Training Command

In Partial Fulfillment of the Requirements for the

Degree of Master of Science in Astronautical Engineering

Scott A. Biehl, Jr., B.S.

1st Lt, USAF

March 2016

AFIT-ENY-MS-16-M-198

Multi-CubeSat Deployment Strategies: How Different Satellite Deployment Schemes Affect Satellite Separation and Detection for Various Types of Constellations and Missions

Scott A. Biehl, Jr., B.S.

1st Lt, USAF

Committee Membership:

Maj Christopher D. Geisel, Ph.D.
Chair

Eric D. Swenson, Ph.D.
Member

Maj Stuart A. Stanton, Ph.D.
Member

Abstract

As economics drive an increased demand for small satellites and, consequently, an increase in the number of satellites deployed per launch, different deployment schemes and their effects on both near and long term satellite dynamics must be well understood. CubeSats are a rapidly growing subsection of small satellites that allow several satellites to be deployed during a single launch. While there are advantages to deploying multiple satellites at once, users may have trouble with tracking, identifying, and communicating with their satellites. This investigation examines the deployment of eight 3U CubeSats, and the resulting motion relative to each other and the deployer. Both the distance between any two satellites within a constellation and the volume of a polygon encompassing a constellation are used to analyze the satellite dynamics within a constellation. The distance and volume metrics detail how the relative motion within a constellation affect satellite separation and detection for different deployment schemes. Deployment schemes are distinguished from one another by varying the deployment geometry, by delaying the ejection of specific CubeSats relative to one another, by varying the deployment location along the orbit path, and by varying the separation velocity imparted upon the CubeSats for various mission types. This investigation examines three time periods: (1) the first 24 hours after deployment, (2) the first few weeks after deployment, and (3) the first three years after deployment. This investigation presents several conclusions. Delaying the deployment of part of a constellation increases the maximum volume of the constellation over the first 24 hours while varying long term effects. Deployments into the plane normal to the velocity vector of the deployer result in minimal dispersal of a constellation. Lower constellation deployment altitudes disperse a constellation faster. Finally, deploying multiple CubeSats along the same deployment vector can result in an increased risk of conjunctions.

Table of Contents

Page

List of Figures

Page

List of Tables

Page

Multi-CubeSat Deployment Strategies: How Different Satellite Deployment Schemes Affect Satellite Separation and Detection for Various Types of Constellations and Missions

I. Introduction

1.1 Overview

The purpose of this investigation is to identify trends in the behavior of how different deployment schemes affect the separation and detection of a constellation once it is deployed. While the term 'constellation' generally describes a collection of satellites used to perform a given mission, for this investigation, it simply refers to the satellites that are deployed during a single launch. The study of how different deployment strategies affect various mission types over crucial time periods can influence how effectively a mission is performed, and, ultimately, if a mission is deemed a success or a failure. This investigation attempts to determine how different deployment strategies affect CubeSat separation. Various mission types (communication, imagery, and formation flying missions) are studied in order to expand the overall mission space to which this investigation can be applied. The specific mission types affect the priorities of the behavior of the deployed constellation, which, in turn, affect how the deployment schemes should be designed.

1.2 Motivation

The use of small satellites in both the military and civilian sectors is steadily becoming more common. In 2014, 158 satellites weighing between one and fifty kilograms where launched, over a 71% increase from 2013 and a growth of over 40% per year since 2009.[1] In a separate study of small satellites launched between 2009 and 2013,

it was found that 49% of all small satellites were funded by the United States (94 of 191) and that 50 of those 94 were funded by the US military.[2] It is readily apparent that not only are small satellites becoming more prevalent but, also, that the US military is a major driver in the development of this trend.

1.3 Research Questions and Methodology

This investigation aims to answer the following questions:

1. How do different deployment strategies affect satellite separation and detection for various types of constellations and mission types?
2. How does changing the altitude and inclination of a constellation affect these deployment schemes?

To answer the questions above, Systems Tool Kit® (STK)[3] is utilized to implement different deployment schemes for a set number of satellites and analyze how the separation of the constellation is affected. The individual test cases differ from one another by varying altitude and inclination. The majority of the test cases are in circular low Earth orbits with altitudes ranging from 300 km to 1,000 km and inclinations between 0 and 90 degrees. For each set of test cases, four parameters have been identified as being the variables that are adjusted in order to study how they affect the separation of the individual satellites. Those four variables are:

1. Separation velocity
2. Geometry (direction of the separation velocity vector relative to the velocity vector of the control satellite)

3. Location of deployment within the orbit (argument of latitude of a circular orbit)
4. Delay time between deployment of individual satellites in a given constellation

More detail on the methodology of this investigation is presented in Chapter 3.

1.4 Background on CubeSats

A popular subsection of small satellites is defined as CubeSats. CubeSats are satellites that are composed of one or more ten-centimeter cubes combined together to form the structure of a satellite.[4,5] CubeSats are popular because, when compared with other satellite systems, they are relatively cheap and easy to construct. CubeSats consisting of three units, commonly referred to as 3U, are the focus of this study.

CubeSats are often secondary or tertiary payloads of a larger launch vehicle. Since the weight of multiple CubeSats is often negligible when compared to the overall lifting capacity of a large launch vehicle, and because of their small size, many CubeSats can be deployed during a single launch. While deploying multiple satellites at once is advantageous as it allows for many CubeSats to be inserted into orbit, the user may experience difficulties with tracking, identifying, and communicating with their satellite(s).[6]

CubeSats that are launched as secondary payloads of large launch vehicles are frequently stored in commercial dispensers attached to an ESPA (Evolved Expendable Launch Vehicle Secondary Payload Adapter) ring.[7,8] The CubeSats that are stored in these dispensers are ejected by a compressed spring at the appropriate time once the door

of the container is released.[9] If multiple CubeSats are stored within the same dispenser, the individual CubeSats are required to place spring plungers on their feet to aid satellite separation.[5,10] Recent problems with conjunctions, tracking, identification, and communication, that have been experienced by missions utilizing CubeSats, will be used as examples to analyze how effective certain deployment schemes are at reducing the possibility that these problems occur during a deployment.

1.5 Research Focus Areas

This study focuses on three time periods after deployment that are of importance to a satellite operator. The three time periods are: (1) the first 24 hours after deployment, (2) the time period after deployment in which the initial identification and tracking of the individual satellites is being conducted, and, (3) during the operational lifetime of the satellite, which, for the purposes of this investigation, is 3 years, unless the satellite deorbits before that period of time. Each of the time frames has specific areas of focus that are of particular importance during that time period. Avoiding conjunctions between the individual CubeSats during the first phase (initial deployment of a cluster of CubeSats), and with the deployment vehicle itself, is of the upmost importance. Once all of the individual satellites have been deployed successfully without colliding with another object, the focus is shifted to the time period after deployment where the initial identification and tracking of the satellite is being conducted. This marks the transition from the first to the second phase.

During the second phase, prioritizing the separation of CubeSats, particularly when many are launched over a short time period, can help facilitate identification and

tracking. One of the key takeaways of the Space Environmental NanoSatellite Experiment (SENSE) mission is the difficulty of identification and tracking of CubeSats that are deployed in swarms.[6] Note that, for the purposes of this investigation, 'swarm' and 'constellation' are interchangeable. For this particular mission, the goal while deploying the CubeSats is to maximize the dispersal of the swarm. Conversely, if the mission requires that a group of CubeSats operate close to one another, then the separation of the individual satellites during this time frame should be minimized (or at least controlled to stay within the required specifications). It should be noted that even if the individual CubeSats have propulsion systems, the propulsion systems might not be utilized during this time frame as the satellite operators wait for accurate ephemeris data and perform initial system checks on the satellite.

During the third phase, the movement of individual satellites with respect to one another over the operational lifetime is of importance if the individual satellites are part of the same constellation. While the full length of this time frame is more focused on CubeSats that do not have propulsion capabilities, this is of importance regardless of whether the satellites have propulsion systems onboard. If the satellites do have propulsion capabilities, this analysis could identify how long the satellite would naturally drift while conserving valuable fuel.

In order to make this investigation applicable to the current and possible future use of CubeSats by the US Air Force, relevant orbits must be utilized within this study. This study focuses on two types of orbits. The first is low Earth orbits (LEO), which, for the purposes of this study, is defined as orbits with an altitude between 300 km and 1,000 km. LEO is the natural operating environment for CubeSats due to the reduced power

requirements necessary for communication, specific payload requirements (e.g., resolution of an imagery satellite), the many different opportunities to launch into LEO, the relatively low cost to insert a payload into LEO, and a possible natural lifetime until deorbit less than the international regulation of 25 years. An important subset of LEO orbits is Sun-Synchronous orbits. Sun-Synchronous orbits are specific orbits that have their operating altitude and inclination selected so the angle in which sunlight is illuminating the surface of the Earth is nearly the same every time the satellite passes over a point on Earth. These types of orbits are very useful for imaging satellites.

The second type of orbit that is studied is highly elliptical orbits. Highly elliptical orbits are orbits designed so that they have a low altitude perigee and a high altitude apogee. Some communication satellites are placed in highly elliptical orbits because these types of orbits have long dwell times over certain areas, and can be used as alternatives to geostationary satellites for locations in the high latitudes. The particular type of highly elliptical orbit that is focused on is a Molniya orbit. Molniya orbits have an inclination of 63.4°, which is necessary to keep the rate of change of the argument of perigee equal to zero, and a period of one half of a sidereal day.[11] These particular orbital parameters combined with an argument of perigee of 270° gives satellites in Molniya orbits long dwell times over the northern hemisphere.

1.6 Terminology and Simplifying Assumptions

The term ‘constellation’ is used throughout this investigation and generally describes a collection of satellites performing a given mission. For this investigation, it simply refers to the satellites that are deployed during a single launch. The term ‘swarm’

and ‘cluster’ are, for this investigation, other ways to refer to a constellation. In a number of figures presented in this investigation, the acronym ‘SV’ is utilized. ‘SV’ stands for separation velocity. The term ‘phasing’ refers to the movement of a satellite along the orbit path. The last term defined in this section is ‘anti-velocity vector’. The anti-velocity vector refers to the vector in the opposite direction of the velocity vector of the deployer.

This investigation utilized a number of assumptions to complete both the simulations and the analysis. The first assumption is that all maneuvers are impulsive. This investigation does not use a full force model to simulate the dynamics of satellite motion. The dynamics model used incorporates two-body dynamics, air drag, and a 2x2 Earth gravity model, while neglecting third body gravity for satellites operating with an altitude at or below 1,000 km, solar radiation pressure, and the higher order terms of the gravity model. Another assumption used in this investigation is that the individual satellites have no propulsion systems onboard. This investigation also assumes that the ballistic coefficient of the individual satellites is fixed throughout time. This implies that both the satellite’s mass and attitude are fixed throughout the simulation. This investigation also sets the number of satellites in a deployment to eight. This is part of the initial methodology but does impose a limitation on the number of deployment vectors per plane that can be studied. The last limitation of this study is that the operational lifetime of an individual constellation is limited to three years.

1.7 Document Summary

This document consists of five chapters, the first of which is an introduction. The second chapter is a review of the applicable literature and background material. Within

Chapter 2 is an overview of recent history concerning the utilization of CubeSats, with examples of specific missions being used to provide context on the problems that current deployments are facing. Chapter 2 also provides information on the history of astrodynamics and the specific governing dynamics that are used in the simulations presented in this investigation, which includes the two-body problem, conic sections, and perturbations due to air drag and the Earth's geopotential. Also included in Chapter 2 are explanations of the various reference frames and orbital elements that are used in this investigation. Explanations of the Clohessy Wiltshire Equations, sun-synchronous, and Molniya orbits are also provided. Chapter 2 concludes with a review of relevant research that is being conducted concerning the deployment of CubeSats.

Chapter 3 covers the methodology used in this investigation. Chapter 3 is an overview of how each test case is laid out. This is followed by an overview of how each simulation is set up using STK. This chapter also contains details on how the post simulation analysis is conducted, with specific attention being paid to both how the volume of a constellation is calculated, and how a delayed deployment scenario is implemented in this investigation.

Chapter 4 contains the analysis, results, and discussion completed during this investigation. Chapter 4 describes the individual test case analysis for low Earth, sun-synchronous, and Molniya orbits and is followed by trend analysis for altitude, inclination, geometry, separation velocity, argument of latitude, and delayed deployment. Chapter 4 concludes with a discussion of how the results of this investigation compare to recent research related to the deployment of CubeSats. Analysis and discussion on how the results of this investigation can be applied to resolve the problems experienced during

recent CubeSat missions and how they can be applied in the future are also included in the final section of Chapter 4.

Chapter 5 contains the conclusions of this investigation and recommendations for future work. Both the overall conclusions and the conclusions specific to various types of missions are presented. An overview of the significance of this investigation is explained and is accompanied by a review of the limitations, weaknesses, and assumptions used during this investigation. Chapter 5 concludes with recommendations for follow-on research. The document also includes an Appendix, which contains a list of all of the test cases conducted and the associated deployment parameters that are tested for each.

II. Literature Review and Background Material

2.1 Chapter Overview

Chapter 2 focuses on explaining the material necessary to discuss the results of this investigation. A brief synopsis of the growth of the use of small satellites over recent years is presented and is followed by a description of a few missions that are conducted using CubeSats and the problems encountered. The nomenclature and the governing dynamics of the two-body problem and the associated perturbations caused by air drag and the Earth's 2x2 gravity model used in this investigation are presented and explained. Also included in Chapter 2 are explanations of the various reference frames and orbital elements that are used in this investigation. Explanations of the Clohessy-Wiltshire Equations, sun-synchronous, and Molniya orbits are provided. This chapter concludes with a summary of relevant work conducted on the development of satellite deployment schemes.

2.2 Recent History of Small Satellites

In recent years, there has been remarkable growth in the prevalence of small satellites, and a popular subsection of small satellites referred to as CubeSats has seen a similar growth. For the purposes of this study, a 'small satellite' is defined as weighing less than 250 kg. Between 2009 and 2013, 244 small satellites were launched.[2] Of those 244 satellites, 55% of those missions complied with the CubeSat standard.[2] Most CubeSats less than 3U in size are used for either educational or technology demonstration purposes. For 3U CubeSats, 45% of these satellites are used for educational or technology demonstration, while the remaining 55% are classified as being used for

science, communications, or imaging.[2] This ratio is nearly identical to the breakdown of small satellites that do not conform to the CubeSat Standard.[2] This shows that the CubeSats 3U in size or larger can provide mission focused capability.

In order to better understand both the US's and the US military's role in the development of small satellites, Table 1 breaks down the source of funding for said development.

Table 1: US vs. Non-US Funding Source – adapted from Richardson[2]

Category	United States	Foreign
Civil	30	59
Commercial	14	15
Military	50	21
Total	94	97

It was found that 49% of all small satellites launched between 2009 and 2013 were funded by the US (94 of 191) and that 50 of those 94 were funded by the US military.[2] While the funding source for the development of small satellites is primarily government organizations, only 22% are actually developed by government organizations (military and civil). Most small satellites that are funded by government organizations are built either by commercial developers or educational institutions.[2] The above information conveys two key points. The first key point is that the US military is financially invested in the growth of small satellites. The second key point is that, while the US is responsible for nearly half of the small satellites launched between 2009 and 2013, the other half are controlled by foreign entities, for which the US may not have input on how they operate.

Deconfliction may need to occur if these satellites share a launch vehicle or operate in the same mission space.

In 2014, 158 satellites weighing between one and fifty kilograms were launched.[1] This is nearly a 72% increase when compared to launches in 2013 and a growth of over 40% per year since 2009.[1] 107 of the 158 satellites launched are operated by commercial entities.[1] In early 2015, SpaceX and OneWeb each announced their plans to deploy very large constellations of small satellites (SpaceX – 4025, OneWeb – 648).[1] Each of the OneWeb satellites is planned to weigh around 150 kg,[12] while SpaceX expects their satellites to weigh several hundred kilograms each.[13] Clearly, the growth in the use of small satellites is causing, and will continue to cause, space around the Earth to be congested.

Between 2010 and 2013, the number of launches has remained relatively constant, with an average of 80 attempts per year,[14] with an increase to 92 worldwide launches in 2014.[15] It has been estimated that satellites weighing between one and ten kilograms could be launched on 60-70% of launches.[16] This means that nanosatellites can be deployed and inserted into many diverse orbits. It should be noted that since most satellites weighing between one and fifty kilograms are launched in large clusters as secondary payloads, a single failure in one of the satellites can result in significant loss amongst the constellation.[1] This wide range of possible orbits and the cost of a potential failure mean that different deployment schemes must be evaluated over a wide range of possible orbits.

2.3 Recent CubeSat Missions and Operational Concerns

Recent missions involving CubeSats highlight many of the concerns that are addressed in this investigation. The Space Environmental NanoSatellite Experiment (SENSE) was a pathfinder mission to show that CubeSats can be used to perform US Air Force missions. The mission consisted of two 3U CubeSats that were launched on November 19, 2013 into LEO as part of the ORS-3 Enabler mission.[6] The SENSE mission experienced difficulties while identifying, acquiring, and communicating with both vehicles. This was initially thought to be caused by a large number of satellites orbiting in a cluster[6] (28 CubeSats were launched as part of the ORS-3 mission[17]). While problems with the attitude control system and the deployment of the solar array were later determined to be the main cause of many of the difficulties experienced, the large number of satellites orbiting in a cluster did contribute to the difficulties identifying, acquiring, and communicating with the CubeSats.[6] Intermittent vehicle signals were the only way to distinguish the two SENSE CubeSats from the other 26 deployed CubeSats during the first two weeks on orbit, which delayed the acquisition of accurate Two Line Element (TLE) sets until December 6, 2013, 17 days after launch.[6]

While the SENSE mission experienced difficulties due to multiple CubeSats operating within a cluster, other missions involving CubeSats may prioritize some individual satellites staying close to one another. One such mission is the Canadian Advanced Nanospace experiments 4 and 5 (CanX-4 and CanX-5) formation-flying mission. The CanX-4 and CanX-5 CubeSats were released separately from the same launch vehicle and drifted thousands of kilometers apart from one another in the time that it took to bring one of the CubeSats online.[18] The autonomous formation flying

algorithms utilized by CanX-4 and CanX-5 relied upon an Inter-Satellite Link between the spacecraft, which requires the two satellites to be within a few kilometers of each other.[18] Since the two spacecraft drifted 2,300 km apart, 2.03 m/s of the available delta-v was spent on drift recovery maneuvers.[18] While this does not seem like a lot, only 0.81 m/s of delta-v was used to accomplish the primary mission.[18] If a more efficient way of deploying the satellites was utilized, more delta-v could have been available for the primary mission.

Another risk of deploying multiple satellites over a short period in time is the inability to precisely locate a single satellite in a cluster of deployed satellites.[19] The ability to launch large numbers of CubeSats and deploy over a short period of time has made older techniques and tools for performing discrimination of each object deployed far less effective.[19] This also includes the increased risk of unanticipated conjunctions between satellites.[19] Another issue which makes the tracking and identifying of the CubeSats within the cluster more difficult is the potential lack of radio frequency deconfliction.[19] This can result in multiple satellites within the cluster operating on the same or overlapping frequencies.[19] Combined, these risks can result in a poorly defined cluster of CubeSats operating in close proximity to one another.[19]

2.4 Brief History of Astrodynamics

Nicholas Copernicus (1473-1543) ended a long period of inactivity in the development of astrodynamics.[20] Copernicus's model of the solar system placed the sun at the center as opposed to the Earth.[20] Copernicus's model also deviated from the, at the time, accepted Ptolemaic theory on the details of planetary motion.[20] While Copernicus

continued to rely on circular motion to explain the motion of the planets, his model did include some modifications to account for observed irregularities.[20]

Galileo Galilei (1564-1642) carried on the development of astrodynamics through the use of the telescope for scientific research. Galileo offered verbal explanations of the motion that was later detailed by Isaac Newton's laws of motion.[21] Galileo served as an important link in the development of astrodynamics, bridging the work of Copernicus and the work of Brahe, Kepler and Newton.[20]

The work of Tycho Brahe (1546-1601) and Johann Kepler (1571-1630) represents the next leap forward in the field of astrodynamics.[20] After Brahe's death, Brahe's precise measurement data was used by Kepler to develop what are now known as Kepler's three laws of planetary motion.[20] Those laws are as follows:[20]

1) The orbit of each planet is an ellipse with the Sun at one focus.
2) The line joining the planet to the Sun sweeps out equal areas in equal times.
3) The square of the period of a planet is proportional to the cube of its mean distance to the Sun.

The first law states that planets travel in ellipses, but other types of conic sections, which are generated by the intersection of a plane and a right circular cone, result in possible orbits as well. More on this is presented in Section 2.6. As important as these laws are, they did not explain and solve the dynamics of motion, which were unresolved until Isaac Newton (1642-1727) solved them.

Isaac Newton, at the request of Edmond Halley (1656-1742),[21] discoverer of Halley's Comet, finished his (Newton's) work on planetary motion, *Mathematical*

Principles of Natural Philosophy. In Book I of his *Principia*, Newton introduced his three laws of motion, which are as follows:[20]

1) Every body continues in its state of rest, or of uniform motion in a right [straight] line, unless it is compelled to change state by forces impressed upon it.
2) The change in motion is proportional to the motive force impressed and is made in the direction of the right line in which that force is impressed.
3) To every action there is always opposed an equal reaction: or, the mutual actions of two bodies upon each other are always equal and directed to contrary parts.

How Newton's laws of motion apply to planetary motion is presented in the next section.

2.5 Two-Body Dynamics

Newton's second law and his universal law of gravitation are solid starting points for studies of orbital motion.[20] Newton's second law for a fixed mass system, shown in Equation (1), states that the time rate of change of linear momentum is equal to the net force applied.[20] Note that the following derivation follows the process presented by Vallado.[20]

$$\sum \vec{F} = \frac{d(m\vec{v})}{dt} = m\vec{a} \tag{1}$$

In Equation (1), $\vec{F}$, the sum of all of the forces that act on a body, is equal to the mass, *m*, multiplied by the acceleration, $\vec{a}$, of that body.

Newton's universal law of gravitation, applied to an Earth-satellite system, is shown in Equation (2), where $\vec{F}_g$ is the gravitational force, G is the universal gravitational constant, m_e is the mass of the Earth, m_{sat} is the mass of the satellite, and $\vec{r}$ is the position of the satellite with respect to the center of the Earth.[20]

$$\vec{F}_g = -\frac{Gm_e m_{sat}}{r^2}\left(\frac{\vec{r}}{r}\right) \tag{2}$$

The equation for the position of the satellite with respect to Earth, $\vec{r}$, is given in Equation (3), while the second time derivative of Equation (3), which is the satellite's relative acceleration with respect to Earth, is shown in Equation (4).[20] $\vec{r}_{sat}$ and $\vec{r}_e$ are the positions of the satellite and Earth in an inertial coordinate frame.

$$\vec{r} = \vec{r}_{sat} - \vec{r}_e \tag{3}$$

$$\ddot{\vec{r}} = \ddot{\vec{r}}_{sat} - \ddot{\vec{r}}_e \tag{4}$$

Equation (5) and Equation (6) are created by rewriting Equation (2) using the nomenclature from Equation (4).

$$\vec{F}_{g_{sat}} = m_{sat}\ddot{\vec{r}}_{sat} = -\frac{Gm_e m_{sat}}{r^2}\left(\frac{\vec{r}}{r}\right) \tag{5}$$

$$\vec{F}_{g_e} = m_e\ddot{\vec{r}}_e = \frac{Gm_e m_{sat}}{r^2}\left(\frac{\vec{r}}{r}\right) \tag{6}$$

The result of combining Equation (4) through Equation (6) is shown in Equation (8), which reduces to Equation (9).

$$\ddot{\vec{r}} = -\frac{Gm_e m_{sat}}{m_{sat}r^2}\left(\frac{\vec{r}}{r}\right) - \frac{Gm_e m_{sat}}{m_e r^2}\left(\frac{\vec{r}}{r}\right) \tag{7}$$

$$\ddot{\vec{r}} = -\frac{Gm_e}{r^2}\left(\frac{\vec{r}}{r}\right) - \frac{Gm_{sat}}{r^2}\left(\frac{\vec{r}}{r}\right) \tag{8}$$

$$\ddot{\vec{r}} = -\frac{G(m_e+m_{sat})}{r^2}\left(\frac{\vec{r}}{r}\right) \tag{9}$$

If it is assumed that the mass of the satellite is much smaller that the mass of the primary body, then $G(m_e + m_{sat}) \cong Gm_e$ because $m_e << m_{sat}$.[20] This assumption, combined with replacing Gm_e with the gravitational parameter, μ, is used to develop the equation of motion for a system comprised of two bodies, which is shown in Equation (10). Note that $\vec{r}$ is the relative position vector of the satellite with respect to the center of the Earth, and Equation (10) assumes the Earth's center is inertially fixed.

$$ {}_I\ddot{\vec{r}} = -\frac{\mu\vec{r}}{|\vec{r}|^3} \tag{10} $$

There are four main assumptions used to develop the restricted two-body problem equation of motion. Those assumptions are: (1) The mass of the satellite is much smaller than the mass of the primary body, (2) The values used for the position vector are obtained from an inertial coordinate system, (3) The bodies of the satellite and primary body are spherically symmetrical, with uniform density, which allows for both to be treated as point masses, and (4) no other forces act on the system except for gravitational attraction acting along the line connecting the center of the two bodies.[20]

In order to gain insight into the behavior of the system, it is helpful to examine the properties of the motion that remain constant. Two quantities that are conserved, along with the linear momentum of the system, are specific mechanical energy and specific orbital angular momentum. 'Specific' indicates that the quantity is per unit mass of the spacecraft. Specific mechanical energy, ε, shown in Equation (11), is the total energy per unit mass. Within Equation (11), $\frac{1}{2}v^2$ represents the kinetic energy per unit mass and $-\frac{\mu}{r}$ represents the potential energy per unit mass, where v is the speed of the satellite.[11]

$$ \varepsilon = \frac{1}{2}v^2 - \frac{\mu}{r} \tag{11} $$

Solving for v, shown in Equation (12), gives some insight into the nature of the solution.

$$v = \left(2\varepsilon + \frac{2\mu}{r}\right)^{1/2} \tag{12}$$

Three types of orbits that can result from Equation (12), and the three types of orbits are:[11]

1) If ε is negative, there is a maximum *r* that yields a non-imaginary speed. This means that once the orbiting satellite reaches that radius, it must come back to the primary body. This results in a circular or elliptical orbit that is repeating in nature.
2) If $\varepsilon = 0$ the orbiting body can reach a radius of infinity with a non-imaginary speed ($v = 0$). This represents the minimum energy that is required to escape the primary body. These orbits are parabolic in shape.
3) If ε is positive, the orbiting body can reach a radius of infinity with a positive speed. These orbits are hyperbolic in shape and are used to leave the primary body.

The second conserved quantity that provides insight into the behavior of the system is specific angular momentum, which is shown in Equation (13).

$$\vec{r} \times \dot{\vec{r}} = \vec{H} \tag{13}$$

Since $\vec{H}$ is a constant, the orbit of the satellite about the Earth must lie in the plane that is perpendicular to $\vec{H}$. If $\vec{H}$ is constant, then the satellite's orbit will stay in the same plane forever. It is important to remember that this constant of motion is derived for the two-body problem, the assumptions of which are not entirely accurate.[11] Small perturbations

on the two-body problem caused by other forces will account for changes in the orbit plane. The other forces, such as air drag and the effects of the Earth's oblateness, will be explained later in this chapter. Equation (13) will be used in the next section to calculate the period of an orbit.

2.6 Conic Sections

From Kepler's first law, the orbit of a planet around the sun is a conic section. A conic section is generated by the intersection of a plane and a right circular cone. There are five types of conic sections: the circle, ellipse, parabola, hyperbola, and straight line.[11] Four of the conic sections are shown in Figure 1, with the fifth, the straight line, being generated by slicing the cone along an edge. All five conic sections are possible orbits. Every conic section has two foci. In astrodynamics, the gravitational center of attraction coincides with one focus for all orbital motion, and is called the primary focus. Parabolic and hyperbolic orbits are both considered open because the satellite does not repeat its position, while closed orbits will, ideally, retrace its position over time. Open orbits are not utilized in this investigation.

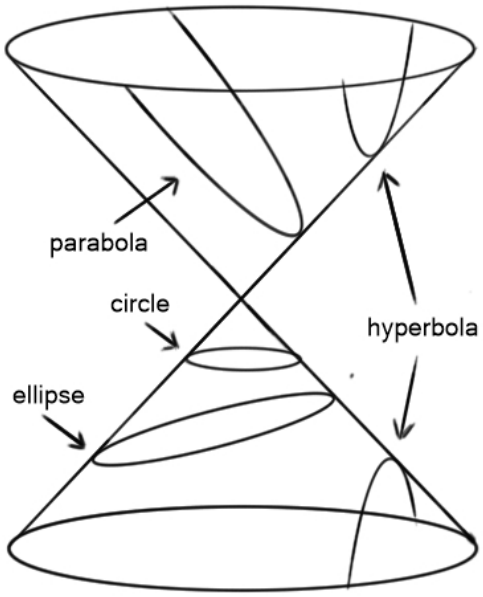

Figure 1: Conic Sections - adapted from Wiesel[11]

Figure 2 illustrates a geometrical concept of a closed orbit. Conic sections are scaled by the major axis. The minor axis and the distance between the two foci are other parameters used to describe the size of a conic section. Typically, half values of these parameters are used and are known as semi-major axis, *a*, semi-minor axis, *b*, and half the distance between the foci, *c*. The eccentricity, *e*, is a fixed constant for each type of conic section and indicates the orbits shape (i.e., how round or flat the shape of the orbit is).[11] The eccentricity is never negative.[11] Table 2 provides a summary of the five types of conic sections and their associated semi-major axis, *a*, and eccentricity, *e*, values.

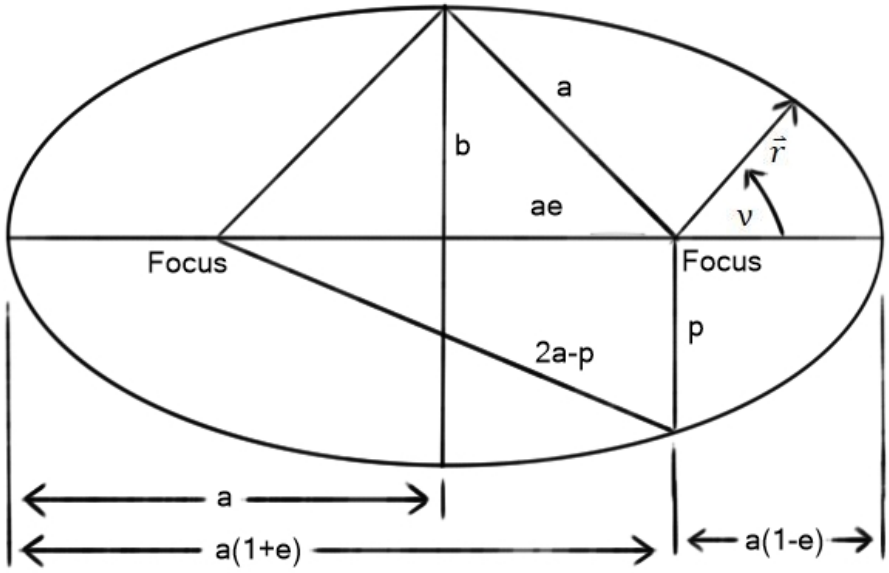

Figure 2: Geometry of an Ellipse - adapted from Wiesel[11]

In Equation (14), *r* is distance from the focus to the satellite's current position. *p* is the semilatus rectum, which, in Figure 2, is the vertical distance from the focus to a point along the trajectory. *v* is the true anomaly, which is described in detail in Section 2.8. Equation (14) is referred to as the trajectory equation and is the polar coordinate form of a conic section with the central body at one of the foci.[20,36] Equation (14) is used to calculate the distance from the focus to a satellite's current position and is the result of a proof confirming Kepler's first law.[20,36]

$$r = \frac{p}{1 + e\cos\nu} = \frac{a(1 - e^2)}{1 + e\cos\nu} \tag{14}$$

Table 2: Conic Sections – adapted from Wiesel[11] and Zurita[35]

Semi-major axis	Eccentricity (e)	Conic Section
a = r	0	Circle
a > 0	0 < e ≤ 1	Ellipse
a → ∞	1	Parabola
a < 0	e ≥ 1	Hyperbola
a(ε), a is a function of ε	e = 1	Line: Degenerate Ellipse, Parabola, or Hyperbola

Equation (13) can be used to calculate the period of an orbit. An alternate equation for $\vec{H}$ is shown in Equation (15).

$$\left|\vec{H}\right| = |\vec{r} \times \vec{v}| = |\vec{r}||\vec{v}| \sin\theta = rv\sin\theta \tag{15}$$

Figure 3 depicts the area swept out by an orbit after an incremental period of time.

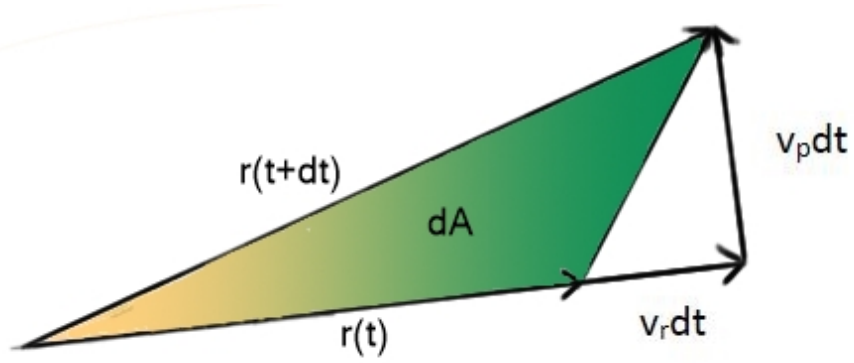

Figure 3: Area Swept Out by an Orbit - adapted from Wiesel[11]

Therefore, the area swept out in a time period of *dt* is *dA*. Equation (16) shows a reduction of the series of equations, where θ is the angle between $\vec{r}$ *and* $\vec{v}$.

$$dA = \frac{1}{2}(r + v_r dt)v_p dt - \frac{1}{2}v_r dt\ v_p dt$$

$$dA = \frac{1}{2}\left(r v_p dt + v_r v_p dt^2 - v_r v_p dt^2\right)$$

$$dA = \frac{1}{2} r v_p dt$$

$$dA = \frac{1}{2} r v \sin\theta dt \tag{16}$$

Substituting Equation (15) into Equation (16) results in Equation (17), which shows that an orbit sweeps out equal areas in equal times (Kepler's second law).

$$\frac{dA}{dt} = \frac{1}{2}\left|\vec{H}\right| = constant \tag{17}$$

For closed orbits, the orbit is an ellipse (or a circle). To calculate the period of an orbit from Equation (17), the total area enclosed by an orbit must be known. For an ellipse, the area is equal to πab, where a is the semi-major axis of the ellipse and b is the semi-minor axis of the ellipse. Integrating Equation (17) over the period of the orbit results in Equation (18), which relates the area to the orbital period.

$$\int_0^T \frac{dA}{dt} dt = \int_0^T \frac{1}{2} H dt$$

$$A = \pi ab = \frac{1}{2} HT \tag{18}$$

Substituting Equation (19) and Equation (20) into Equation (18) results in Equation (21), which reduces to Equation (22). Equation (22) solves the period of the orbital while also proving Kepler's third law.[36]

$$b = \left(a\sqrt{1-e^2}\right) \tag{19}$$

$$H = \sqrt{\mu a(1-e^2)} \tag{20}$$

$$T = \frac{2\pi a^2\sqrt{1-e^2}}{\sqrt{\mu a(1-e^2)}} \tag{21}$$

$$T = 2\pi\sqrt{\frac{a^3}{\mu}} \tag{22}$$

Mean motion, *n*, is the mean angular rate of the orbital motion and is measured in radians per unit time. Equation (23) shows that as the semi-major axis of an orbit decreases, the mean motion of that orbit increases. Mean anomaly, *M*, is an angle defined by Equation (24) measured from perigee, where *t* is the current time and t_0 is the time of perigee passage. Mean anomaly corresponds to the constant angular motion about a circle with radius *a*. Note that mean anomaly only measures the angle from perigee to the satellite's current position for the entire orbit if the orbit is circular.

$$n = \frac{2\pi}{T} = \sqrt{\frac{\mu}{a^3}} \tag{23}$$

$$M = n(t - t_0) \tag{24}$$

2.7 Reference Frames

This section describes the two coordinate frames that are used during this investigation. The two coordinate frames are the J2000 frame and the radial, transverse, and normal (RTN) frame. The J2000 coordinate system is an Earth-Centered Inertial (ECI) frame. The origin of an ECI frame is at the Earth's center of mass.[20] The $\hat{\imath}$-axis of an ECI frame is in the vernal equinox direction.[11] The vernal equinox is when the plane of the Earth's equator passes through the center of the sun on the first day of spring in the Northern Hemisphere, and the direction of the $\hat{\imath}$-axis points to the sun at that moment. The $\hat{k}$-axis is aligned with the Earth's axis of rotation, and the $\hat{\jmath}$-axis is defined to complete a right-handed coordinate system.[11] Specifically, for the J2000 coordinate system, the $\hat{\imath}$-axis is defined as the vernal equinox, γ, on January 1, 2000 at 12:00.[11] The J2000 frame, shown in Figure 4, is a specific type of ECI frame that is also a geocentric equatorial frame. As the name suggests, the origin of a geocentric equatorial frame is at the center of the Earth, and the x and y coordinates (or $\hat{\imath}$ and $\hat{\jmath}$ directions) are in the plane of the Earth's equator.

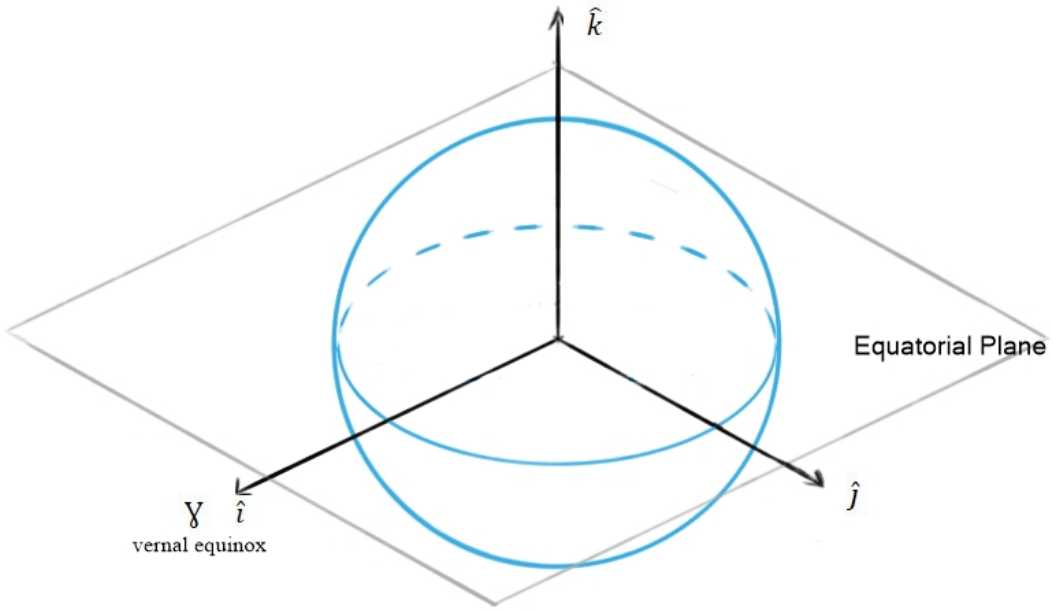

Figure 4: J2000 Frame - adapted from Vallado[20]

The RTN frame, shown in Figure 5, also referred to as the Local-Vertical, Local-Horizontal (LVLH) frame, is centered on the satellite.[20] The r̂-axis always points from the Earth's center along the radius vector toward the satellite.[20] The t̂-axis points in the direction of the velocity vector and is perpendicular to the r̂-axis.[20] If the satellite is in a circular orbit, the velocity vector and the t̂-axis are aligned, but they are not aligned in general.[20] The n̂-axis is normal to the orbit plane, completing a right-handed coordinate system. The RTN frame is used to describe relative positions from one satellite to another.[20]

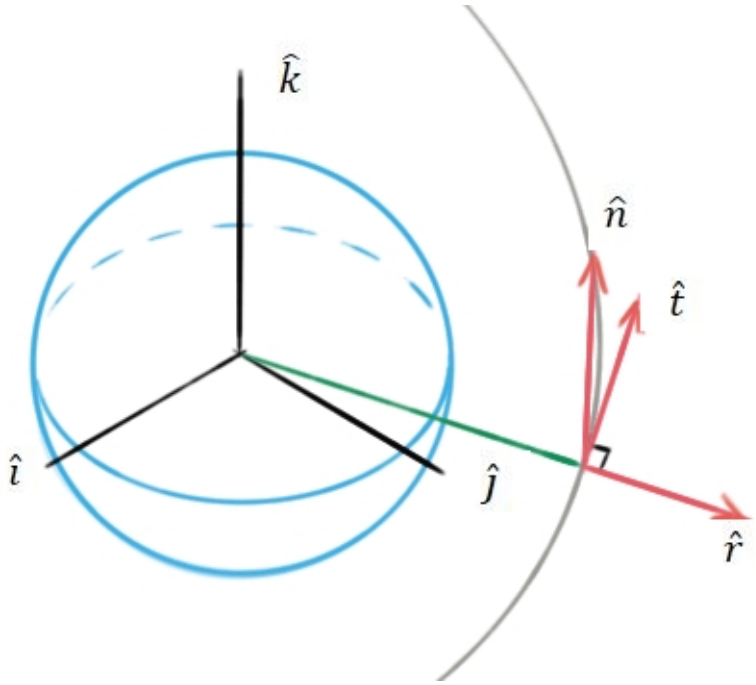

Figure 5: RTN Frame - adapted from Vallado[20]

2.8 Classical Orbital Elements

While defining the position and velocity vectors of a satellite sufficiently constrains a satellites orbit, six parameters are traditionally defined to help with the visualization of an orbit (see Figure 6). The six values are commonly referred to as the six classical orbital elements (COEs) and they are shown in Table 3.

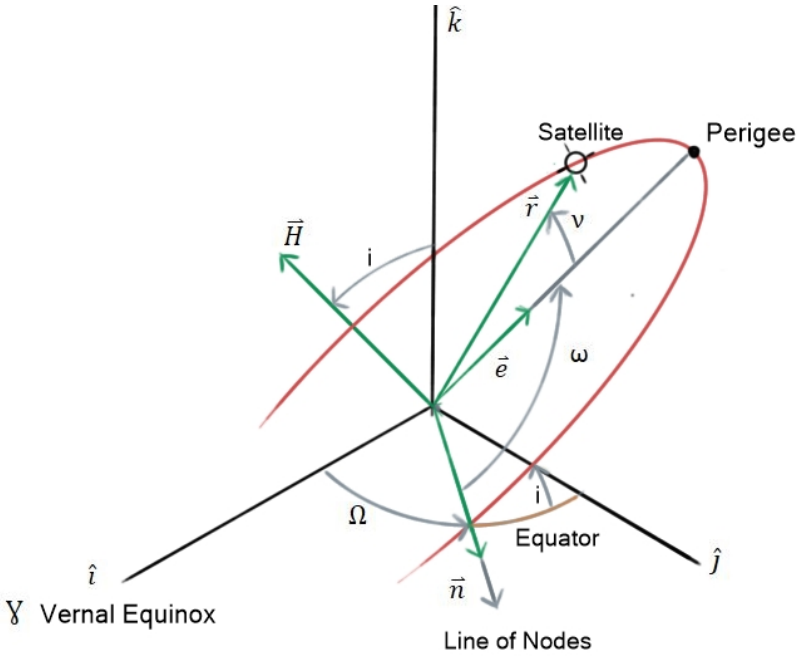

Figure 6: Classical Orbital Elements – adapted from Wiesel[11]

Table 3: Classical Orbital Elements for Earth Centered Orbit – adapted from Wiesel[11]

Semi-major axis	*a*	Defines the size of the orbit. For circular orbits, this value is equal to the orbital radius.
Eccentricity	*e*	Defines the shape of the orbit. For circular orbits, this value is equal to 0.
Inclination	*i*	The angle between the equatorial plane of the Earth and the satellite's orbital plane.
Right Ascension of the Ascending Node (RAAN)	Ω	The angle from the vernal equinox direction to the satellite's line of nodes (vector from center of Earth to the point where the satellite crosses from the southern to northern hemisphere [called the ascending node]). Not defined for an orbit with an inclination of 0° (or 180°).
Argument of Perigee	*ω*	The angle from the ascending node to perigee. Not defined for a circular orbit.
True Anomaly	*v*	Defines where along the orbit the satellite is. Measured from perigee to the satellite's location. Not defined for a circular orbit.

2.9 Alternate Orbital Elements

Table 3 shows that for three of the COEs (RAAN, argument of perigee, and true anomaly) there are types of orbits in which these values cannot be defined. Those three types of orbits are circular ($e = 0$), equatorial ($i = 0°$ or 180°), and circular equatorial ($e =$

0 and i = 0° or 180°). For a circular orbit, there is no perigee, so argument of perigee and true anomaly are undefined. In this case, the alternate orbital element that is utilized is argument of latitude (u).[22] Argument of latitude is the angle measured from the ascending node to the spacecraft's current position.[20] For an elliptical orbit with an inclination of 0° or 180° (equatorial), there is no ascending node, so RAAN and argument of perigee are undefined. In this case, the alternate orbital element that is utilized is the longitude of perigee (Π).[20] Longitude of perigee is the angle measured from the vernal equinox of the coordinate system ($\hat{\imath}$-axis) to perigee in the direction of the spacecraft's motion.[20] For a circular equatorial orbit, there is no perigee or ascending node, so RAAN, argument of perigee, and true anomaly are undefined. In this case, the alternate orbital element that is utilized is true longitude (λ).[20] True longitude is the angle measured from the vernal equinox of the coordinate system ($\hat{\imath}$-axis) to the spacecraft's current position, measured in the direction of the spacecraft's motion.[20] This information is summarized in Table 4.

Table 4: Alternate Orbital Elements

Element	Name	Description	Type of Orbit
u	Argument of latitude	Angle from ascending node to spacecraft's current position	Circular
Π	Longitude of perigee	Angle from $\hat{\imath}$-axis to perigee	Elliptical Equatorial
λ	True longitude	Angle from $\hat{\imath}$-axis to spacecraft's current position	Circular equatorial

2.10 Clohessy-Wiltshire Equations

To predict the initial behavior of a deployed CubeSat, the Clohessy-Wiltshire or CW equations[23] (also known as Hill's equations[24]) are utilized and are shown in Equation (27) and Equation (28), where Equation (25) and Equation (26) are the relative position and velocity at the initial time, respectively. Note that the CW equations are approximate solutions, not the exact solution. A major assumption in relative motion is that the chief and deputy satellites are in nearly circular orbits.[20] The CW equations also assume that the initial displacement of the deputy satellite relative to the chief satellite is small. In Equation (25), δr_0 is the initial displacement in the radial direction, $r_0\delta\theta_0$ is the initial displacement along the velocity vector, and δz_0 is initial displacement in the cross-track direction. Note that the *n* present in Equation (28) is equal to the mean motion of the reference orbit. Figure 7 is provided to illustrate the reference frame used in the CW equations, which is the RTN frame discussed earlier.

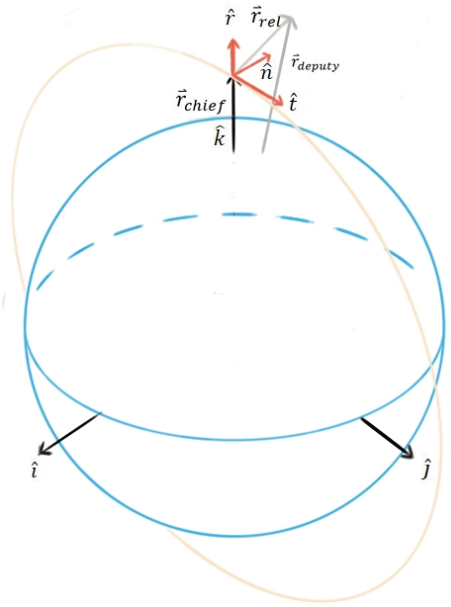

Figure 7: Reference Frame for CW Equations - adapted from Vallado[20]

$$[\delta\vec{r}_0]^T = [\delta r_0 \quad r_0\delta\theta_0 \quad \delta z_0] \tag{25}$$

$$[\delta\vec{v}_0]^T = [\delta\dot{r}_0 \quad r_0\delta\dot{\theta}_0 \quad \delta\dot{z}_0] \tag{26}$$

$$\begin{bmatrix} \delta r(t) \\ r_0\delta\theta(t) \\ \delta z(t) \\ \delta\dot{r}(t) \\ r_0\delta\dot{\theta}(t) \\ \delta\dot{z}(t) \end{bmatrix} = \Phi \begin{bmatrix} \delta r_0 \\ r_0\delta\theta_0 \\ \delta z_0 \\ \delta\dot{r}_0 \\ r_0\delta\dot{\theta}_0 \\ \delta\dot{z}_0 \end{bmatrix} \tag{27}$$

$$\Phi = \begin{bmatrix} 4-3\cos(nt) & 0 & 0 & {}^{1}/_{n}\sin(nt) & {}^{2}/_{n}[1-\cos(nt)] & 0 \\ 6[\sin(nt)-nt] & 1 & 0 & {}^{2}/_{n}[\cos(nt)-1] & {}^{4}/_{n}\sin(nt)-3t & 0 \\ 0 & 0 & \cos(nt) & 0 & 0 & {}^{1}/_{n}\sin(nt) \\ 3n\sin(nt) & 0 & 0 & \cos(nt) & 2\sin(nt) & 0 \\ 6n[\cos(nt)-1] & 0 & 0 & -2\sin(nt) & 4\cos(nt)-3 & 0 \\ 0 & 0 & -n\sin(nt) & 0 & 0 & \cos(nt) \end{bmatrix} \tag{28}$$

Φ is the state transition matrix and is a function of the current time and the mean motion of the reference (chief) satellite.

While the CW equations are very useful with respect to terminal guidance,[11] this investigation is set up in such a way that the initial displacement of the deployed satellites is 0. In test cases where the separation velocity does not have a component in the in-track direction (i.e., $r_0\delta\dot{\theta}_0 = 0$), all of the terms that are proportional to *t* go to 0. According to the CW equations, this means that the two satellites will not see an in-track drift relative to one another. In the model used in this investigation, there is an in-track drift, which is

caused by slight differences in the mean motion of the two satellites. Due to this difference, the CW equations are only used as a quick reference to the initial motion of the deployed satellite relative to the control satellite.

2.11 Perturbations on the Two-Body Problem

In addition to the gravitational influence of the Newtonian point mass of the primary body, there are several perturbations that are common in orbital mechanics.[11] Historically, the most studied perturbation is caused by a 'third' body.[11] The greater the distance between the orbiting bodies, the more important this perturbation is, but for orbiting bodies close to the primary body, this is not as important.[11] In this investigation, perturbations caused by 'third' bodies are not taken into account for satellites operating with an altitude at or below 1,000 km. Small, artificial satellites have increased the relevance of other perturbations.[11] Artificial satellites can operate very close to the atmosphere, where the atmosphere is more dense, making air drag a large perturbation at low altitudes, but only a small, or negligible perturbation at higher altitudes.[11] The second perturbation accounted for in this investigation is created by the Earth's geopotential. The Earth is not a perfect sphere of uniform density, so the gravitational potential is not of a point mass.[11] Small deviations from a perfect sphere can cause large perturbations at altitudes all the way out to geosynchronous orbit (a = 42,164 km).[11] This effect does become less of a factor as the distance between the orbiting bodies grows.[11] More information about perturbations caused by air drag and the Earth's gravitational field is presented in the next three sections.

2.11.1 Effects of Air Drag

Air drag, shown in Equation (29), is a non-conservative force that acts in the opposite direction of the motion of a satellite. In Equation (29), C_d is the drag coefficient, A is the presented area, m is the mass of the satellite, ρ is the atmospheric density, and v is the speed of the satellite.[11] Equation (30) defines the ballistic coefficient, B^*, which is a measure of how much the size, shape and mass of an object affect the amount of air drag that an object experiences. It is important to note that different sources define B^* as the reciprocal of the right side of Equation (30), so one must make sure of what definition an investigation is using before comparisons can be made.

$$a_d = \frac{1}{2}\frac{C_d A}{m}\rho v^2 \tag{29}$$

$$B^* = \frac{C_d A}{m} \tag{30}$$

The overall effect of air drag is to lower the altitude of the orbit until, over time, the satellite reenters the atmosphere.[20] If the orbit is eccentric, the orbit will experience a contraction due to drag, during which the radius of perigee will remain close to constant, while the radius of apogee will shrink until the orbit circularizes.[20] Once the orbit circularizes, the radius of the circular orbit will decrease as air drag continues to act on the satellite until reentry.

The period of an orbit, as discussed earlier and shown again in Equation (31), is a function of the semi-major axis, a, and the standard gravitational parameter, μ. The

standard gravitational parameter is constant for Earth, which means that the period of a satellite squared is proportional to the semi-major axis cubed. More specifically, as the semi-major axis of the orbit decreases, the period of the satellite will also decrease. Small differences in the semi-major axis of the satellites within the cluster will cause the satellites within the cluster to have slightly different orbital periods, which will cause the satellites within the cluster to move along the orbital path with respect to one another.

$$T = 2\pi\sqrt{\frac{a^3}{\mu}} \tag{31}$$

Another way of conceptualizing this relative motion is by observing differences in mean motion, which is shown in Equation (23). This means that the satellite in that orbit will travel around the orbit faster, which will cause the satellites within the cluster to separate along orbital path with respect to one another.

2.11.2 Secular Effects of J_2

Besides air drag, the fact that the Earth bulges around its equator by nearly 20 km, more specifically the mass associated with that bulge, results in secular effects to the right ascension of the ascending node (RAAN) (Ω) (Equation (32)), argument of perigee (ω) (Equation (33)), and mean anomaly at epoch (M_0) (Equation (34)) of an orbiting satellite.[11,20] Secular effects are non-periodic changes (growing with time) to various orbital elements of an orbiting satellite. For Equation (32) through Equation (34), *a*, *e*, and *i* are defined in Section 2.8 (Table 3). J_2 has only small periodic effects on *a*, *e*, and *i*.

The variable, n, is the mean motion of the satellite. R_e is the radius of the Earth, and J_2 is a dimensionless number that characterizes how much the Earth departs from a sphere due to the oblateness of the Earth. For the Earth, the value of J_2 is 0.001082.

$$\dot{\Omega} = -\mathrm{n}\left(\frac{3}{2}J_2\frac{R_e^2}{a^2(1-e^2)^2}\cos i\right) \tag{32}$$

$$\dot{\omega} = -\mathrm{n}\left(\frac{3}{2}J_2\frac{R_e^2}{a^2(1-e^2)^2}\left[\frac{5}{2}sin^2\, i - 2\right]\right) \tag{33}$$

$$\dot{M}_0 = -n\left(\frac{3}{4}J_2\frac{R_e^2}{a^2(1-e^2)^{3/2}}\left[3\, sin^2\, i - 2\right]\right) \tag{34}$$

Equation (32) affects where the orbit crosses from the Southern to the Northern Hemisphere. This will not affect the relative drift between two satellites, but it will cause separation between the orbit planes of the individual satellites.

2.11.3 Geopotential

The Earth's equatorial bulge is not the Earth's only deviation from a spherical body. For numerical propagation that requires high precision, the Newtonian point mass potential $V = -\mu/r$ is replaced with the full geopotential,[25] which is given in Equation (35).

$$V = -\frac{\mu}{r}\sum_{n=0}^{\infty}\sum_{m=0}^{n}\left(\frac{r_e}{r}\right)^n P_n^m(\sin\delta)(C_{nm}\cos m\lambda + S_{nm}\sin m\lambda) \quad (35)$$

In Equation (35), r_e is the Earth's equatorial radius, λ is the longitude and δ is the latitude. The P_n^m terms are the associated Legendre polynomials, which are solutions to Legendre's differential equations. A table of C_{nm} and S_{nm} coefficients is termed a gravity model.[25] The Earth's equatorial oblateness is the C_{20} term, which is related to J_2.[25] A 2x2 gravity model is utilized in this research. While this does account for J_2, it also includes the C_{22} and S_{22} terms in the gravity model. The C_{22} and S_{22} terms essentially model the Earth's two major continental blocks and the two oceans that separate them.[25] J_2 (C_{20}) is the dominant term in the Earth's geopotential and has an order of magnitude of 10^{-3}, while the C_{22} and S_{22} terms have an order of magnitude of 10^{-6}. This investigation is concerned with the relative motion of the satellites compared to one another, not with the precise position of the satellites relative to the Earth, so a 2x2 gravity model is used.

2.12 Sun-Synchronous and Molniya Orbits

In this investigation, two types of orbits are utilized that are designed to specifically take advantage of the Earth's oblateness effects. One of those orbits is a sun-synchronous orbit. A sun-synchronous orbit is designed so that the ascending node progresses precisely 360° per year.[11] This is achieved by adjusting the semi-major axis, *a*, eccentricity, *e*, and inclination, *i*, of an orbit until $\dot{\Omega}$ in Equation (32) is equal to +360° per year. This will lock the orientation of the orbital plane relative to the sun.[11] Satellites inserted into a sun-synchronous orbit will pass over points on the Earth with a constant

sun-angle, which is advantageous for imagery satellites.[11] For Earth, sun-synchronous orbits are slightly retrograde.

The second type of orbit in this investigation that is specifically designed to take advantage of the Earth's J_2 effects is a Molniya orbit. Molniya orbits are named after Russian Molniya communication satellites and are designed so the rate of change in the argument of perigee, $\dot{\omega}$ (Equation (33)), is 0 and typically have a period around 12 hours.[11] This, when applied to an eccentric orbit, will cancel the drift of where on the Earth the satellite is over when the satellite reaches apogee and perigee. This can be used as an alternative to geostationary satellites for high latitudes. If the perigee of the orbit is in the Southern Hemisphere, the satellite will have long coverage times over the Northern Hemisphere. To drive the expression in Equation (33) to zero, the bracketed portion of Equation (33), shown in Equation (36), is set to zero. Solving for the inclination, shown in Equation (37), yields the result that there are two critical inclinations that will result in no rate of change in the argument of perigee. Those inclinations are 63.4349° and 116.5650°, with an inclination of 63.4349° being used for Molniya orbits.[11]

$$\frac{5}{2}\sin^2 i - 2 = 0 \tag{36}$$

$$i_c = \sin^{-1}\frac{2}{\sqrt{5}} \tag{37}$$

2.13 Previous/Relevant Research on CubeSat Deployment Strategies

Work on the design of deployment strategies for CubeSats has been conducted prior to this investigation. Puig-Suari, Zohar, and Leveque,[26] hereinafter referred to as Puig-Suari, and Kilic, Scholz, and Asma,[27] hereinafter referred to as Kilic, conducted the two examples that have the strongest correlation with the work conducted in this investigation. The work conducted by Puig-Suari is focused on maximizing the dispersal along an orbit path by varying deployment timing and direction for individual CubeSats in a single launch.[26] His work indicates that simple deployment strategies can be utilized to create efficient constellation geometries.[26] Puig-Suari's investigation assumed all of the deployed satellites are identical 3U CubeSats, with minimal or no propulsion capabilities. Puig-Suari's findings include that although variations in values for the ballistic coefficient, B^*, limit the absolute accuracy of the positions of the individual satellites in a simulation that utilizes fixed values for B^*, STK will accurately predict the relative positions of the deployed spacecraft.[26] Note that Puig-Suari defines B^* the same way as in this investigation (Equation (30)).

In Puig-Suari's work, an initial deployment scheme involving delayed deployment along the anti-velocity vector (opposite direction of the velocity vector of the deployer) is attempted, which resulted in minimal dispersal of the deployed satellites.[26] By analyzing the Clohessy-Wiltshire equations, Puig-Suari then decided to vary the magnitude of the different deployment velocities along the deployment path. To accomplish this while still maintaining a constant ejection velocity from the deployer, a radial semi-circular deployment is implemented. A radial semi-circular deployment scenario ejects the first satellite along the velocity vector and the last satellite along the

anti-velocity vector.[26] All of the remaining satellites are ejected into the upper half of the plane containing both the velocity vector and radial vector (see Figure 8). Eight 3U CubeSats are ejected using two versions of this deployment scenario. The first version deploys the satellites with a constant angle between deployments, while the second version varies the angle of the satellite deployments to create a constant differential between the magnitudes of the component of the separation velocity along the velocity vector of the deployer. Both versions populated the constellation in the same amount of time, but the deployment scenario that utilized a constant differential in in-track separation velocity resulted in a more even distribution along the orbit path.[26] Puig-Suari also conducted analysis on how varying the altitude of the orbit affected how fast a deployment scheme populated an orbit path. The results indicate that the lower the altitude of the initial deployment, the faster the constellation populates the orbit path.[26]

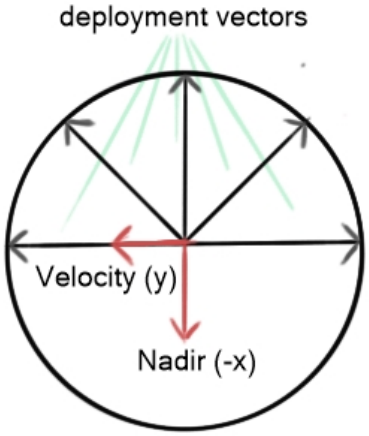

Figure 8: Radial Semi-Circular Deployment - adapted from Puig-Suari[23]

While Puig-Suari is focused on the overall dispersal of a deployment scheme, Kilic's work is focused on both the overall dispersal of a deployment scheme and the collision risks between the individual CubeSats after deployment, specifically for 2U

CubeSats being developed for the QB50 mission.[27] The deployment variables that Kilic used to develop deployment schemes are deployment direction, sequence (order), and frequency (timing).[27] The overall goal of Kilic's investigation is to minimize the risk of collisions while optimizing both the lifetime and distribution of the individual CubeSats.[27] Kilic does implement parameters specific to the deployment vehicle in the simulation to model the behavior the deployment vehicle, while using a constant separation velocity of 1.5 m/s.[27] The initial orbit has an altitude of 320 km, an inclination of 79°, eccentricity of 0, RAAN of 40°, and an argument of latitude of 155°.[27] Kilic's investigation resulted in multiple conclusions regarding how to avoid collisions immediately after deployment. Those conclusions are that CubeSats should be ejected from minimum 'ballistic coefficient' to maximum 'ballistic coefficient,' that ejection of satellites perpendicular to the velocity vector leads to an elevated risk of collisions, and that the safest deployment scenario is in the anti-velocity direction.[27] Note that Kilic defines 'ballistic coefficient' as the reciprocal of how B^* is defined in this investigation (Kilic defines ballistic coefficient as $\frac{m}{C_d A}$). This means that Kilic concluded that the lightest CubeSats (assuming the same $C_d A$) should be ejected first.[27]

2.14 Chapter Summary

In this chapter, it is shown that the US military is a driving force in the development of small satellites and that some recent missions have experienced difficulties that could be mitigated through the implementation of better deployment schemes. The nomenclature and governing dynamics are presented and explained. Also included in Chapter 2 are explanations of the various reference frames and orbital

elements that are used in this investigation. Explanations of the Clohessy-Wiltshire Equations, sun-synchronous, and Molniya orbits are also provided. This chapter concludes with a synopsis of the work that has been conducted over the last few years concerning the development and implementation of satellite deployment schemes. The work on overall dispersal shows that an orbit path can be populated using CubeSats without propulsion, and that the lower the dispersal altitude, the faster the orbit path is populated. The work on the avoidance of collision risks concludes that CubeSats should be ejected (assuming the same $C_d A$) from lightest satellite to heaviest satellite, that ejection of satellites perpendicular to the velocity vector leads to an elevated risk of collisions, and that the safest deployment scenario is in the anti-velocity direction.

III. Methodology

3.1 Chapter Overview

This chapter delves into methodologies that are used to set up the individual test cases, run the simulations, and conduct the post-simulation analysis. Metrics based on various measurement instruments used to track satellite position are also included in the post-simulation analysis. This chapter also includes details on how the volume of a constellation of satellites is calculated and on how this investigation implements the delayed deployment of part of the constellation.

3.2 Test Case Layout

In Chapter 1, four deployment variables are called out as being variables for the test setup. As a quick reminder, those four variables are separation velocity, geometry, location of deployment within the orbit, and the delay time between deployments. Altitude and inclination are associated with the orbit of a single 3U satellite that does not undergo any changes in the four variables. This creates a default orbit for a particular set of test cases that is used to explore the effect of separation velocity, geometry, and the location of, and delay between, deployments within the orbit on the separation of the constellation of CubeSats. The satellite that does not undergo any changes in the last four variables is referred to as the ‘control’ satellite in each test case. The control satellite has the exact same properties as all of the other satellites in the scenario, and while it is not considered part of the constellation, it is used as a common reference point to compare the relative motion of the rest of the satellites in the constellation. A table containing a

comprehensive list of all of the test cases completed and their specific variable settings is available in the Appendix.

In every test case, eight satellites are ejected into a deployment plane. The numbering scheme applied to each individual test case is presented in Figure 9. All eight satellites are ejected into the same plane for a given test case and are deployed such that a single satellite is deployed every 45° within the deployment plane. Figure 10 and Figure 11 have been provided in order to give a visual representation of how this would look immediately after separation. Note that the acroymn 'SV' in the caption of Figure 10 and Figure 11 stands for separation velocity. Figure 10 and Figure 11 are specifically for test case 101, which has a deployment plane normal to the velocity vector of the control satellite. The red and yellow vectors shown in both figures represent the velocity and nadir vectors from the control satellite, respectively.

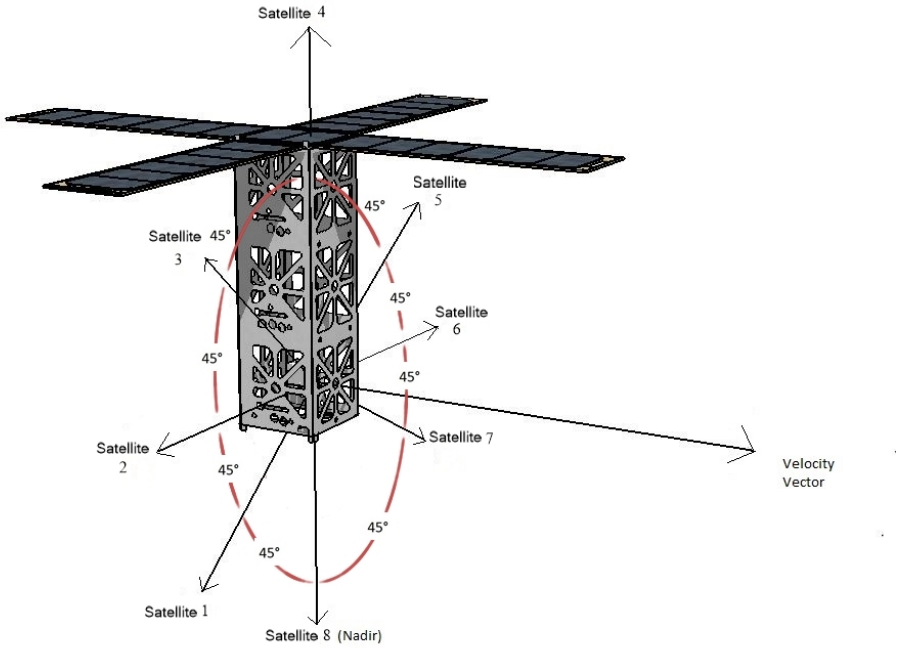

Figure 9: Numbering Scheme for Deployed Satellites

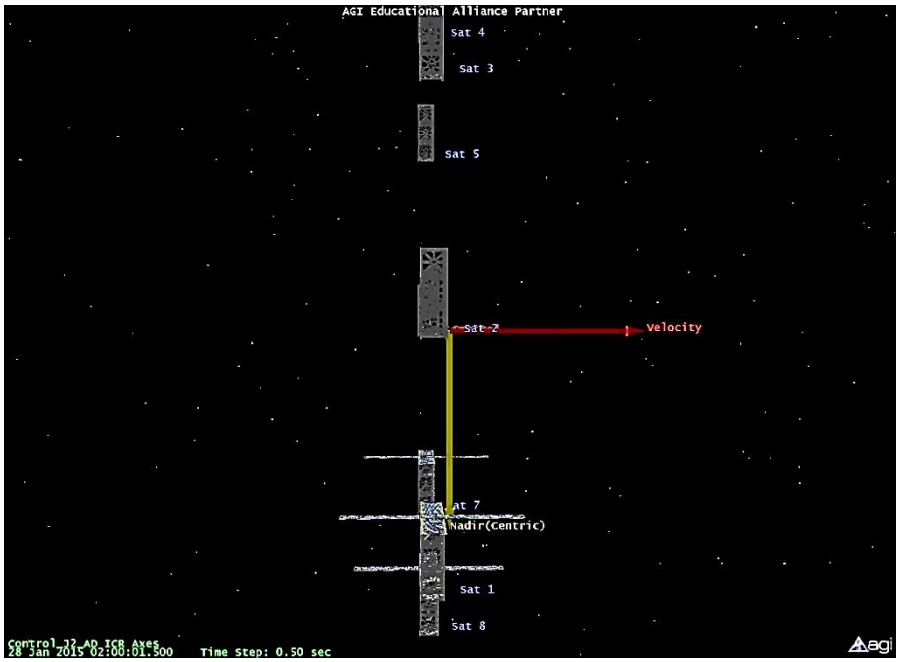

Figure 10: Side View of Test Case 101 Deployment (Alt = 300 km – Inc = 30° - Offset = 0° - SV = 1 m/s) –STK screenshot[3]

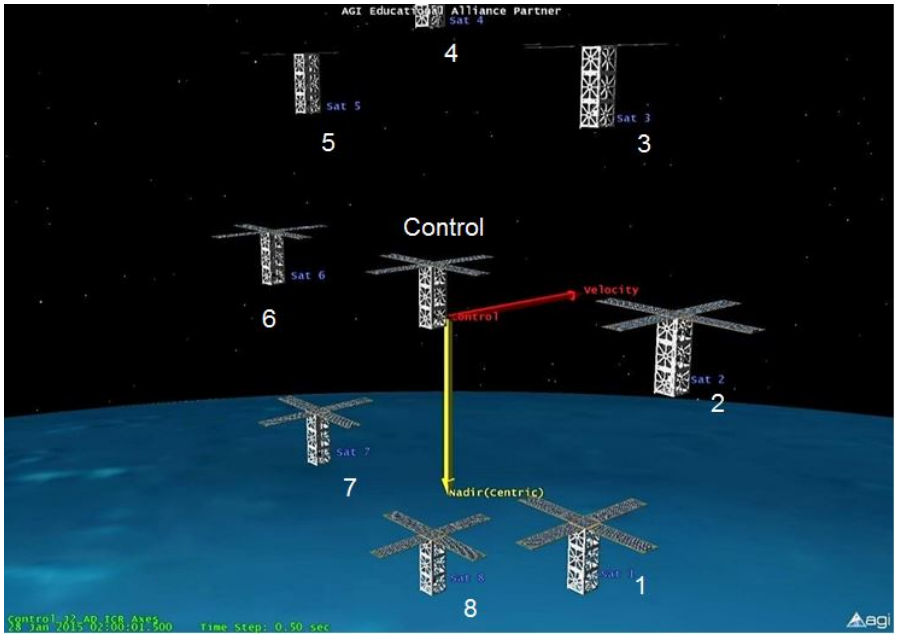

Figure 11: Perspective View of Test Case 101 Deployment (Alt = 300 km – Inc = 30° - Offset = 0° - SV = 1 m/s) – STK screenshot[3]

For future reference, when the deployment plane is normal to the velocity vector, the offset is 0°. A visual of the offset deployment variable is shown Figure 12(b), Figure 13(a), and Figure 13(b). Offsets of 0°, 45°, 90°, and 135° are tested in this investigation. For an offset of 45°. the normal vector of the deployment plane is the result of rotating the velocity vector of the control satellite 45° around the nadir vector. This is best shown in Figure 13(b) as the angle measured from the velocity vector of the control satellite (red) to the normal vector of the deployment plane (blue). For an offset of 90°, the rotation is 90°. These offsets are used for all unique control satellites to test the effects of geometry on a constellation of CubeSats. For every offset tested, two separate separation velocities are used, 1 m/s and 2 m/s, with the exception of the geometries tested with an altitude of 300 km and an inclination of 30°. For these specific geometries, an additional separation velocity of 1.5 m/s is also tested. A visual of the separation velocity deployment variable is shown in Figure 12(a).

Orbits with altitudes of 300, 400, 500, 750, and 1,000 km, with an inclination set to 30°, are utilized to investigate how altitude affects the dispersal of a constellation. Similarly, inclinations between 0° and 90°, with test cases every 15°, are set up to test the effects of inclination. To study the effect of argument of latitude, an orbit with an inclination of 30° and an altitude of 300 km is utilized. The argument of latitude that the deployment occurs at is then varied from 0° to 360° by steps of 30°. A visual of the argument of latitude deployment variable is shown in Figure 12(c). The last variable to be tested is the delay time between orbits. How this variable is tested is discussed later in this chapter.

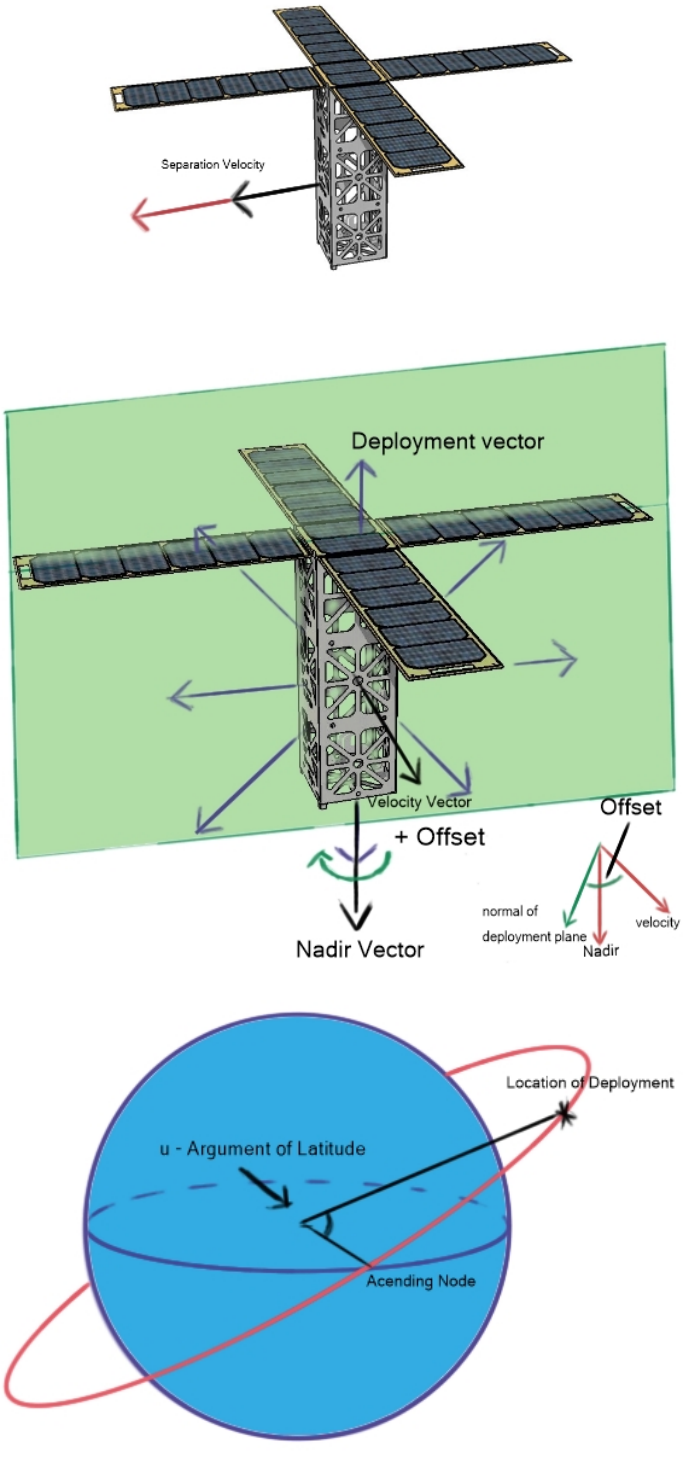

Figure 12: Visual Representations of Deployment Variables

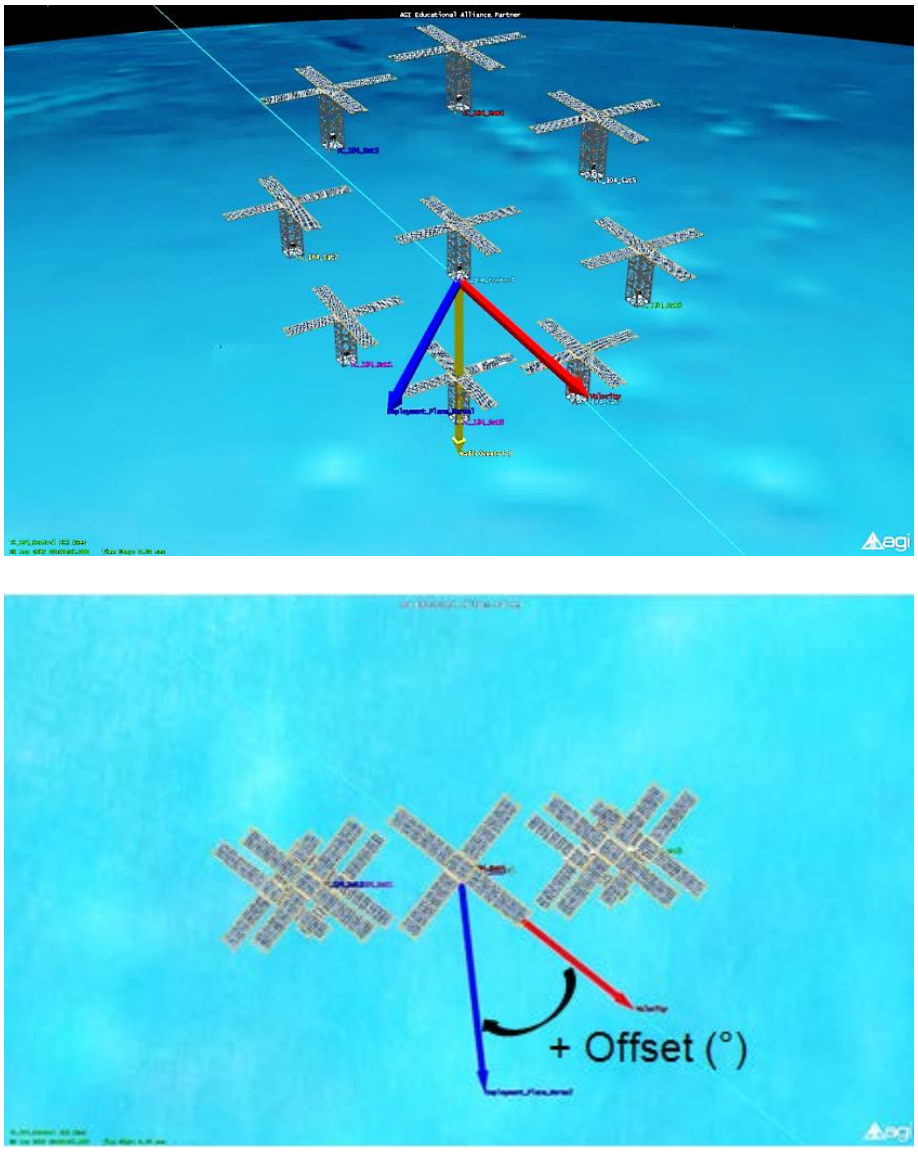

(a)

(b)

Figure 13: Additional Visual Representations of Offset – STK screenshots[3]

3.3 Systems Tool Kit® (STK) Simulation Setup

The initial start time of every test case is January 28, 2015, 0200 UTCG. For each set of test cases, a 'control' satellite is created within STK in order to acquire its position and velocity vectors in the J2000 reference frame. When creating the initial 'control' satellite for each set of test cases, the six classical orbital elements (COEs) must be

inputted. The altitude (semi-major axis) and inclination are defined for each test case. All of the test cases, with exception to those focused on Molniya orbits, have an eccentricity of 0, which also prevents the use of argument of perigee and true anomaly. Altitude, inclination, and eccentricity account for three of the inputs.

Since there is no argument of perigee or true anomaly, this necessitates the use of argument of latitude, which is the sum of the argument of perigee and true anomaly, if they were defined. Since these variables are not defined for a circular orbit, the argument of latitude is defined as the angle between the nodal vector and the satellite's position vector. For most test cases, the argument of latitude is set to 0°, which is indicative of a deployment occurring over the equator, specifically at the ascending node. The test cases that do not have an argument of latitude set to 0° fall into three subsets. One subset is used to test how the location of the deployment (argument of latitude) effects the dispersal of the constellation of CubeSats, in which case the argument of latitude is set to a desired test setting. The second subset is used to construct the deployments that involve the delayed deployment of part of the constellation. More on how this is accomplished is presented later in this chapter.

The last subset that does not involve an argument of latitude equal to zero is for test cases involving Molniya orbits. Due to the eccentricity of a Molniya orbit, there are only two places on the orbit where the velocity vector and nadir vectors are perpendicular to one another, apogee and perigee. The way the deployment parameters are defined for this investigation is based on the velocity and nadir vectors being perpendicular so, for Molniya orbits, the argument of perigee is set to 270° and the true anomaly is set to 0°. This causes the deployment of the constellation to occur at perigee. This is a limitation of

the algorithm used to create the deployment vectors for the individual satellites in this investigation. The final input is the right ascension of the ascending node (RAAN), which is also set to 0°.

The position and velocity vectors are then inputted into a MATLAB®[28] script that recreates the control satellite within a new scenario and creates the eight satellites of the specific constellation for that particular test case based off of the deployment geometry, separation velocity, and location in the orbit that is assigned to that test case.

STK's High Precision Orbit Propagator (HPOP) is used in order to propagate each satellite forward in time. HPOP is more computationally intensive than STK's analytical propagators and must integrate from an initial state to determine the satellite's state at any other time.[29] This propagator is used because it allows the user greater control of which specific forces are used during the simulation.

During the creation of each satellite in the simulation, which is automated using MATLAB®, the force model that is used by HPOP is programmed. The first two programmed settings concern third body gravity. Neither the gravitational effects of the Moon or the Sun on the constellation are taken into account. Similar to third body gravity, solar radiation pressure experienced by the individual satellites is also not taken into account. These effects were not accounted for during the simulations because, for satellites in LEO, these effects are dominated by the presence of drag and the J_2 effects caused by the Earth's oblateness.[20]

STK has multiple standard Earth gravity models that can be utilized for various simulations. The WGS84.grv model[30] (World Geodetic System) is utilized for this investigation. The WGS84_EGM96.grv model[30,31] (Earth Gravitational Model 1996) is

more commonly used but, since only a 2x2 gravity model is utilized in the simulations, the differences between the two gravity models is very small (the largest difference in any coefficient used is $1*10^{-9}$). A 2x2 gravity model is utilized using the HPOP in order to accurately model J_2 effects while also accounting for atmospheric drag.

The main reason for using HPOP within STK as opposed to the much faster J_2 or J_4 propagators is that it allows the user to also model atmospheric drag. A spherical Jacchia-Roberts atmospheric density model is applied for all of the test cases. A drag coefficient, C_D, of 2.2 and an area to mass ratio of 0.005 m^2/kg is used. The area to mass ratio used is the area to mass ratio of a 3U CubeSat with a mass of 6 kg. Note that by using a fixed area to mass ratio, two assumptions are being made. The first assumption is that the satellites' mass does not change over time. The second assumption is that the body of the spacecraft is either spherical or has a fixed orientation with respect to the Earth. The second assumption is due to the cross-sectional area of the satellite not changing during the simulation. Since the body of a 3U CubeSat is not spherical, the assumption is that the orientation of the satellite's body is fixed with respect to the Earth. Figure 14 is a screenshot from STK of the propagator specific force model that is utilized for the simulations.

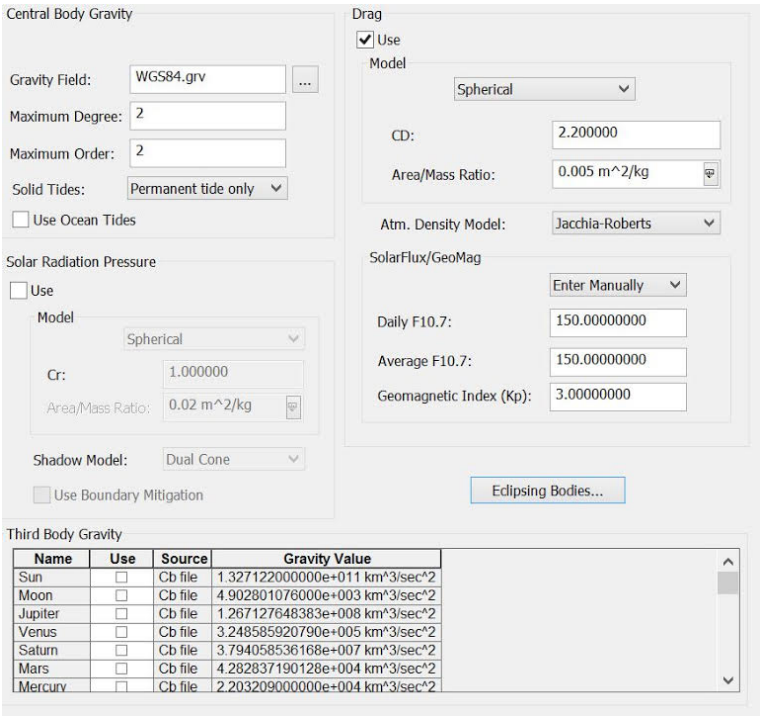

Figure 14: STK HPOP Force Model Settings – STK screenshot[3]

The duration of each test case is determined by the lifetime of the individual satellites contained within the test case. Each simulation is terminated once either all nine satellites deorbit or after three years, whichever duration is shorter.

3.4 Post Simulation Analysis

All analysis of the data is conducted utilizing MATLAB®. While the satellite's state is defined by 6 state variables, 12 are provided by STK in this investigation. Those twelve variables are: Position (x, y, z – J2000 frame), Velocity ($\dot{x}$, $\dot{y}$, $\dot{z}$ – J2000 frame), Semi-major axis, Eccentricity, Inclination, Right Ascension of the Ascending Node (RAAN), Argument of Perigee, and True Anomaly. These twelve variables are recorded and outputted every 60 seconds. The data from STK is imported into MATLAB® and saved in test cases specific .mat files for future use.

The first calculation that is completed is finding the straight-line distance from every satellite to every other satellite within the constellation. After this has been completed, the minimum and maximum distance between any single satellite pair in the constellation is computed. The responsible pair for both the minimum and maximum distance is also recorded. The next analysis of the constellation that is conducted involves calculating the volume occupied by the eight deployed satellites using the methods described later in this chapter. The minimum and maximum volume is also found by stepping though the data with a step size equal to the initial period of the orbit and finding the minimum and maximum volume over that period in time.

Once this analysis is completed, plots are created for all of the above calculations for four separate time periods. Those time periods are 1 day, 1 week, 1 month, and 3 years or the lifetime of satellite, whichever is shorter. Once all of the plots have been compiled for an individual test case, two videos are created to show the relative motion of the eight deployed satellites with respect to the control satellite for the first 24 hours and the first month after deployment. The videos are very helpful to understand how certain physical behaviors represent themselves within the plots. Figure 15 shows a progression of three screenshots depicting the motion of the individual satellites relative to the control satellite.

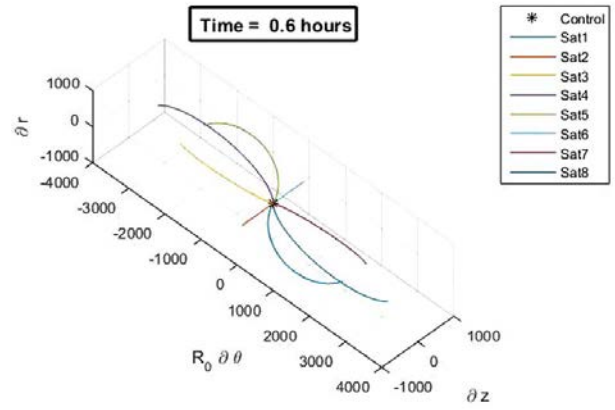

(a)

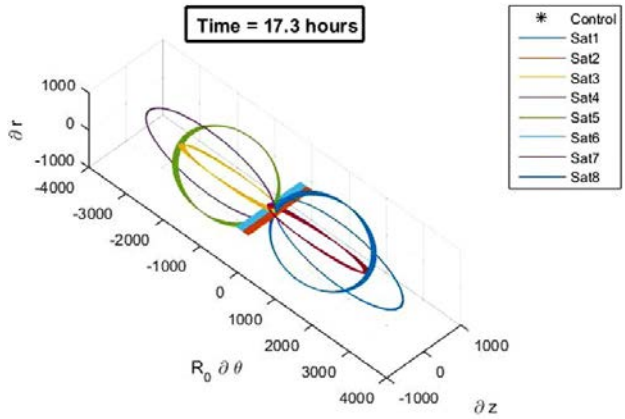

(b)

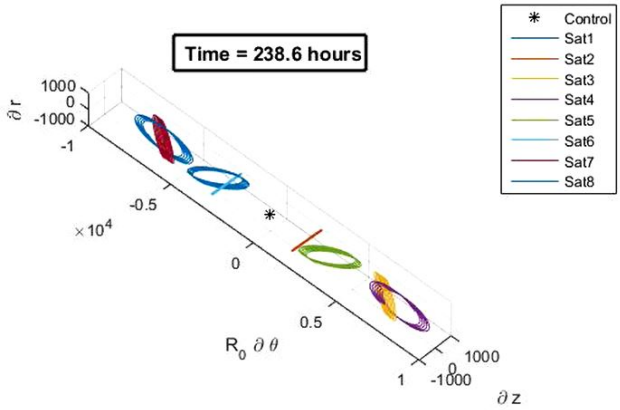

(c)

Figure 15: Progression of Relative Motion of the Individual Satellites - (Alt = 300 km – Inc = 30° - Offset = 0° - SV = 1 m/s)

The difficulties of tracking and identifying multiple CubeSats deployed over a short period in time is discussed in Chapter 2. Table 5 displays the observation accuracy of four different types of devices that are used to determine a satellite's position in space. While some of the measurement devices are quite accurate, others that are in use may not be able to resolve two satellites from one another if they are closer than 300 m away from one another. Deployment parameters that result in individual satellites operating within this distance should be avoided if one desires to minimize these difficulties.

Table 5: Observation Accuracy of Various Satellite Position Measurement Instruments (1,000 km) – adapted from Vallado [20]

Measurement Type	Accuracy
High-precision laser	60 cm
High-precision radar	8 m
Interferometer	200 m
Low-precision radar	300 m

Conversely, keeping a set number of CubeSats close to one another is of importance if those CubeSats are meant to operate in proximity with one another. While the set of satellites should still be far enough apart to facilitate tracking and identification, initially keeping the CubeSats within close proximity to one another would reduce the amount of time and fuel necessary to bring the set of CubeSats within the proximity required to begin operations, which would allow the operational phase of the mission to begin sooner while also leaving more fuel available for the operational lifetime of the satellite. Conjunctions between satellites are always a concern, but, for this investigation, avoiding conjunctions over the first 24 hours is prioritized. Deployment parameters that result in a satellite pair possibly colliding with one another are noted for future

deconfliction. Table 6 lists distances and the associated trait that can be linked between the satellite pair responsible for the measurement.

Table 6: Distance Links to Satellite Pair Traits

Distance (km)	Associated Satellite Pair Trait
1-3	Formation Flying Inter-Satellite Link
5,000	Optimal Spacing
13,000-15,000	Opposite Sides of Orbit Path

The final time period that is investigated is the operational lifetime of the satellite, during which the priorities concerning the behavior of a constellation may be different from the two other time periods that are examined in this investigation. For instance, over the operational lifetime of a constellation, multiple CubeSats being in range of a single ground station simultaneously may be less than optimal if the ground station does not have the ability to communicate with both CubeSats simultaneously. If that is the case, the various distance metrics can identify a potentially redundant pair of CubeSats within the constellation. The final metric utilized in this investigation is the volume metric, which can show constellation growth and dispersal and highlight potential coverage gaps.

The volume metric does not intuitively convey a sense of what is a ‘good’ volume verse a ‘bad’ volume, and the ultimate determination of what volume is desired is mission dependent. However, some volumes are linked to particular traits in a constellation. For example, 0.113 km^3 is the volume of a sphere with a radius of 300 m. From the measurement parameters presented in Table 5, tracking of a constellation with this volume may be difficult. If the constellation must operate in close proximity to one

another, like the CanX-4 and CanX-5 formation flying mission, a constellation volume of 4.189 km^3 to 113.09 km^3 is more desirable. 4.189 km^3 to 113.09 km^3 represent the volumes of spheres with radii of 1 km and 3 km, respectively. If a mission requires that the individual satellites populate the entire orbit path, volumes on the order of 10^8 km^3 are desired. This order of magnitude is the initial limit for constellations with altitudes between 300 km and 1,000 km, and corresponds to the volume of a cylinder with a radius equal to the orbital radius of the constellation and a height of 2 km, which is approximately the observed out of plane motion with a constellation. Volumes higher than 10^8 km^3 can be achieved over long durations, and this is indicative of the separation of the orbit planes of the individual satellites occupying a constellation. This information is summarized in Table 7.

Table 7: Volumetric Links to Constellation Traits

Volume (km^3)	Associated Constellation Trait
10^{-1}	Possible difficulties with tracking and identification
$10^0 – 10^2$	Advantageous for proximity operations
$10^8 – 10^9$	Constellation populates entire orbit path
$> 10^9$	Orbit planes of individual satellites have separated

3.5 Volumetric Calculations

In this investigation, the volume of a constellation of satellites is calculated using Delaunay Triangulations and Convex Hulls. A Delaunay triangulation is based off of the work of Russian mathematician Boris Nikolaevich Delone.[32] Delaunay triangulation is first used on points that lie on a plane to connect all of the points to one another to form

triangles with the original points as vertices. Furthermore, any Delaunay triangulation of a set of points maximizes the minimum angle over all triangulations of a particular set of points.[33] When applied to points in 3-dimensional space, instead of triangles, tetrahedrons are formed.[34] Once all of the tetrahedrons are formed, the volume of the constellation is calculated using Equation (38). The volume of the constellation can be found from the summation of the volume of all of the individual tetrahedrons using Equation (38), where a, b, c, and d are the points of the four vertices of the tetrahedron. An example volume broken up into tetrahedrons is shown in Figure 16. The *delaunayTriangulation* and *convexHull* commands in MATLAB® are utilized within this study to quickly compute the volume of a constellation at any given point in time.

$$V = \frac{|(a-d)\cdot((b-d)\times(c-d))|}{6} \tag{38}$$

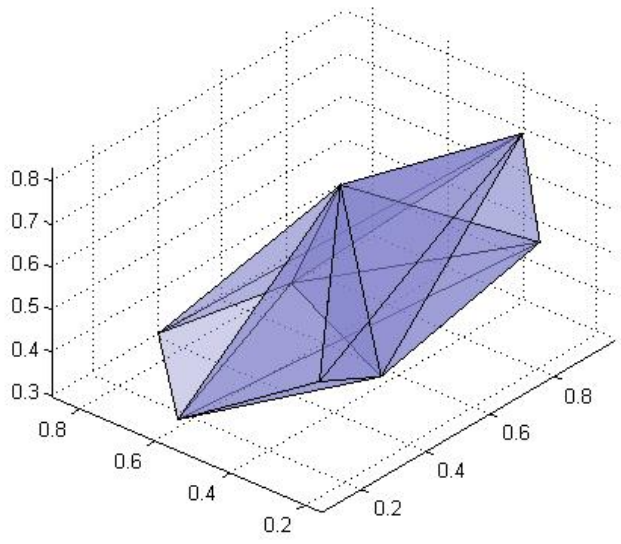

Figure 16: Random Volume Split into Tetrahedrons

3.6 Creation of a Delayed Deployment Constellation

The creation of a constellation in which at least some of the satellites are deployed at a time after the initial deployment is conducted differently than the rest of the test cases. To create these constellations, the position and velocity vector for the control satellite occupying a circular orbit at an altitude of 300 km with an inclination of 30° is taken over two time periods. The first time period is every minute for the first 7 minutes past the ascending node. The second time period is every 5 minutes for the first 45 minutes past the ascending node. Eight satellites are ejected into a plane normal to the velocity vector for all of these time steps, utilizing a separation velocity of 1 m/s. The position and velocities of the individual satellites are computed until they reenter Earth's atmosphere. These simulations are completed using STK and then imported into MATLAB®. The individual deployment scenarios are constructed and analyzed with

MATLAB®. This means that the final test case never existed separately within STK. This allows for the propagations to be calculated using STK, but for many different permutations of deployment schemes to be analyzed within MATLAB®.

To accomplish this, the data from a numerical propagation is taken out of STK, and the various separation velocities are then applied to the data and then reentered into STK as the initial conditions for new numerical propagations. In order to be able to pick satellites from different scenarios and analyze them as a single constellation, the position and velocity vectors of the control satellites within those scenarios must agree with one another. This was not the case initially. It was found that the truncation of the initial conditions between scenarios differed enough to initially invalidate this method. The root cause of this issue was within the MATLAB® code used to create the constellations within STK, specifically the *num2str* command, internally deciding how many digits of the initial conditions to convert to a string variable before passing that information along to STK to create the desired constellation. Once this issue was identified, studied, and corrected, the creation of test cases within MATLAB® using previously calculated data was implemented to study the behavior of a constellation containing satellites that are deployed at separate times.

3.7 Chapter Summary

In this chapter, the layout of an individual test case is presented and explained. After the individual test cases are explained, the details of how the individual test cases are inputted and simulated in STK are described. Once the data is uploaded into MATLAB® from STK, the distance and volume metrics for the constellation are

calculated. Exactly how this investigation calculates the volume of a constellation of satellites is also presented in this chapter. This chapter concludes with a summary of how a constellation containing satellites whose deployments are delayed with respect to one another is implemented in this investigation.

IV. Analysis, Results, and Discussion

4.1 Chapter Overview

Two different types of analysis are discussed in this chapter. The first type is the analysis of a deployment scenario for three types of orbits: low Earth, sun synchronous, and Molniya. For this analysis, the three phases of interest are discussed. Those three phases are: (1) the first 24 hours after deployment, (2) the first few weeks after deployment in which the initial identification and tracking of the individual satellites is being conducted, and (3) during the operational lifetime of the satellite, which, for the purposes of this investigation, is 3 years, unless the satellite deorbits before that period of time. For this investigation, eight 3U CubeSats are deployed and their behavior, relative to each other, and one control 3U CubeSat, is studied. The numbering scheme applied to each individual test case is presented in Figure 17. To analyze the behavior of a constellation, the distance from any single satellite within the constellation to any other satellite is tracked. From those distances, the minimum and maximum spacing between any two satellites within the constellation is determined. The last metric that is calculated is the volume of a polygon that would encompass the constellation.

The final section of this chapter is a discussion of how the results of this investigation compare to previous research that is being conducting on the deployment of CubeSats. Also included in this section is a discussion of how the results of this investigation can be used to resolve problems that have been experienced by past missions that have been caused by the deployment of CubeSats. The last portion of this

section is a discussion of how the results of this investigation can be applied to specific types of missions.

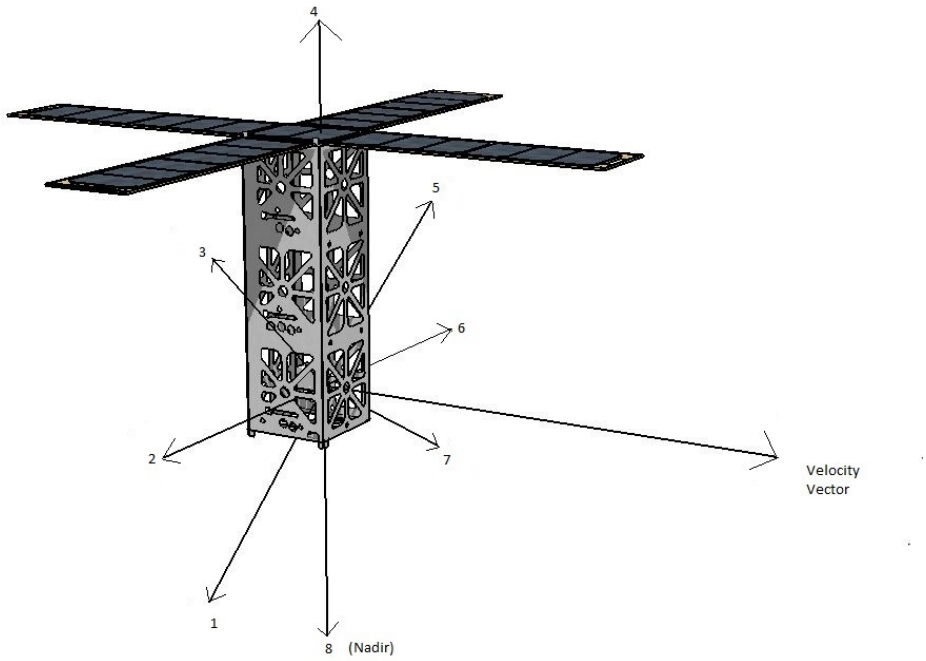

Figure 17: Numbering Scheme for Deployed Satellites

The second type of analysis discussed in this chapter is an overall trend analysis on how varying the type of orbit (altitude and inclination) and the four deployment variables (geometry, delayed deployment, location within the orbit, and separation velocity) affect the distance and volume metrics that are calculated from the individual test case analyses. Table 8 is provided as a quick reference to the satellite parameters that are used for the following analyses.

Table 8: Satellite Parameters

Parameter	Value
Ballistic coefficient	0.011 m^2/kg
Cross-sectional area	0.03 m^2
Mass	6 kg
Coefficient of drag	2.2

4.2 Individual Test Case Analysis

4.2.1 Low Earth Orbits

4.2.1.1 LEO - Deployment Phase Analysis

For this investigation, the deployment phase is the time period consisting of the first 24 hours after deployment. During this phase, the main objectives are to safely deploy the satellites, avoid conjunctions between the individual satellites, and to facilitate tracking and identification. An immediate area of concern is the launch of multiple CubeSats from the same dispenser simultaneously. Figure 18 shows, when the offset of the deployment plane is 0°, the relative difference in position between two satellites launched simultaneously along the same vector, for example, vector 1 in Figure 17, with a 0.5 m/s difference in separation velocity. Separation velocities of 1 m/s and 1.5 m/s are used for the satellites involved in conducting this analysis. There are multiple conjunction opportunities over the first 24 hours and very little overall separation during that time period, leading to problems with the tracking and identification of and the communication with these two satellites. These problems are mitigated if the offset of the deployment plane is set to 45°, shown in Figure 19, but the behavior is still driven by a

difference in the separation velocities of the individual satellites. There may not be such a difference if the satellites are deployed from the same dispenser. The mitigation shown in Figure 19 is caused by the fact that a component of the separation velocity is in the direction of the anti-velocity vector. If the same dispenser is being used to launch multiple satellites, a mechanism should be implemented that will at least separate the deployments in time or separation velocity, preferably both.

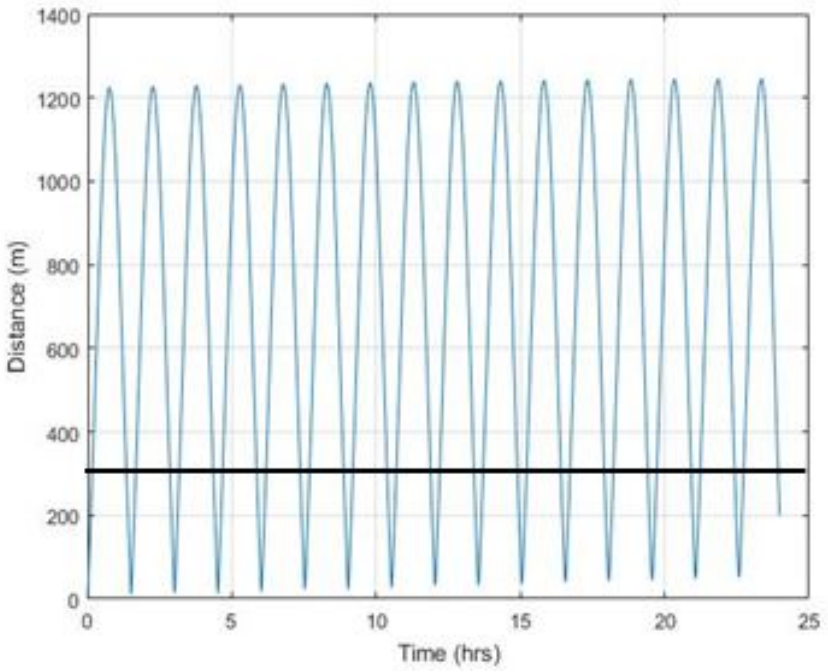

Figure 18: Relative Distance of Two CubeSats Deployed Simultaneously in the Same Direction (0.5 m/s difference in separation velocity – Offset = 0°)

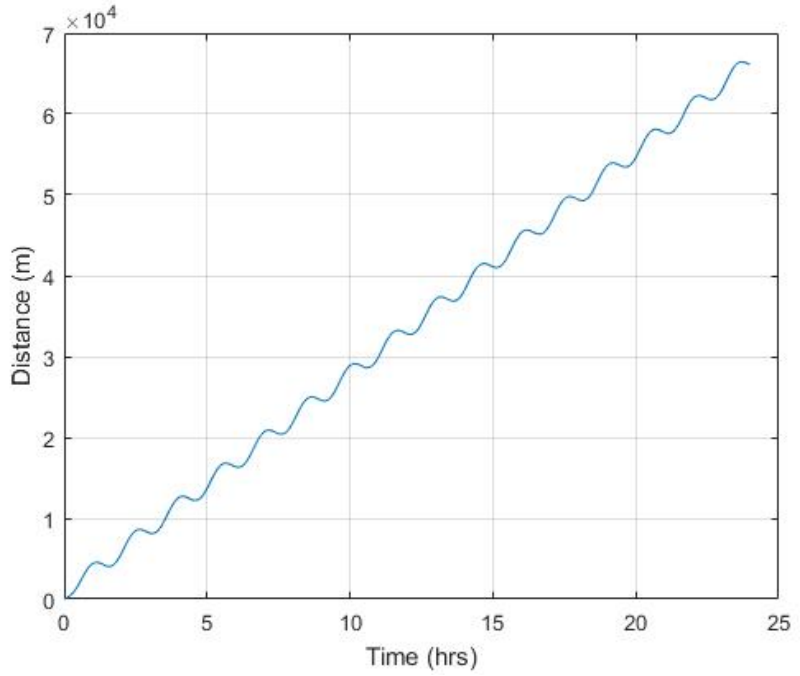

Figure 19: Relative Distance of Two CubeSats Deployed Simultaneously in the Same Direction (0.5 m/s difference in separation velocity – Offset = 45°)

Figure 20 through Figure 22 show the distance from the control satellite to the deployed satellites for a circular orbit with an altitude of 300 km, an inclination of 30°, argument of latitude of 0°, and a separation velocity of 1 m/s. The difference between the three plots is the offset, which is 0°, 45°, and 90° for the 3 figures, respectively. Note that, due to the way offset is investigated, satellites 4 and 8 are the same satellites being used in all three test cases. From observing the behavior of the constellation shown in Figure 20, it can be observed that deploying into the plane normal to the velocity vector of the control satellite does not promote the growth of the constellation. This is because no component of the separation velocity is in the direction of the velocity vector. Another trend that stands out is that satellite 2 and satellite 6, which, for this deployment configuration, only undergo small (approximately .0075°) changes in inclination, have

twice as many pass-by opportunities as other satellite pairs, which shows that deploying satellites in such a way should be avoided to prevent possible conjunctions shortly after deployment.

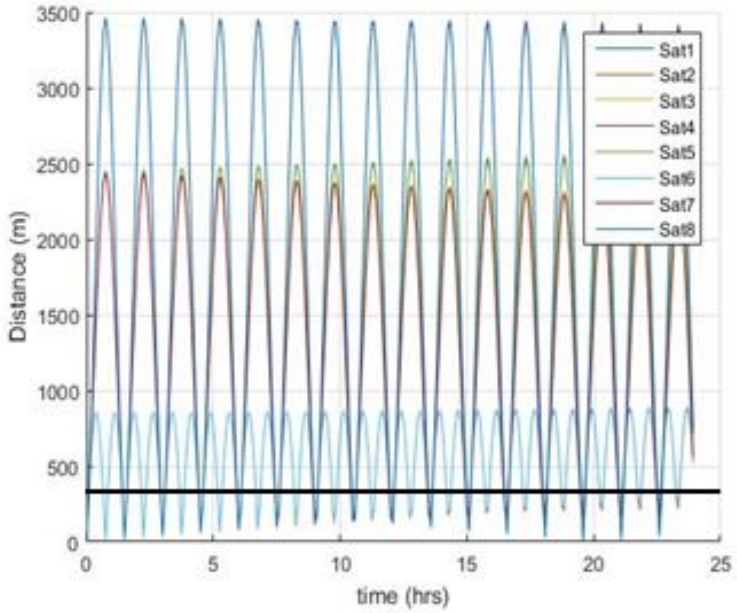

Figure 20: Distance from Control Satellite to Deployed Satellites (1 Day) (Alt = 300 km – Inc = 30° - Offset = 0° - SV = 1 m/s)

In Figure 21, the deployment scheme is set up such that six of the eight satellites have a portion of their separation velocity adding to or subtracting from the initial velocity of the control satellite. With the exception of satellites 4 and 8, the satellites within this constellation move with respect to one another due to the slightly different orbital periods between the individual satellites. Satellites 2 and 6 move faster than the rest of the constellation due to those two satellites receiving a larger change in the direction of the initial velocity vector.

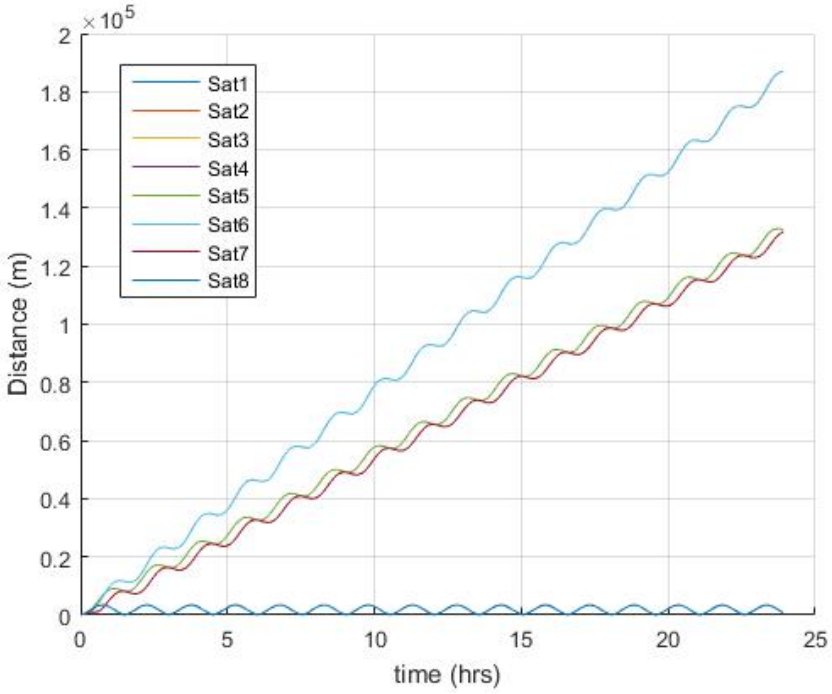

Figure 21: Distance from Control Satellite to Deployed Satellites (1 Day) (Alt = 300 km – Inc = 30° - Offset = 45° - SV = 1 m/s)

A deployment plane offset of 90°, shown in Figure 22, shows similar behavior as a deployment plane offset of 45°. This is because the phasing effects experienced by the constellation are present in both, which causes the distance between the satellites to initially grow with time. ‘Phasing’ refers to how the satellites separate along the orbit path.

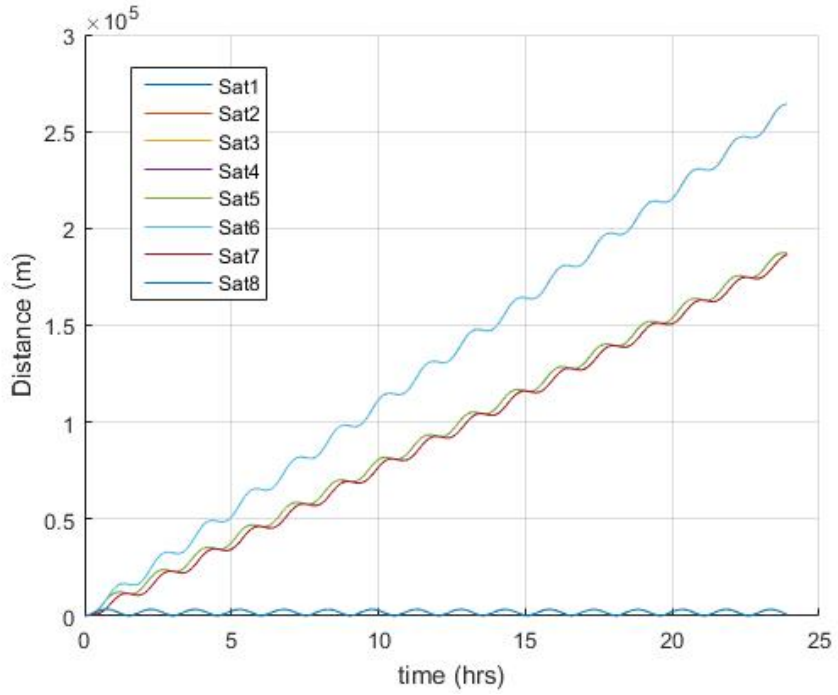

Figure 22: Distance from Control Satellite to Deployed Satellites (1 Day) (Alt = 300 km – Inc = 30° - Offset = 90° - SV = 1 m/s)

Figure 23 through Figure 25 show the maximum distance between any two satellites in the constellation over the first 24 hours after deployment. These figures also show the satellite pair that is responsible for this measurement. For an offset of 0°, satellite 4 and satellite 8 are the two satellites that are farthest away from one another for during the first 24 hours. It is also observed that, for this deployment scheme, once an orbit, no satellite pair in the constellation is more than 500 m away from one another. This shows that multiple of the satellites in this deployment pose conjunction risks to one another, in addition to contributing to difficulties with the tracking and identification of the individual satellites.

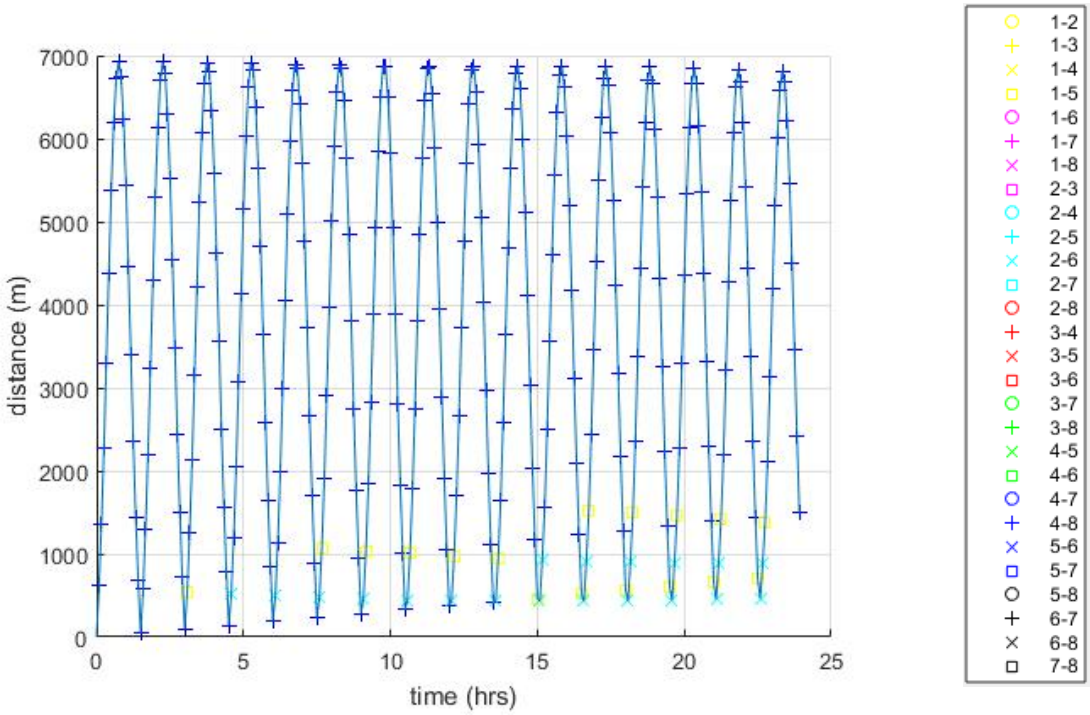

Figure 23: Maximum Distance Between Any Two Satellites (1 Day) (Alt = 300 km – Inc = 30° - Offset = 0° - SV = 1 m/s)

Again, the behavior of deployment schemes with offsets of 45° (Figure 24) and 90° (Figure 25) show similar behavior as each other. The difference between the two plots is the magnitude of the maximum distance between any two satellites. In these two cases, after the first hour, satellites 2 and 6 are the furthest away from one another for the majority of the first day. Satellites 2 and 6 are the furthest away from each other because they have the largest difference between the components of their separation velocities in the direction of the velocity vector of the deployer. It is also observed that satellites 4 and 8, which are the satellites that are the furthest away from one another for the majority of the time when the offset is 0°, and are the same satellites in all 3 test cases, are only the furthest apart for the first few minutes when the offset of the deployment plane is either 45° or 90°.

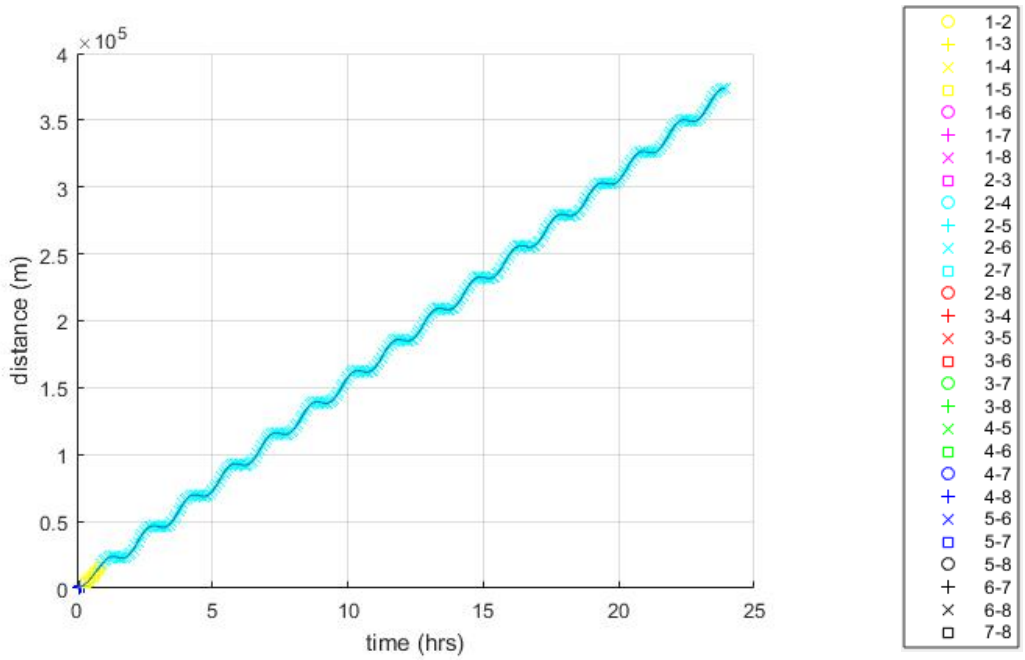

Figure 24: Maximum Distance Between Any Two Satellites (1 Day) (Alt = 300 km – Inc = 30° - Offset = 45° - SV = 1 m/s)

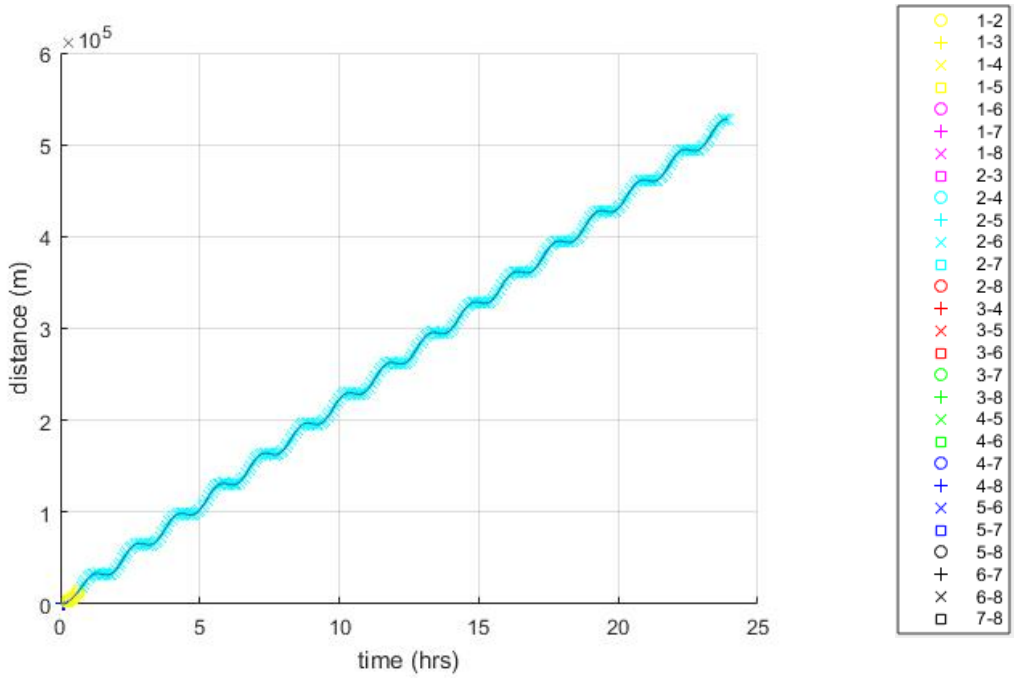

Figure 25: Maximum Distance Between Any Two Satellites (1 Day) (Alt = 300 km – Inc = 30° - Offset = 90° - SV = 1 m/s)

Figure 26 through Figure 28 show the minimum distance between any two satellites in the constellations over the first 24 hours. From Figure 26 it can be seen that during the first 24 hours after deployment, for an offset of 0°, seven different satellite pairs are responsible for the minimum distance within the constellation, five of which occur less than 300 m from each other. This supports the evidence from Figure 20 and Figure 23 that an offset of 0° can lead to problems with both possible conjunctions between satellites and with tracking and identification.

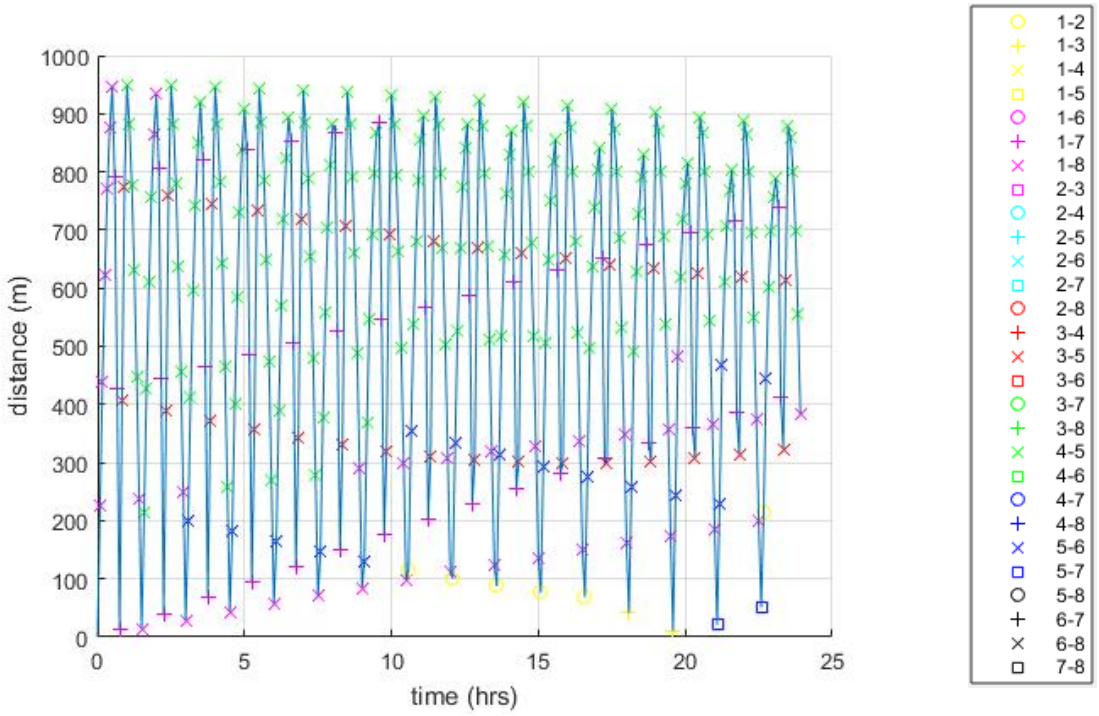

Figure 26: Minimum Distance Between Any Two Satellites (1 Day) (Alt = 300 km – Inc = 30° - Offset = 0° - SV = 1 m/s)

With respect to the minimum distance between any two satellites within the constellation, both Figure 27 and Figure 28 display similar behavior over the first 24

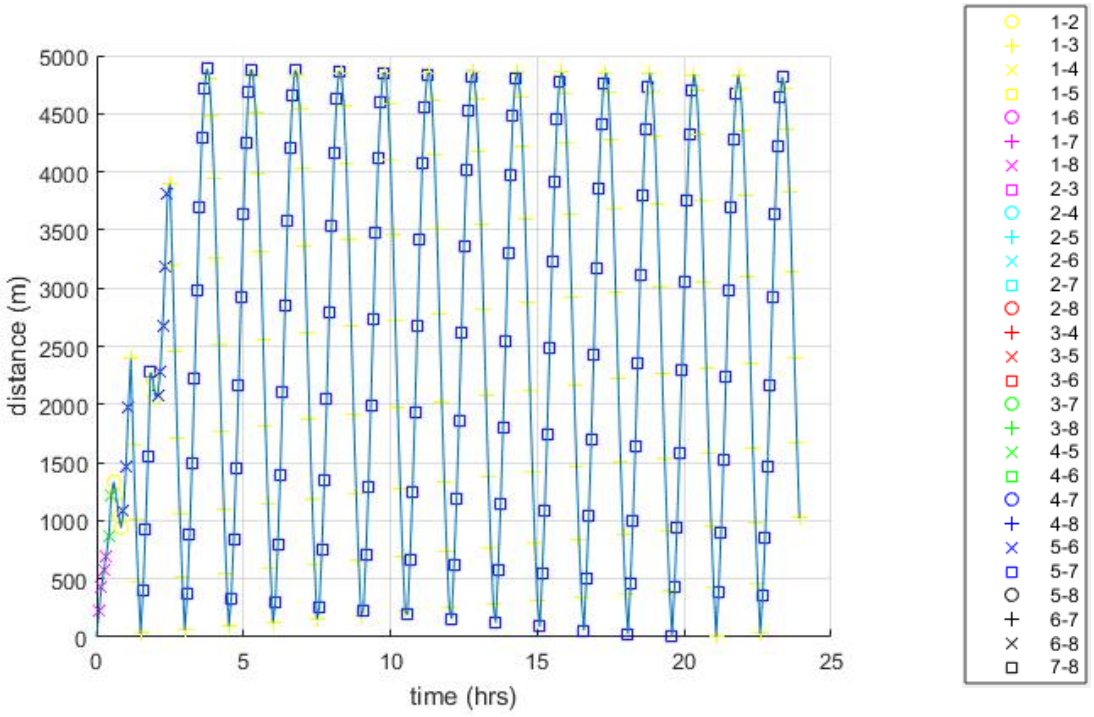

Figure 27: Minimum Distance Between Any Two Satellites (1 Day) (Alt = 300 km – Inc = 30° - Offset = 45° - SV = 1 m/s)

hours. For offsets of 45° and 90°, the satellite pair consisting of satellite 1 and satellite 3 and the satellite pair consisting of satellite 5 and satellite 7 are the satellite pairs responsible for the minimum distance between any two satellites within the constellation. Referring back to Figure 17, it shows that the 1-3 pair and the 5-7 pair both result from separation velocities in the same out of plane (orbit normal) direction. The 1-3 pair and the 5-7 pair both keep their respective satellites close together, while still allowing the individual satellites to be separated by a maximum of 4.5 km per orbit. Note that the value of this separation is dependent on the ballistic coefficient, B^*, of the individual satellites in the constellation. One downside to this particular deployment setup though is that the same pairs also experience a period in which the relative distance between them is very small, leading to the possibility of a conjunction shortly after deployment.

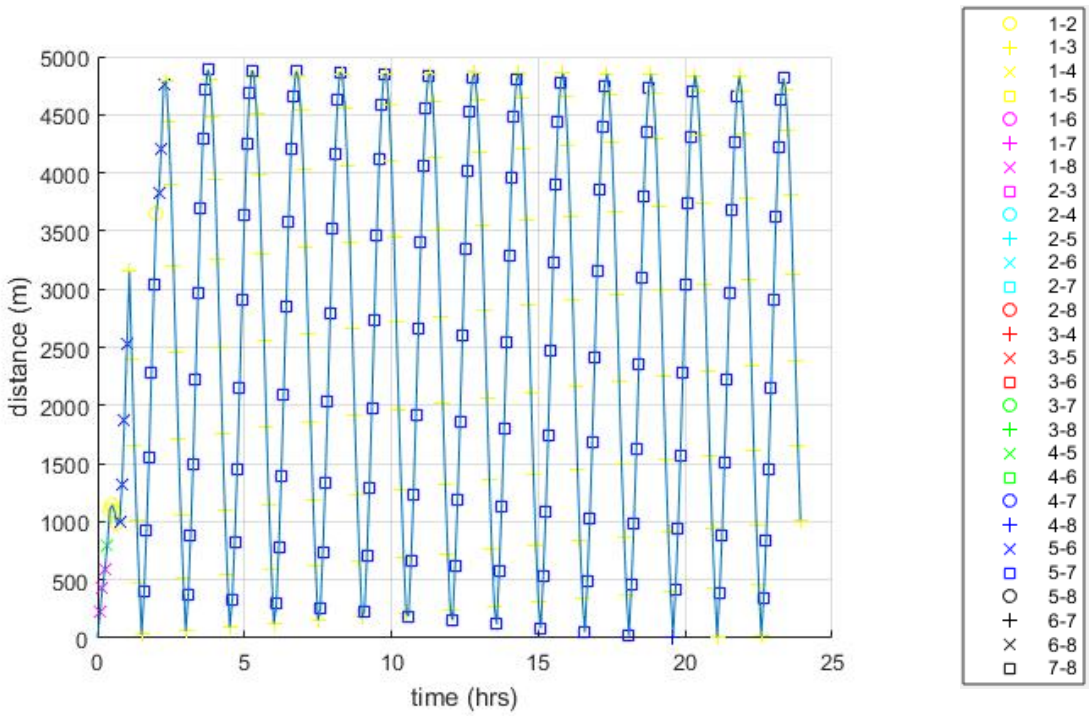

Figure 28: Minimum Distance Between Any Two Satellites (1 Day) (Alt = 300 km – Inc = 30° - Offset = 90° - SV = 1 m/s)

4.2.1.2 LEO - System Checkout Phase Analysis

For this investigation, the system checkout phase is the first week after deployment that is utilized to track, identify, and communicate with the individual satellites. Once the operators are able to communicate with their satellites, the necessary system checks can be carried out so that the operational phase of the mission can begin. During this phase, the main objectives are to facilitate the tracking and identification of, and communication with the deployed satellites.

Figure 29 shows that, for 0° offset, the deployed satellites stay within close proximity to one another. The 0° offset does not cause the satellites within the constellation to start to spread out from one another by the end of the week.

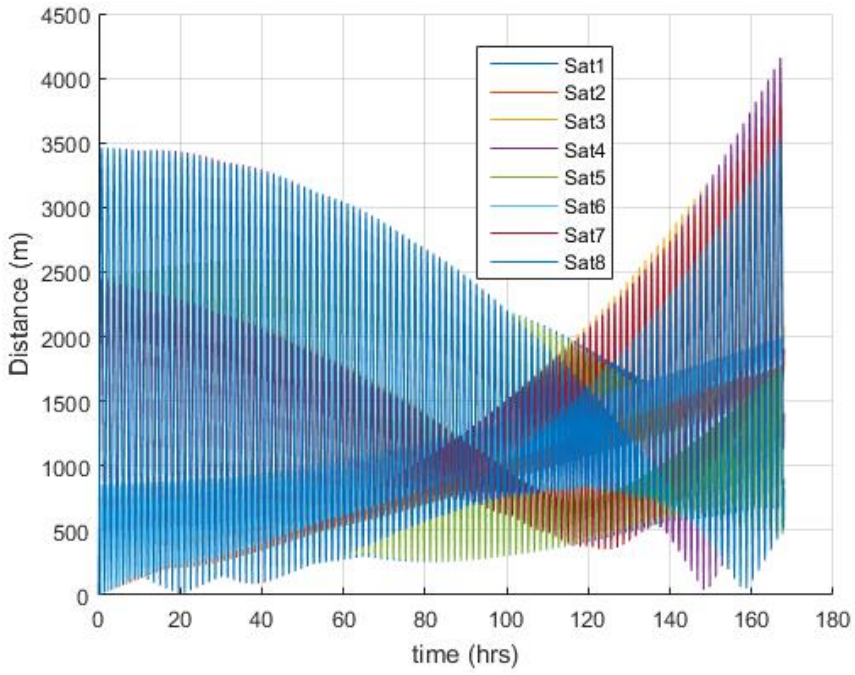

Figure 29: Distance from Control Satellite to Deployed Satellites (1 Week) (Alt = 300 km – Inc = 30° - Offset = 0° - SV = 1 m/s)

Over the first week after deployment, offsets of 45° and 90° do a much better job of separating the satellites, as shown in Figure 30 and Figure 31. The three different groupings shown in Figure 30 and Figure 31 are caused by the different directions of the separation velocities applied to the individual satellites creating small changes in the semi-major axis of the deployed satellites orbit. This changes the value of the mean motion of the individual satellites, causing them to move with respect to one another.

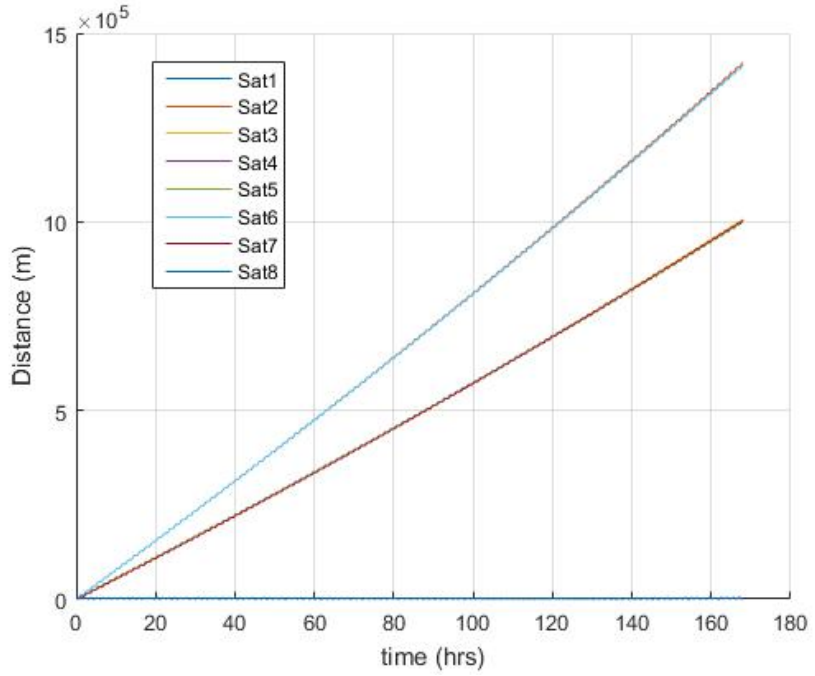

Figure 30: Distance from Control Satellite to Deployed Satellites (1 Week) (Alt = 300 km – Inc = 30° - Offset = 45° - SV = 1 m/s)

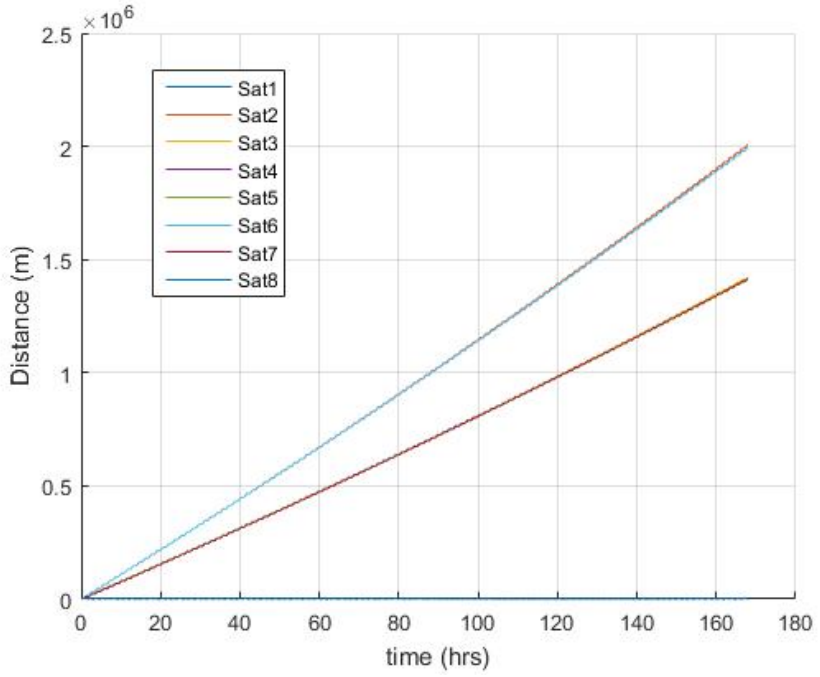

Figure 31: Distance from Control Satellite to Deployed Satellites (1 Week) (Alt = 300 km – Inc = 30° - Offset = 90° - SV = 1 m/s)

Figure 32 shows the maximum distance between any two satellites for a deployment in the plane normal to the velocity vector. Once 50 hours have passed from the time of deployment, two satellites are at least 1 km away from one another. While this shows that some of the satellites are far enough apart to facilitate tracking and identification, Figure 35, which shows the minimum distance between any two satellites, is a better measure of how this constellation facilitates tracking and identification.

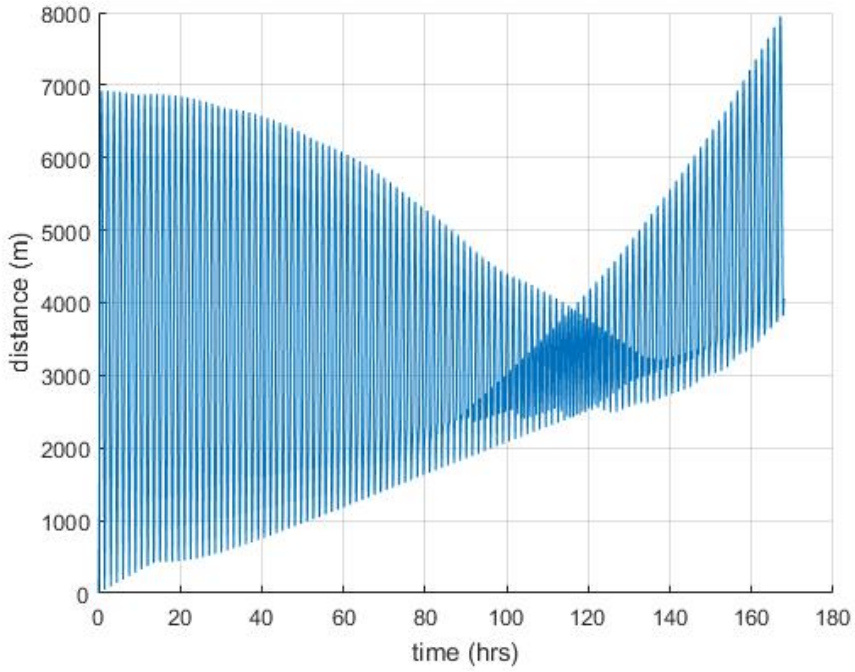

Figure 32: Maximum Distance Between Any Two Satellites (1 Week) (Alt = 300 km – Inc = 30° - Offset = 0° - SV = 1 m/s)

Figure 33 and Figure 34 show the growing distance between satellite 2 and satellite 5 that is a continuation of the behavior observed in Figure 24 and Figure 25. This is due to a difference in mean motion, caused by the two satellites having slightly different magnitudes for semi-major axis, meaning that one satellite completes its orbit slightly faster than the other, causing the distance between the two to grow.

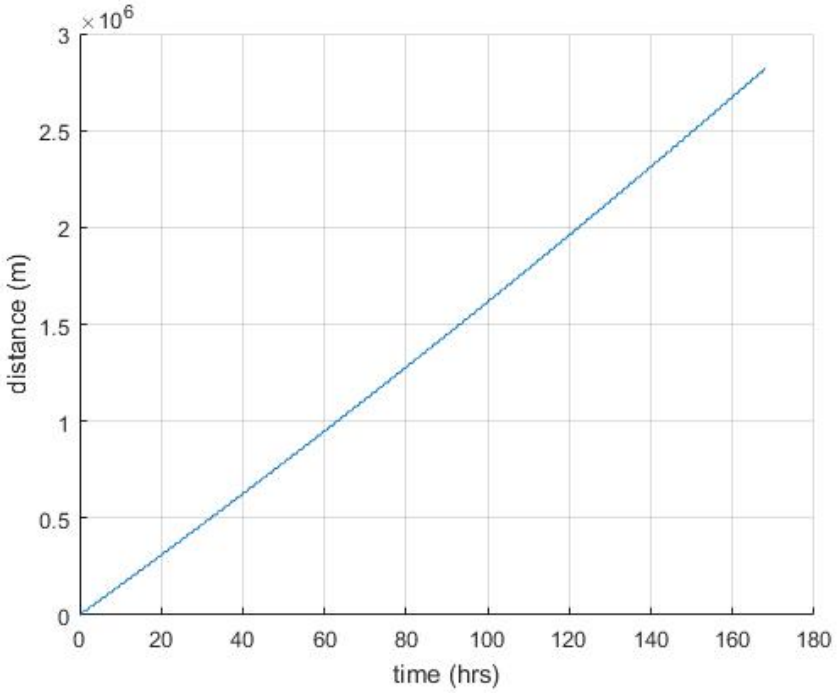

Figure 33: Maximum Distance Between Any Two Satellites (1 Week) (Alt = 300 km – Inc = 30° - Offset = 45° - SV = 1 m/s)

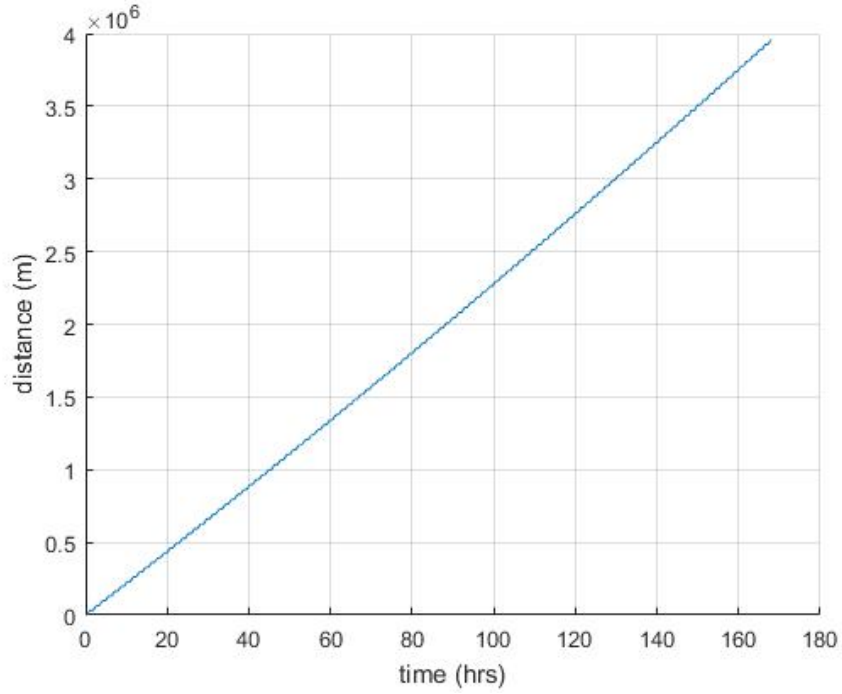

Figure 34: Maximum Distance Between Any Two Satellites (1 Week) (Alt = 300 km – Inc = 30° - Offset = 90° - SV = 1 m/s)

From the minimum distance between any two satellites in the constellation with a deployment plane with an offset of 0°, shown in Figure 35, it is evident that if a less precise means of tracking is used to observe this constellation, for example, low precision radar, which can have accuracies to within 300 m (Table 5[20]), there is only a small window in which none of the satellites are consistently more than 300 m apart. This constellation would be very hard to track and identify due to this.

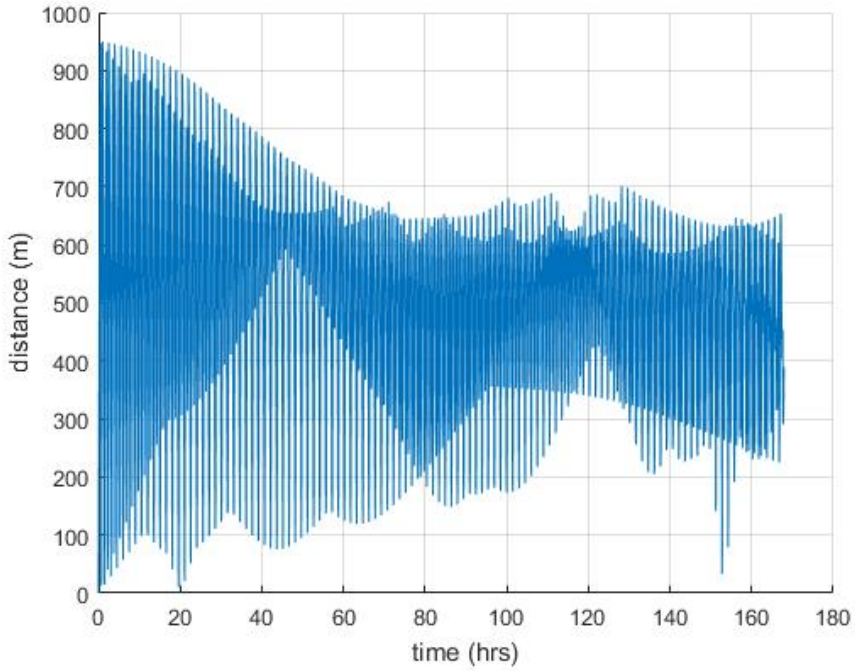

Figure 35: Minimum Distance Between Any Two Satellites (1 Week) (Alt = 300 km – Inc = 30° - Offset = 0° - SV = 1 m/s)

With the exception of the first few hours, Figure 36 and Figure 37 are the same. This is because the minimum distance within constellations with an offset of 45° and 90° are determined to be between the same satellite pair. The satellites that are closest to one another are satellites 4 and 8, which are the same for both scenarios. If the 4-8 satellite pair is driving this metric and the two plots did not agree with one another, the indication would be that there is either an error in the data or in the analysis process. This agreement

shows that the analysis process is consistent between these two test cases and can be used to validate other cases. The data provided in the two figures indicate that the tracking and identification of the entire constellation should not be hampered by two satellites operating too close to one another after 60 hours, though satellites 4 and 8 do temporarily have moments when they do get close to one another toward the end of the week.

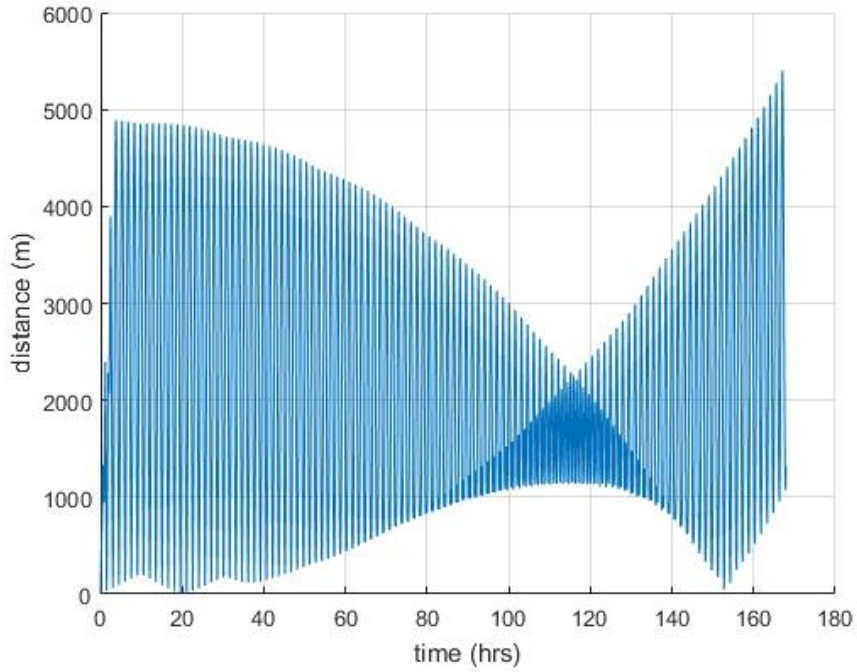

Figure 36: Minimum Distance Between Any Two Satellites (1 Week) (Alt = 300 km – Inc = 30° - Offset = 45° - SV = 1 m/s)

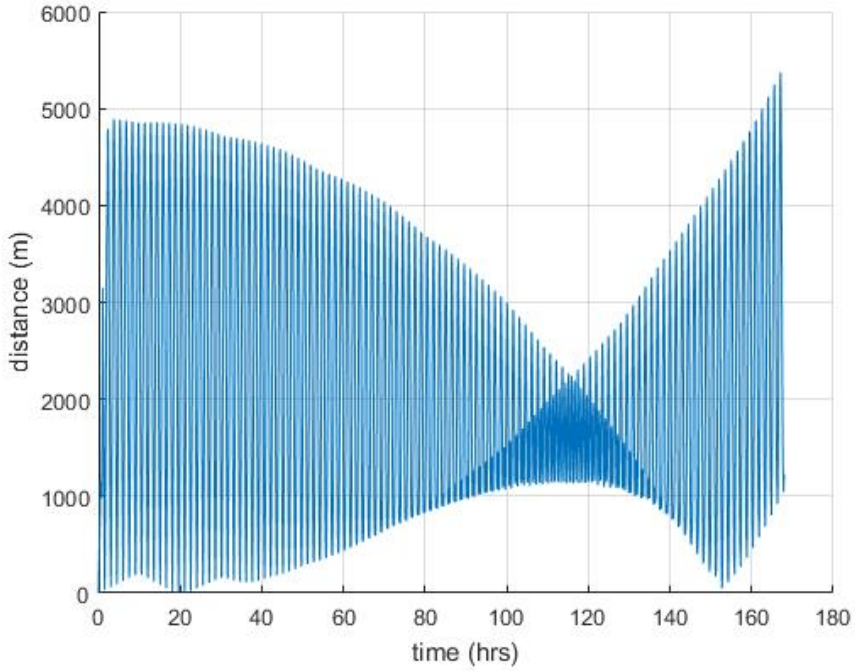

Figure 37: Minimum Distance Between Any Two Satellites (1 Week) (Alt = 300 km – Inc = 30° - Offset = 90° - SV = 1 m/s)

4.2.1.3 LEO - Operational Phase Analysis

During the operational phase, the primary objectives concerning the behavior of the constellation change. Conjunctions between satellites, while still monitored, are not a primary concern. The tracking and identification of the individual satellites has already been completed, so, while the satellites are still tracked, the orbital data of the satellites should be well known at this point in the satellites lifetime. Taking all of this into account, the primary concerns during this phase focus on mission performance, specifically communication and ground coverage.

Figure 38 shows the distance from satellite 4 to all of the deployed satellites in the constellation for when the deployment plane has an offset of 0°. Satellite 4 is chosen because, for this deployment case, it is the first satellite to pass over any given point on

the ground track. The increasing slope present in the distance plots is due to air drag. As air drag causes the altitude of the orbits to decrease, the slight difference in the semi-major axis between the satellites has a greater effect. This causes the rate at which the satellites are travelling with respect to each other to increase, which is shown in Figure 38.

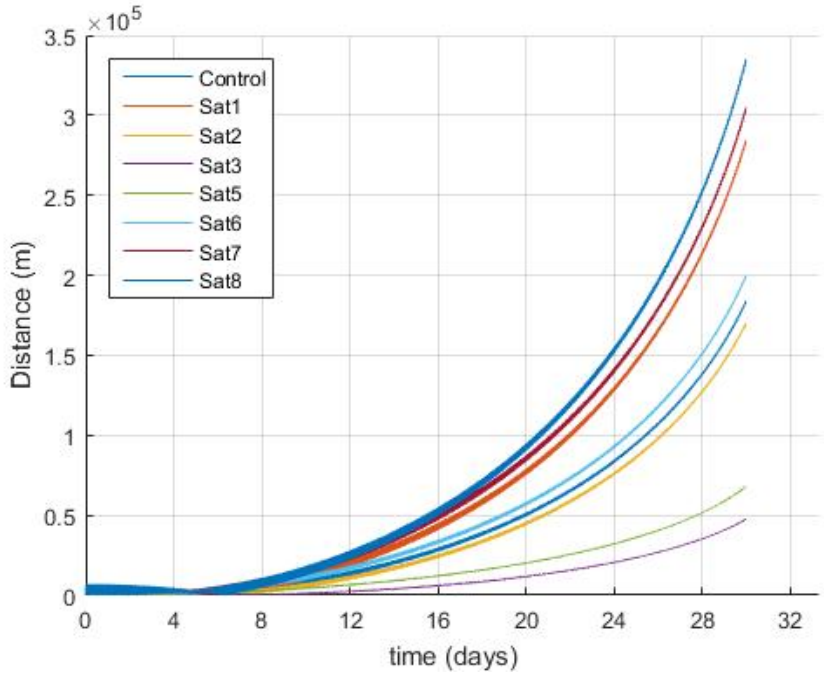

Figure 38: Distance from Satellite 4 to Deployed Satellites (1 Month) (Alt = 300 km – Inc = 30° - Offset = 0° - SV = 1 m/s)

Figure 39 is a plot of the maximum distance between any two satellites in the constellation with a deployment plane offset by 45°. Notice that there are multiple peaks in this distance plot. While this does indicate that satellite 2 and satellite 6 start to get closer to one another toward the end of the first month, it does not indicate their relative motion within the orbit plane. Satellite 2 and satellite 6 are essentially phasing in opposite directions along the orbit relative to the control satellite. This peak simply indicates that satellite 2 and 6 are now on opposite sides of the orbit and their relative phasing is now

bringing them closer together. Once this first peak is achieved, half of the orbit is occupied by the constellation.

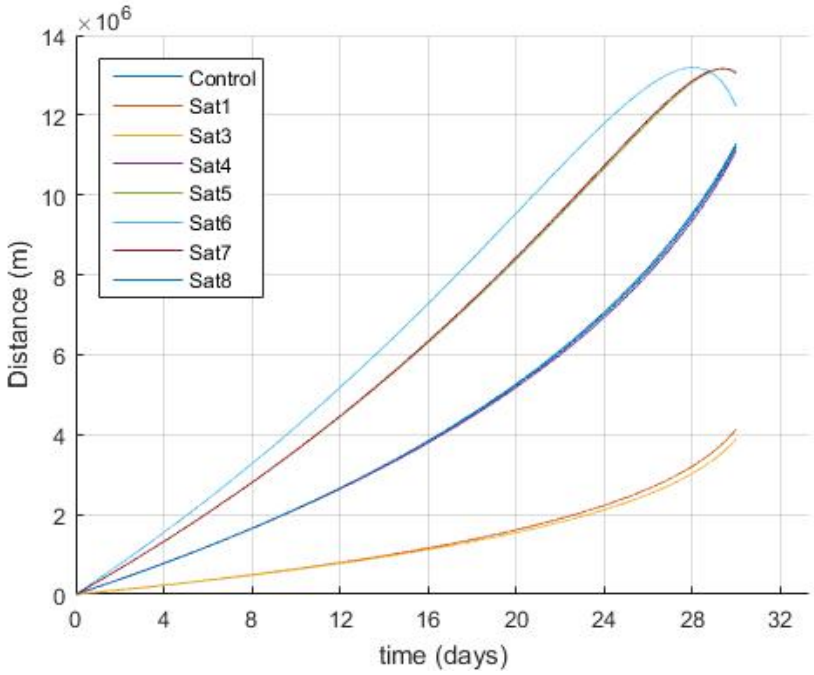

Figure 39: Distance from Satellite 2 to Deployed Satellites (1 Month) (Alt = 300 km – Inc = 30° - Offset = 45° - SV = 1 m/s)

Figure 40 shows that the peaks occur quicker when the deployment plane is offset by 90° when compared to an offset of 45°. This follows the expected results, and these results, when put into practice, can be utilized to populate an orbit plane before reentry for satellites with altitudes around 300 km.

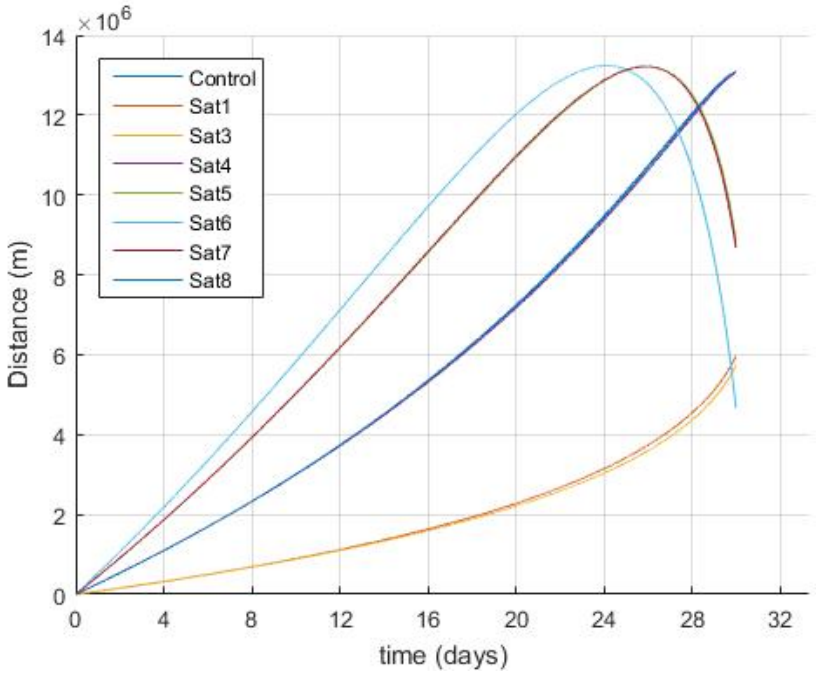

Figure 40: Distance from Satellite 2 to Deployed Satellites (1 Month) (Alt = 300 km – Inc = 30° - Offset = 90° - SV = 1 m/s)

Figure 41 shows that the maximum distance between any two satellites in the constellation with a deployment plane offset of 0° is 650 km over the lifetime of the constellation. Given that satellites in LEO are traveling around 7 km/sec, this distance can be covered in a matter of minutes. A typical LEO has a period slightly greater than 90 minutes. By comparison, it can quickly be determined that very little of the orbit is populated by this constellation, resulting in large gaps in coverage.

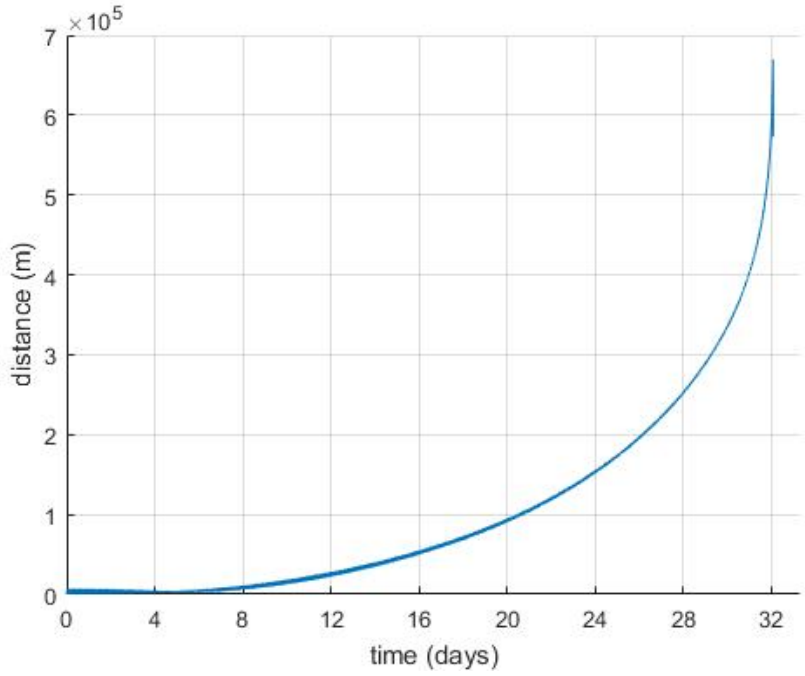

Figure 41: Maximum Distance Between Any Two Satellites (Lifetime) (Alt = 300 km – Inc = 30° - Offset = 0° - SV = 1 m/s)

Figure 42 and Figure 43 are plots of the maximum distance within the constellation for offsets of 45° and 90°, respectively. With the additional phasing present in these two deployment scenarios, it can be observed that there is a maximum in the plots of maximum distance. This occurs when a pair of satellites are on opposite sides of the orbit plane. Under close observation, it can also be seen that the local maxima are getting slightly smaller and smaller as time goes on. This is showing the diameter of the circular orbit decreasing overtime, giving an indication as to when a constellation is about to reenter the atmosphere.

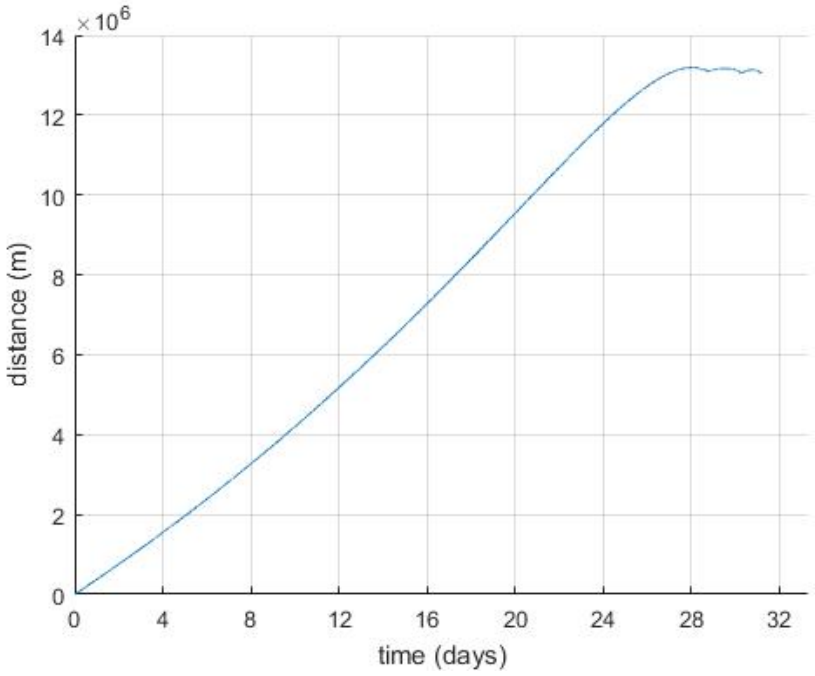

Figure 42: Maximum Distance Between Any Two Satellites (Lifetime) (Alt = 300 km – Inc = 30° - Offset = 45° - SV = 1 m/s)

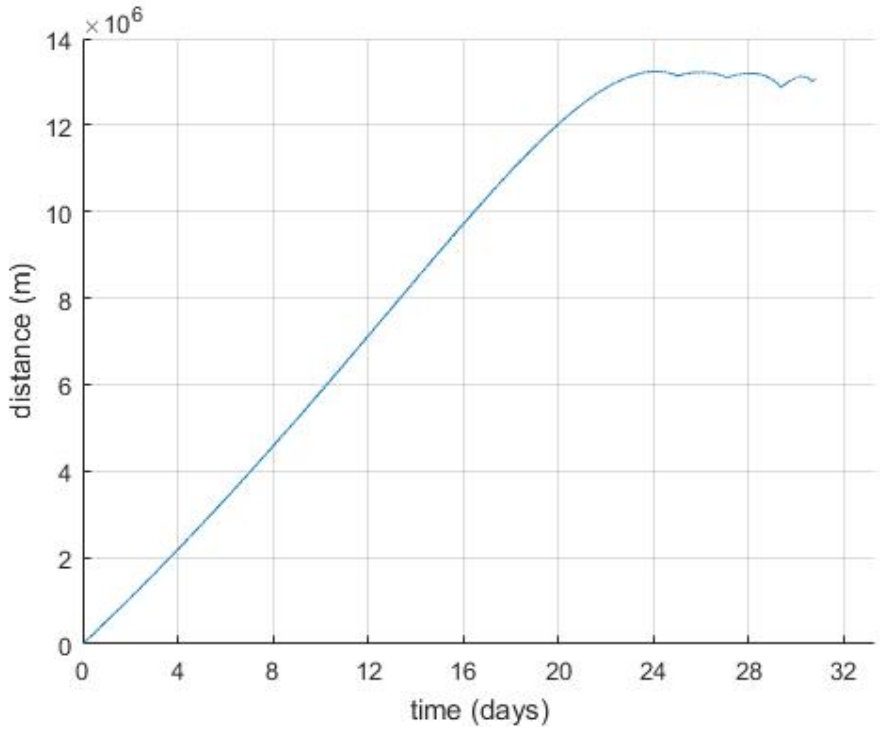

Figure 43: Maximum Distance Between Any Two Satellites (Lifetime) (Alt = 300 km – Inc = 30° - Offset = 90° - SV = 1 m/s)

Figure 44 through Figure 46 show the minimum distance between any two satellites within the constellations with deployment planes with offsets of 0°, 45°, and 90°, respectively. Figure 44 shows that the maximum of the minimum distance plot is just over 35 km, while Figure 45 shows the same maximum around 250 km. The values shown in all three of these plots indicate that there is at least one redundant pair of satellites in all of these constellations. The transition observed in Figure 44 that occurs around 23 days is caused by a swap in the satellite pair that is driving this measurement. The sharp dip (near the vertical line at approximately 30 days) in Figure 46 is not an error. This indicates that two satellites in the orbit plane are phasing past one another in the orbit, causing a lower minimum distance to be measured within the constellation, before the measurement returns to the previous dominant satellite pair.

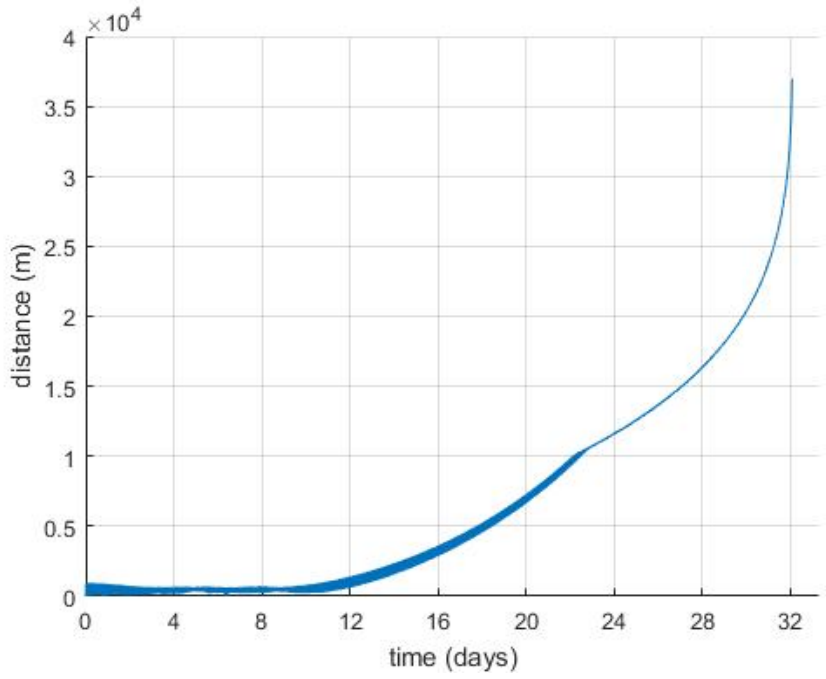

Figure 44: Minimum Distance Between Any Two Satellites (Lifetime) (Alt = 300 km – Inc = 30° - Offset = 0° - SV = 1 m/s)

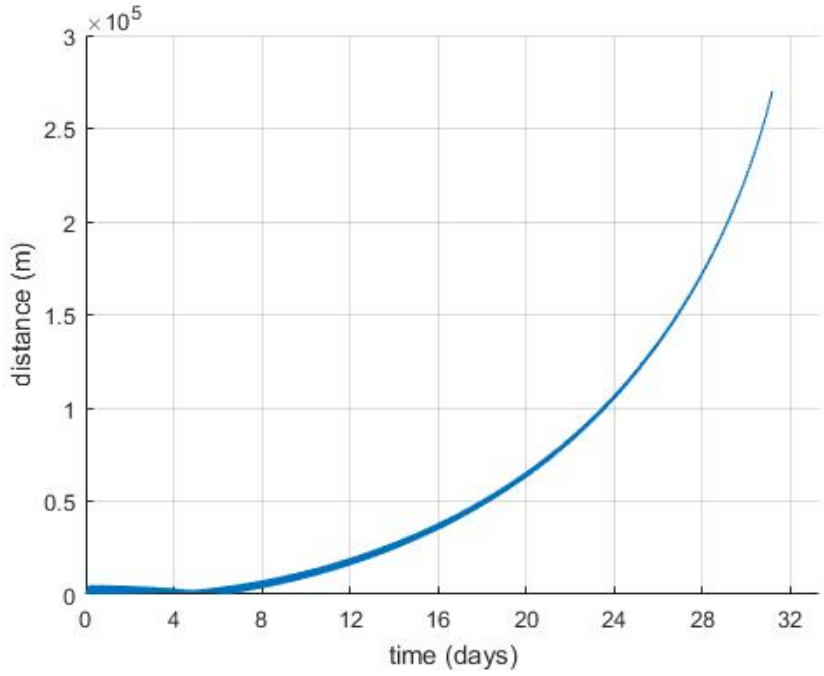

Figure 45: Minimum Distance Between Any Two Satellites (Lifetime) (Alt = 300 km – Inc = 30° - Offset = 45° - SV = 1 m/s)

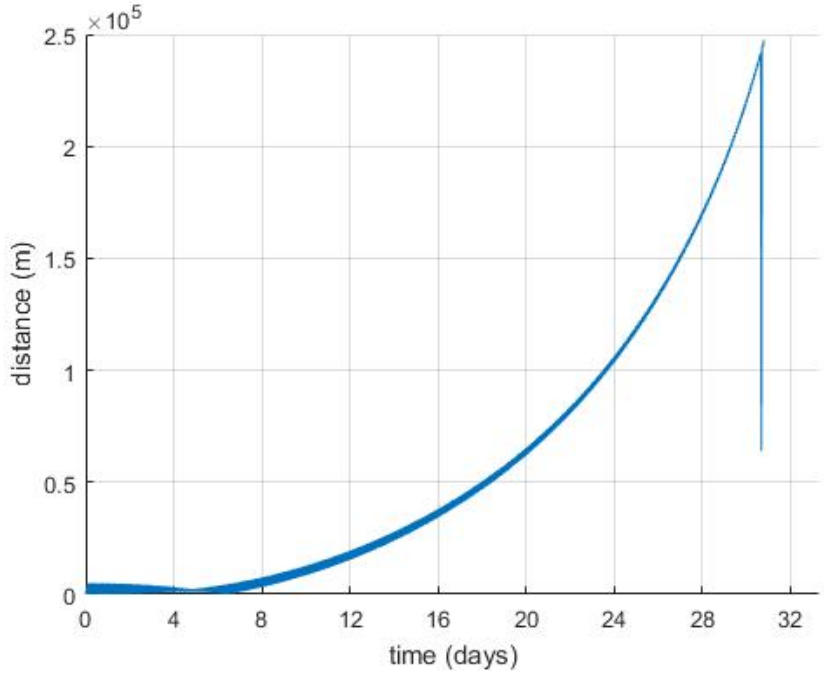

Figure 46: Minimum Distance Between Any Two Satellites (Lifetime) (Alt = 300 km – Inc = 30° - Offset = 90° - SV = 1 m/s)

4.2.2 Sun Synchronous Orbits

The control orbit used to create Figure 47 through Figure 55 is a circular sun synchronous orbit with an altitude of 300 km, an inclination of 96.7425°, an argument of latitude of 0°, and a separation velocity of 1 m/s. The eight deployed satellites are deployed into a plane normal to the velocity vector of the control satellite (offset = 0°).

Similar to Figure 20, Figure 47 shows that deploying satellites in the plane normal to the velocity vector of the control satellite does not promote growth within the cluster over the first 24 hours after deployment. There are multiple instances where the deployed satellites return to within a close proximity to the control satellite, simultaneously, which raises concerns of the possibility that conjunctions may occur within the cluster.

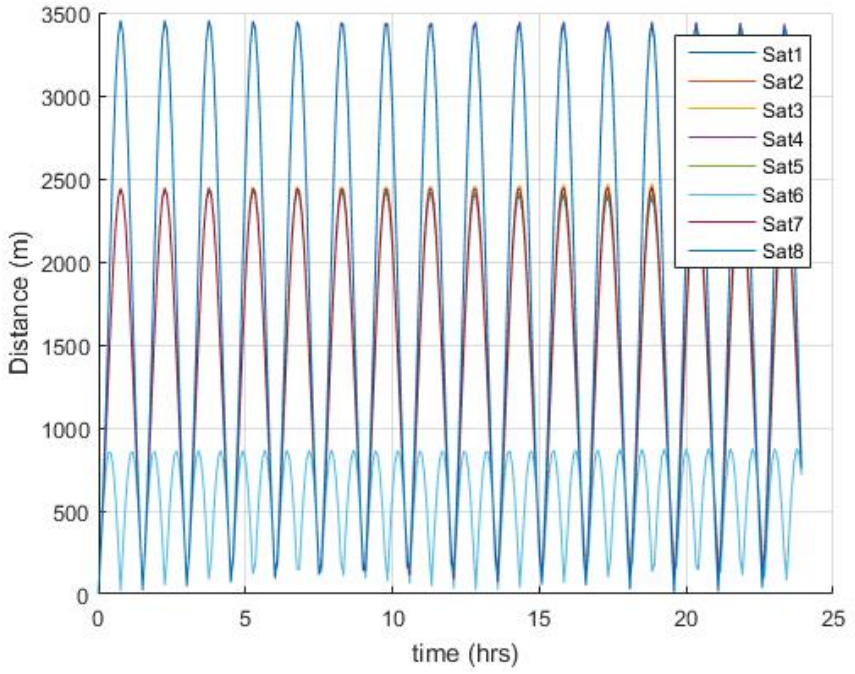

Figure 47: Distance from Control Satellite to Deployed Satellites (1 Day) (Alt = 300 km – Inc = 96.7425° - Offset = 0° - SV = 1 m/s)

Figure 48 displays the maximum distance between any two satellites within the cluster over the first 24 hours after deployment. Figure 48 reinforces the findings gleaned from the analysis of Figure 47, showing that once every orbital period the maximum distance between any two satellites is under 500 m, which means that all of the other distances within the cluster are smaller during that instance in time.

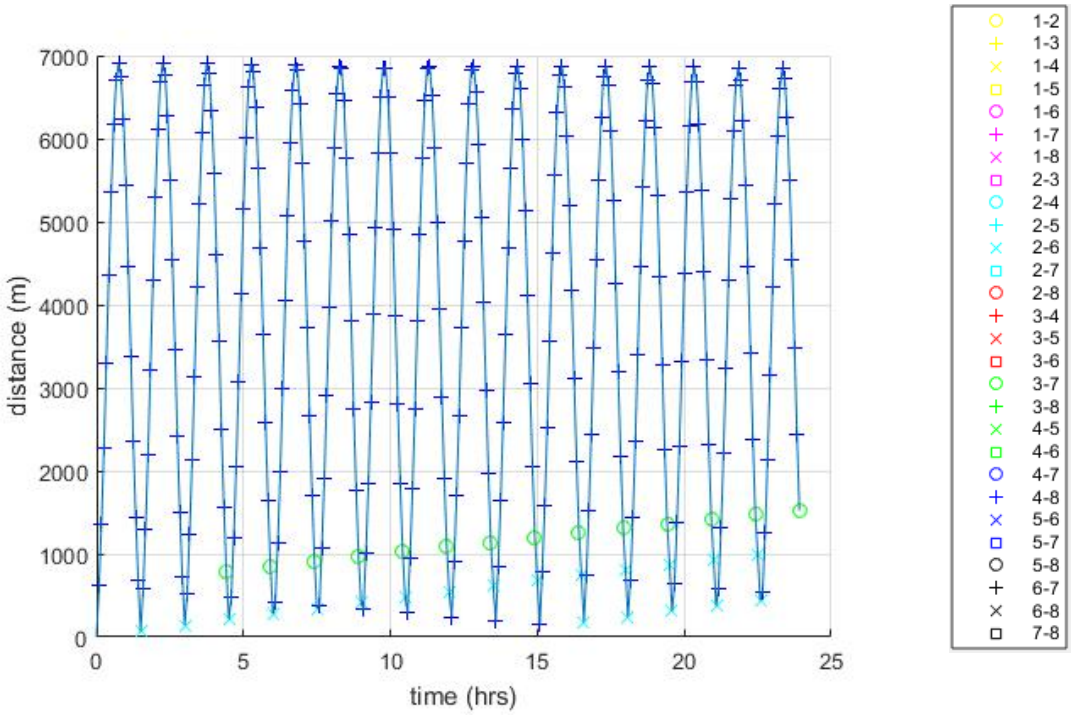

Figure 48: Maximum Distance Between Any Two Satellites (1 Day) (Alt = 300 km – Inc = 97.7425° - Offset = 0° - SV = 1 m/s)

Figure 49 is a plot of the minimum distance between any two satellites within the cluster for the first 24 hours after deployment. Figure 49 shows that, during the first 24 hours, at least 6 different pairs of satellites are within 300 m of one another. That is significant because, from Table 5, 300 m is around the observational accuracy of a low accuracy (low precision radar) satellite position measurement device, which means the

tracking and identification of the individual satellites within the cluster is difficult over the first 24 hours.

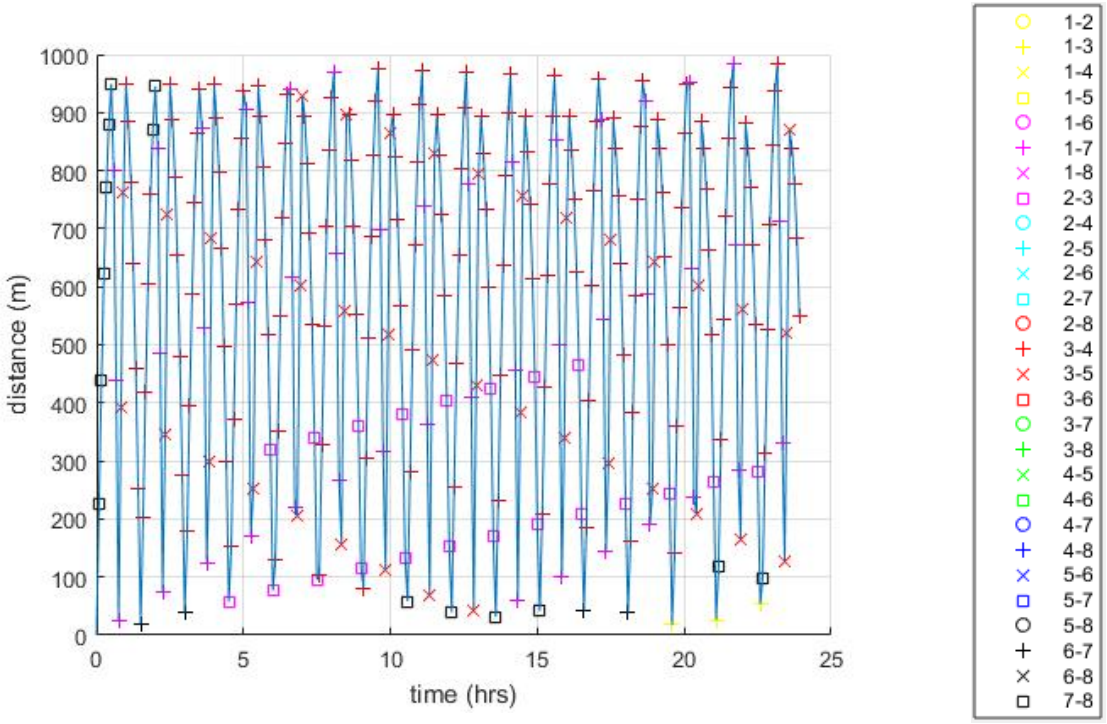

Figure 49: Minimum Distance Between Any Two Satellites (1 Day) (Alt = 300 km – Inc = 97.7425° - Offset = 0° - SV = 1 m/s)

Figure 50 is a continuation of Figure 47, showing the distance from the control satellite to the eight deployed satellites over the first week after deployment. Again, it is noticeable that this deployment scheme does not spread the satellites out from one another.

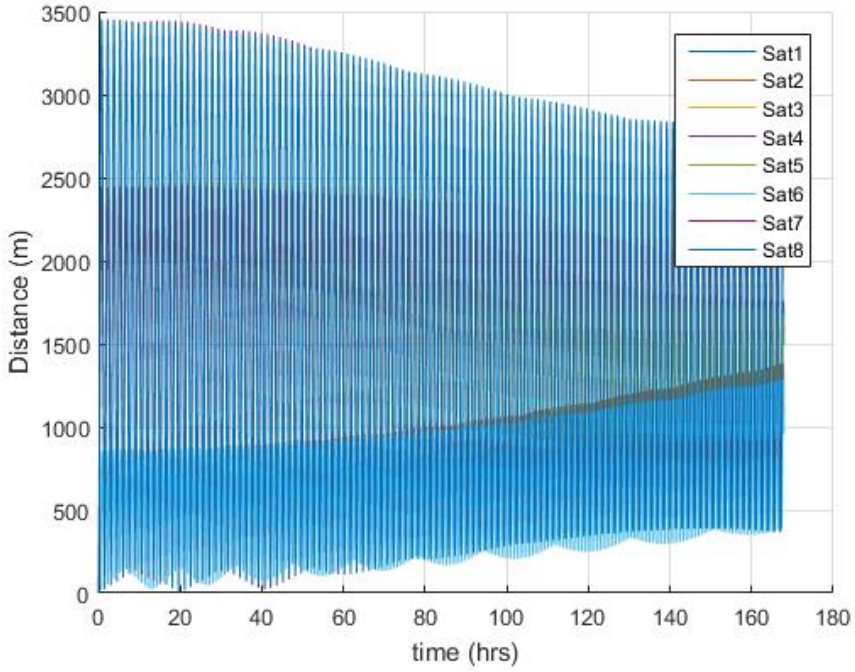

Figure 50: Distance from Control Satellite to Deployed Satellites (1 Week) (Alt = 300 km – Inc = 96.7425° - Offset = 0° - SV = 1 m/s)

Figure 51 displays the maximum distance within the cluster over the first week after deployment. It is observed that the peak maximum distance between any two satellites within the constellation actually decreases during the first week, while the local minima experienced over an orbital period increase over the first week. The decreasing peaks indicate that the points of farthest displacement of satellite 4 and satellite 8, which travel the farthest apart from one another per orbit initially, are moving toward one another. While the rising local minima indicate that the point in which the orbits of the deployed satellites cross the control orbit becoming different for each individual satellite.

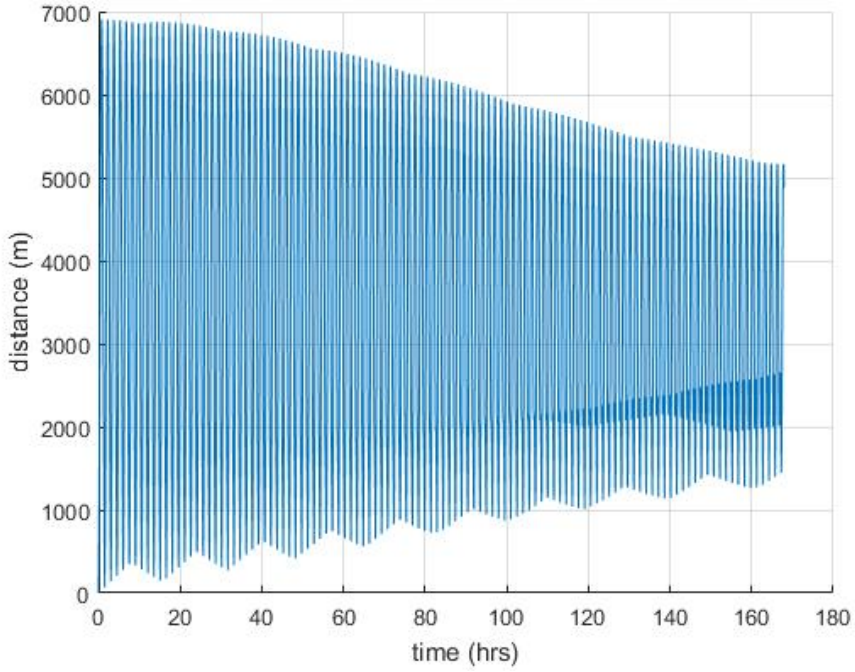

Figure 51: Maximum Distance Between Any Two Satellites (1 Week) (Alt = 300 km – Inc = 96.7425° - Offset = 0° - SV = 1 m/s)

Figure 52 shows the minimum distance between any two satellites within the deployed cluster over the first week after deployment. While the local minima of this plot increase over the first week, at no point in time is every satellite within the cluster over 300 m apart from one another. This indicates that the tracking and identification difficulties present over the first 24 hours may not alleviate themselves over the first week.

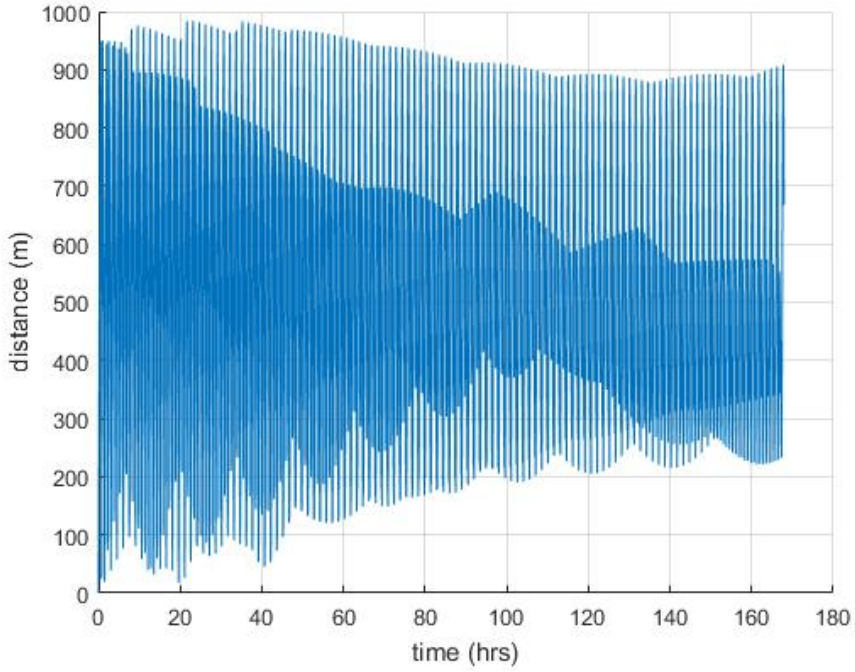

Figure 52: Minimum Distance Between Any Two Satellites (1 Week) (Alt = 300 km – Inc = 96.7425° - Offset = 0° - SV = 1 m/s)

It is in Figure 53 and Figure 54 that the separation of the cluster of satellites is displayed. The increasing slope observed in Figure 53 and Figure 54 is caused by air drag, coupled with the small differences in the orbit from the different directions in which the eight satellites where deployed, causing slight differences in the semi-major axis of the individual satellites. This difference leads to slightly different periods for the satellites, which cause the satellites to separate along the orbit with respect to one another.

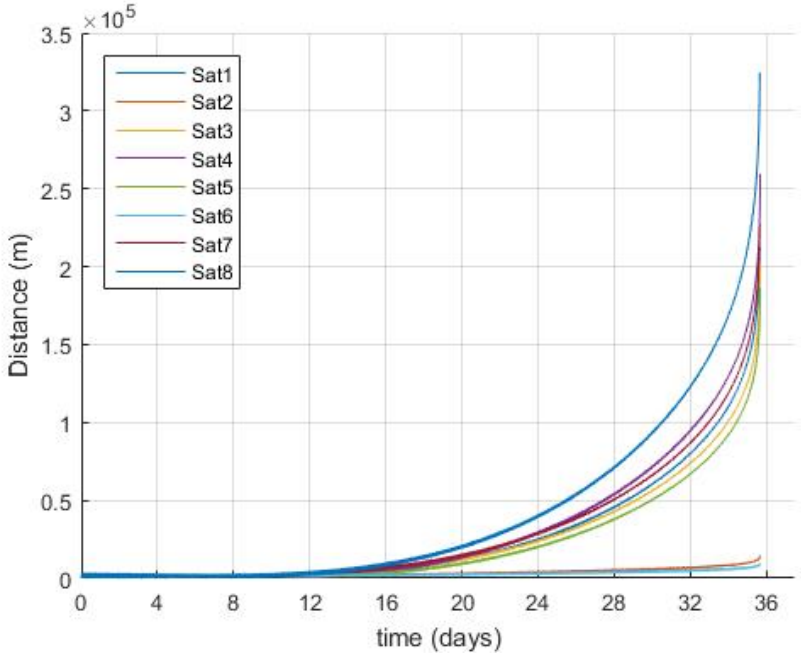

Figure 53: Distance from Control Satellite to Deployed Satellites (Lifetime) (Alt = 300 km – Inc = 96.7425° - Offset = 0° - SV = 1 m/s)

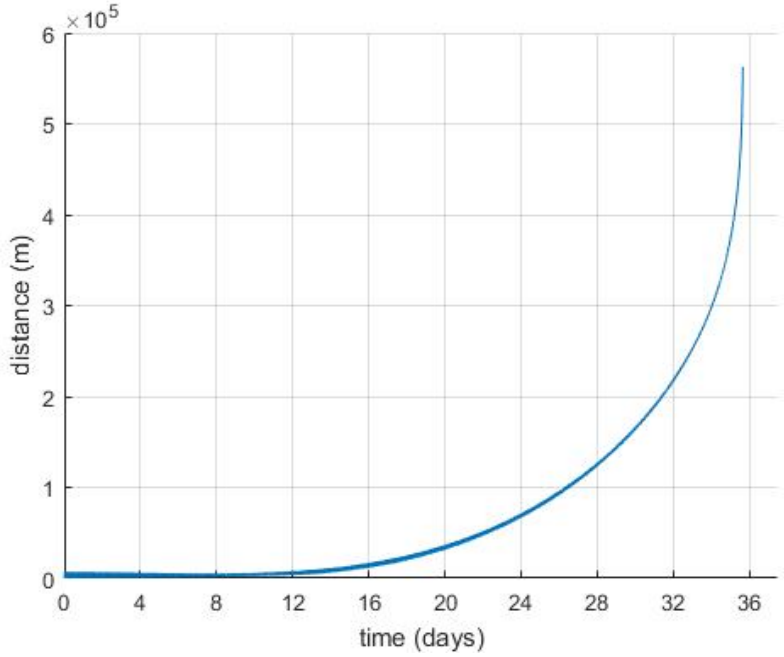

Figure 54: Maximum Distance Between Any Two Satellites (Lifetime) (Alt = 300 km – Inc = 96.7425° - Offset = 0° - SV = 1 m/s)

Figure 55 is a continuation of Figure 52. The behavior shown in the plot is highly periodic. This periodic behavior, combined with the small magnitude of the minimum distance compared to the amplitude of the periodic motion, leads to the behavior shown in Figure 55. One takeaway from Figure 55 is that it may take a few weeks to properly track and identify all of the satellites deployed in a cluster depending on the deployment pattern.

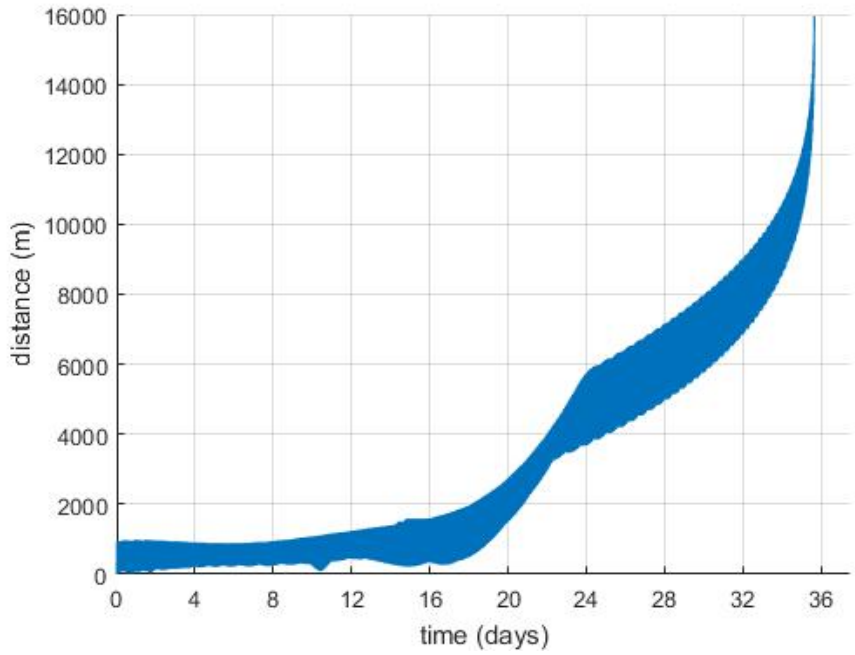

Figure 55: Minimum Distance Between Any Two Satellites (Lifetime) (Alt = 300 km – Inc = 96.7425° - Offset = 0° - SV = 1 m/s)

4.2.3 Molniya Orbits

The control orbit used to create Figure 56 through Figure 64 is a Molniya orbit with a perigee altitude of 300 km, an apogee altitude of 40,050 km, an inclination of 63.3212°, an argument of perigee of 270°, a true anomaly of 0°, and a separation velocity of 1 m/s. The eight satellites are deployed into a plane normal to the velocity vector of the control satellite (offset = 0°).

Figure 56 shows the effect of the much longer orbital period on how much the satellites spread out over the orbit. While the separation velocity and offset of the deployment plane are the same as presented in the analysis of satellites deployed in LEO, the satellites have a much longer time for the separation velocity to take them away from the initial orbit before they return to the initial point of departure.

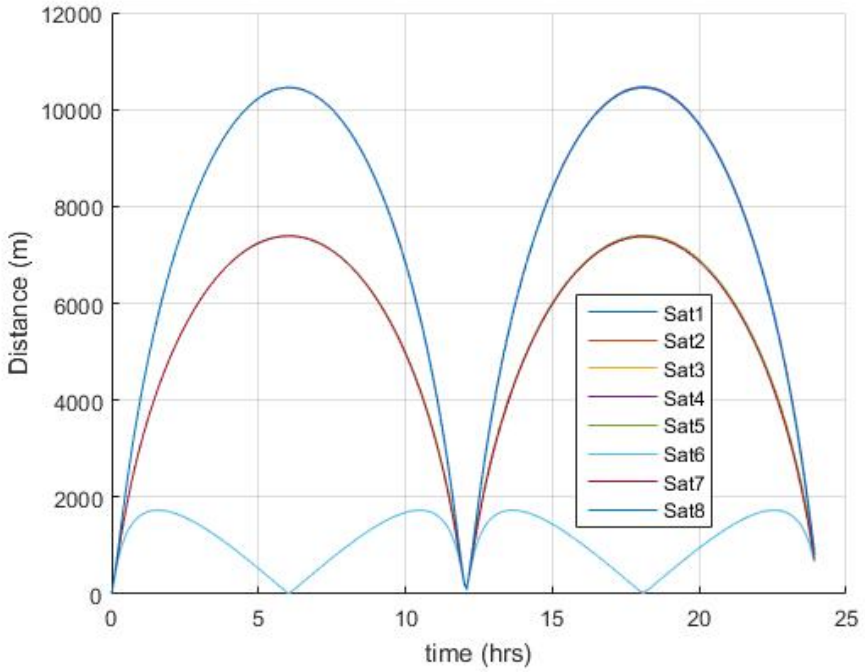

Figure 56: Distance from Control Satellite to Deployed Satellites (1 Day) (Perigee/Apogee) Alt = 300/40,050 km – Inc = 63.3212° - Offset = 0° - SV = 1 m/s)

From Figure 57 it is evident that satellite 4 and satellite 8 are the primary pair dictating the maximum distance between two satellites deployed over the first 24 hours. While the maximum distance within the cluster is large for the majority of the orbit, there is still a concern about conjunctions due to the cluster coming back together after an orbital period.

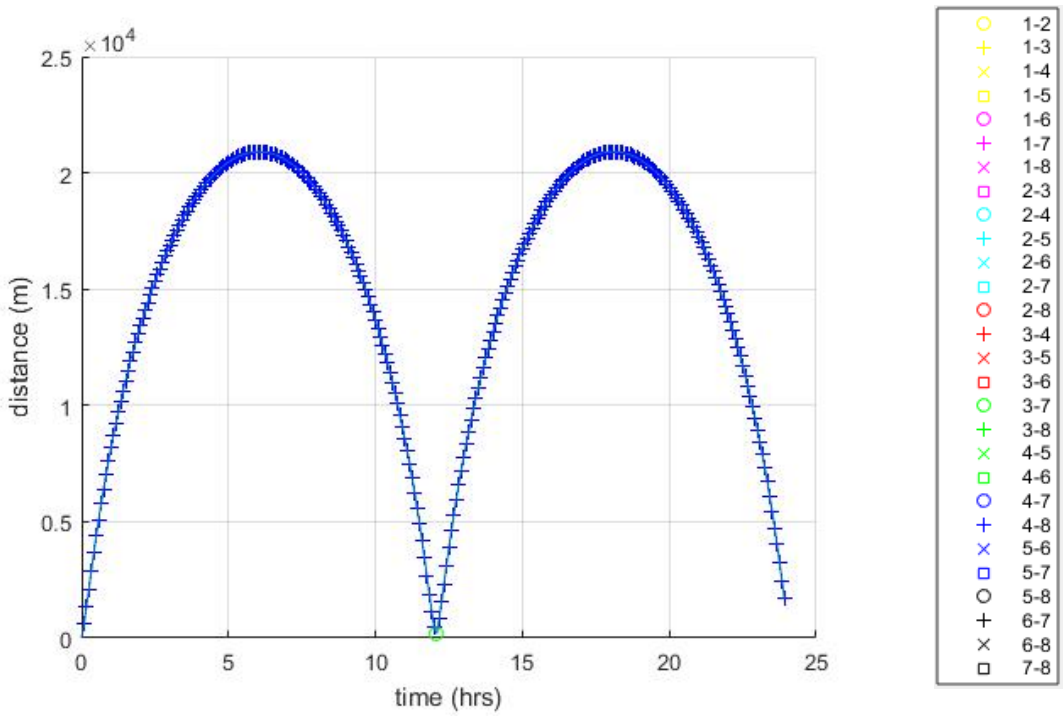

Figure 57: Maximum Distance Between Any Two Satellites (1 Day) (Perigee/Apogee) Alt = 300/40,050 km – Inc = 63.3212° - Offset = 0° - SV = 1 m/s)

Figure 58 is an interesting plot as it shows that, over the majority of the orbit, the minimum distance between any two satellites within the deployed cluster, over the first 24 hours after deployment, is well above 400 m. Note that while a limit of 300 m has been used as the limit for when the tracking and identification of the individual satellites may be difficult for satellites deployed in LEO, the increased altitude of apogee in the Molniya orbit corresponds to a decrease in the accuracy of the low precision radar measurement device used to observe a satellite position.[20] Since the minimum distance is well above 400 m for the majority of the orbit, there should be minimal difficulties with the initial tracking and identification of the individual satellites in the cluster.

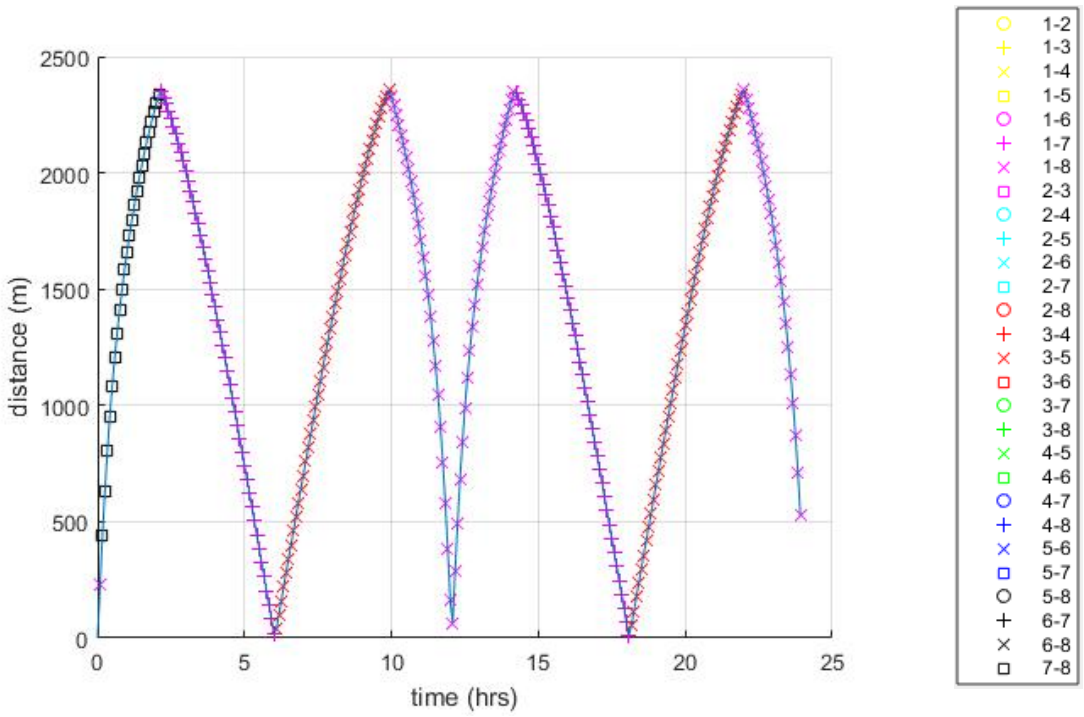

Figure 58: Minimum Distance Between Any Two Satellites (1 Day) (Perigee/Apogee) Alt = 300/40,050 km – Inc = 63.3212° - Offset = 0° - SV = 1 m/s)

Figure 59 through Figure 61 are continuations of the previous three figures. They show the behavior of the cluster over the first month after deployment. From Figure 59 through Figure 61, it is evident that the behavior of the cluster does not change a lot over the first month after deployment. This fact can be used by an operator to design an initial deployment strategy, knowing that the behavior that results from the deployment are maintained for an extended period of time.

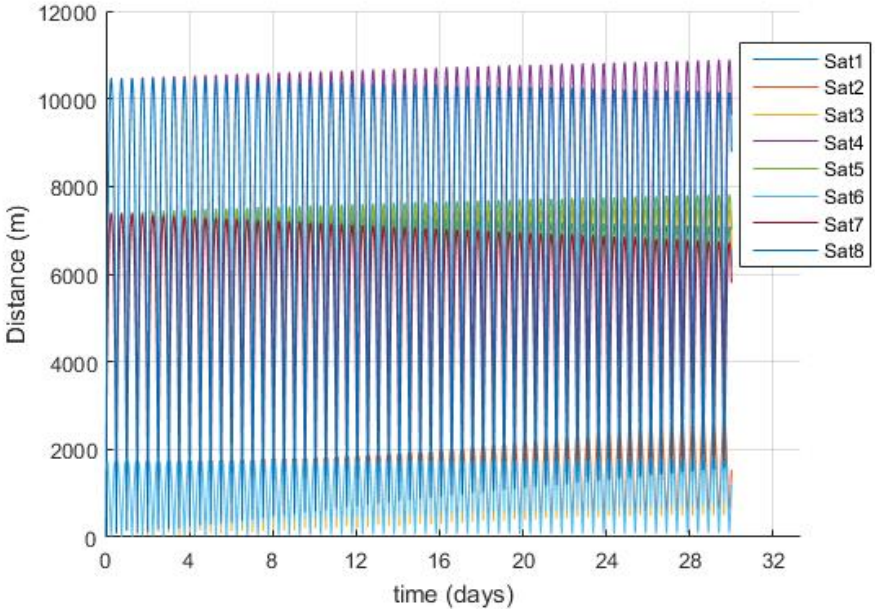

Figure 59: Distance from Control Satellite to Deployed Satellites (1 Month) (Perigee/Apogee) Alt = 300/40,050 km – Inc = 63.3212° - Offset = 0° - SV = 1 m/s)

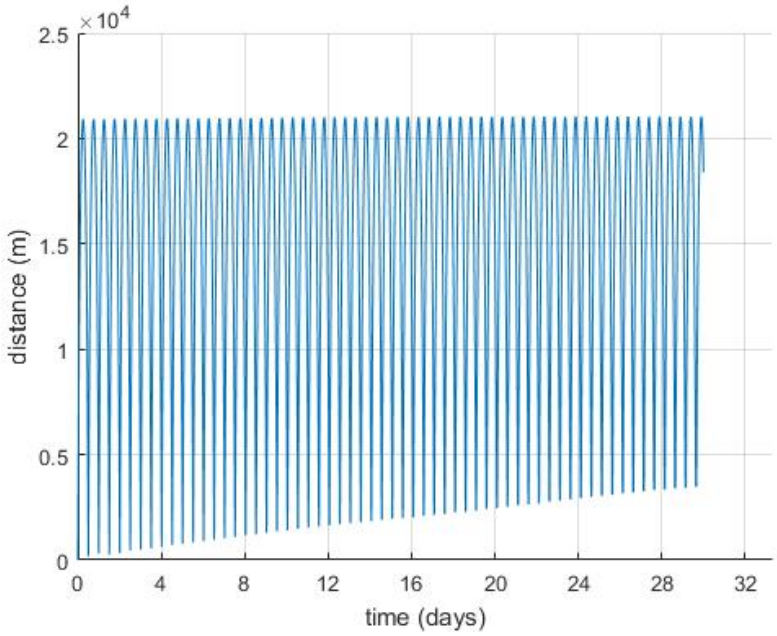

Figure 60: Maximum Distance Between Any Two Satellites (1 Month) (Perigee/Apogee) Alt = 300/40,050 km – Inc = 63.3212° - Offset = 0° - SV = 1 m/s)

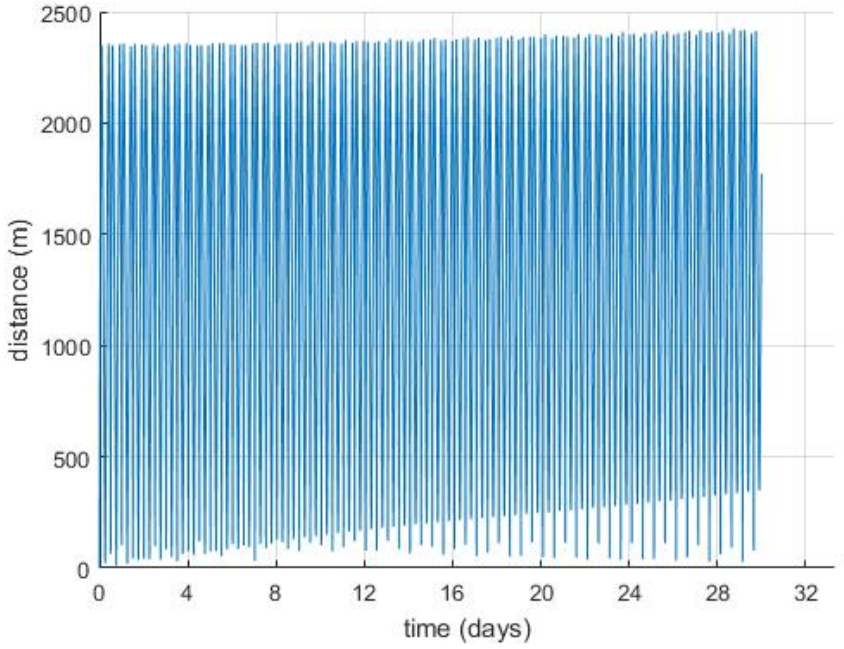

Figure 61: Minimum Distance Between Any Two Satellites (1 Month) (Perigee/Apogee) Alt = 300/40,050 km – Inc = 63.3212° - Offset = 0° - SV = 1 m/s)

The principal takeaway from Figure 62 through Figure 64 is the increased lifetime of a cluster deployed into a 300 x 40,050 km Molniya orbit in comparison to a 300 x 300 circular orbit. While the lifetime of the circular orbit in LEO is about 1 month, the lifetime of the 300 x 40,050 Molniya orbit is 32 months. From the three figures, it is also evident that while the lifetime of the cluster is 32 months, the various distances between the satellites deployed in the Molniya orbit start to vary greatly with respect to one another after 2 years on orbit. If the cluster is meant to operate with each other to accomplish a specific mission, this behavior will need to be taken into account.

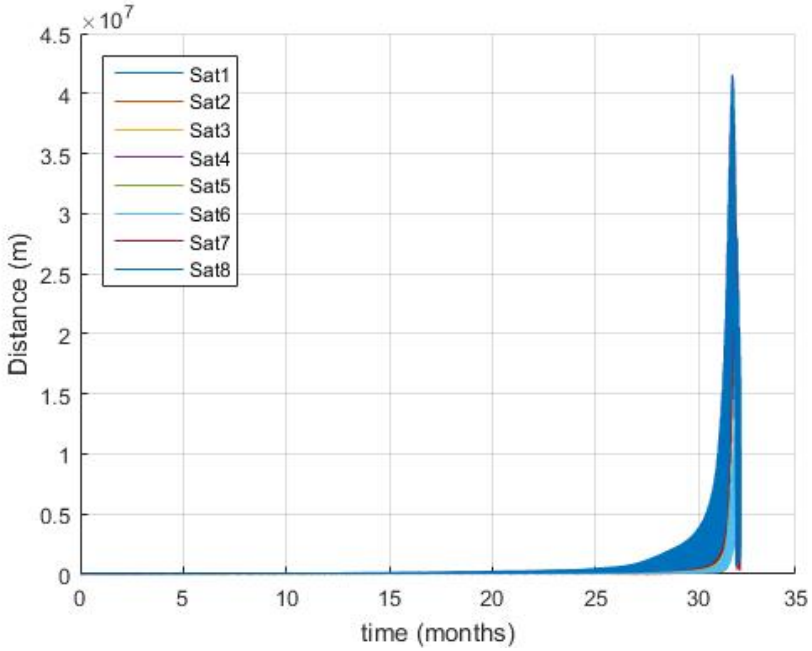

Figure 62: Distance from Control Satellite to Deployed Satellites (Lifetime) (Perigee/Apogee) Alt = 300/40,050 km – Inc = 63.3212° - Offset = 0° - SV = 1 m/s)

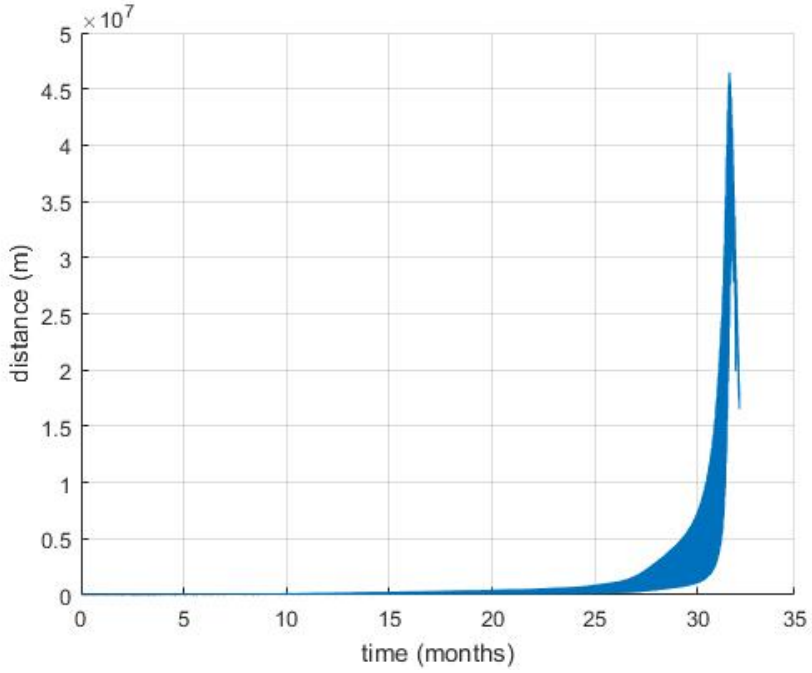

Figure 63: Maximum Distance Between Any Two Satellites (Lifetime) (Perigee/Apogee) Alt = 300/40,050 km – Inc = 63.3212° - Offset = 0° - SV = 1 m/s)

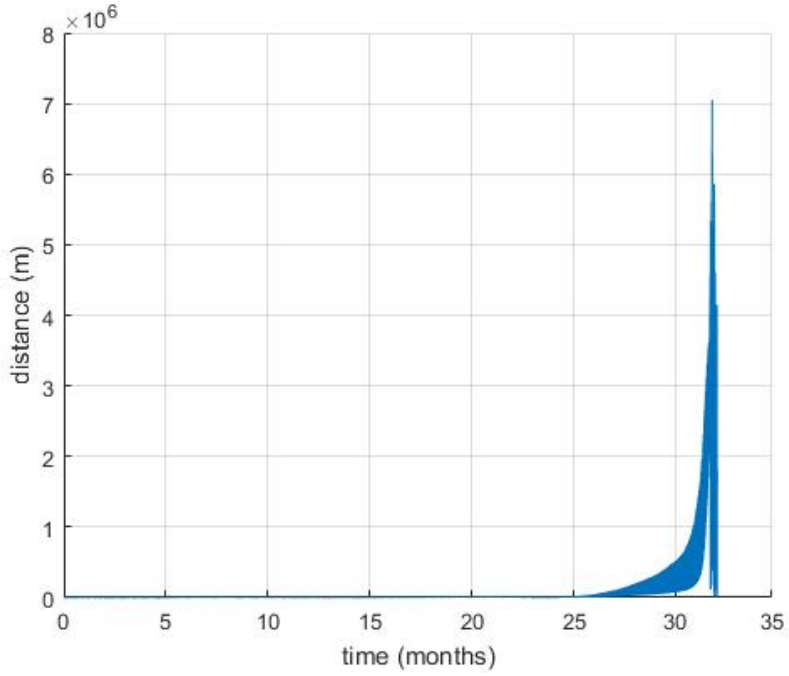

Figure 64: Minimum Distance Between Any Two Satellites (Lifetime) (Perigee/Apogee) Alt = 300/40,050 km – Inc = 63.3212° - Offset = 0° - SV = 1 m/s)

4.3 Altitude Trends

To conduct the altitude trend analysis, the data is parsed into eight sets. For all of the sets, the inclination, RAAN, and argument of latitude are set to 30°, 0°, and 0° respectively. The data is then separated into the eight sets to compare tests cases with the same separation velocity (1 m/s or 2 m/s) and dispersal plane offset (0°, 45°, 90°, or 135°) for circular orbits with altitudes of 300 km, 400 km, 500 km, 750 km, and 1,000 km.

4.3.1 Altitude Maximum Volume Trends

Figure 65 through Figure 67 show how the maximum volume of a constellation varies with altitude for when the separation velocity is equal to 1 m/s and all eight satellites are ejected into a plane normal to the velocity vector (0° offset). This dispersal

pattern produces the smallest overall maximum volume. This is because the separation velocity imparted to the individual satellites has no component in the direction of the velocity vector of the control satellite. This means that the dispersal along the orbit path is due to aerodynamic drag and the subsequent change in semi-major axis. Aerodynamic drag will lower the altitude of the individual satellites, but at independent rates, which will give each of them slightly different orbital periods.

During the investigation, it is found that observing how the maximum volume of a constellation grew over the first day, with respect to altitude, is a convenient and quick way to check the data for test cases that may not have been simulated properly. From the start of the plot shown in Figure 65 it can be seen that, from smallest to largest, the order of maximum volume goes in ascending order according to altitude. This is because satellites in the constellation have periodic motion with respect to one another. The satellites at a higher altitude have a longer period, which, for the same separation velocity, allows for satellites to travel further away from the reference orbit before their periodic motion will bring them back closer to the reference orbit. Figure 65 also clearly shows the maximum volume for orbits at 300 km growing faster than for orbits at higher altitudes. This is due to the effects of aerodynamic drag mentioned above.

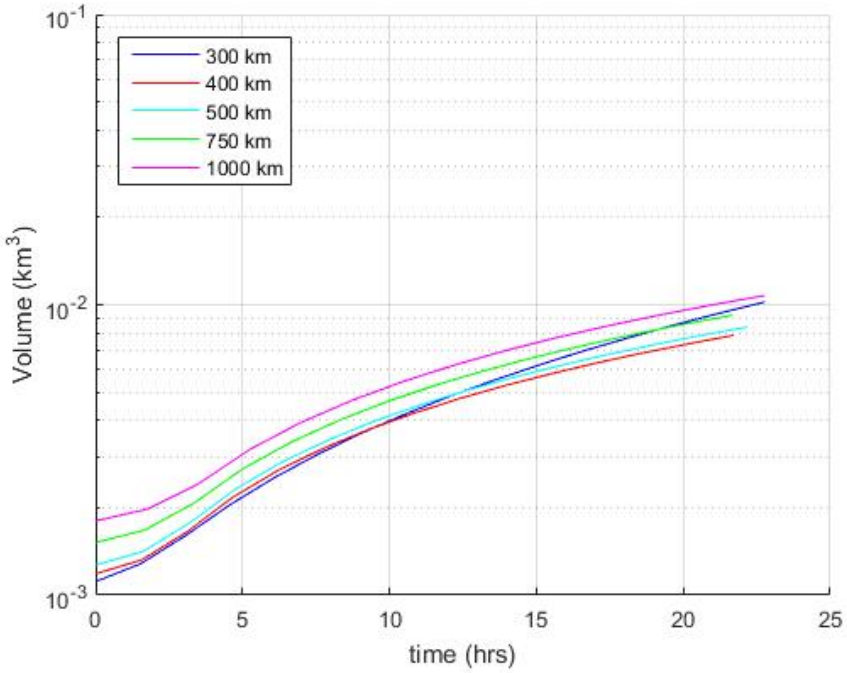

Figure 65: Maximum Volume Enclosing Constellation (1 Day) (SV = 1 m/s & Offset = 0°) (Altitude Comparison)

Figure 66 shows the maximum volume of a constellation with a separation velocity of 1 m/s and an offset of 0° for the first month after separation. The trend observed in Figure 65 continues with the maximum volume of orbits at 300 km quickly surpassing the maximum volume for constellations at the other included altitudes. Similarly, over the first two weeks, the maximum volume for 400 km also starts to grow much quicker than the maximum volume for higher altitudes. This is because the constellation at 400 km is affected by drag, similar to the constellation at 300 km, though to a lesser extent.

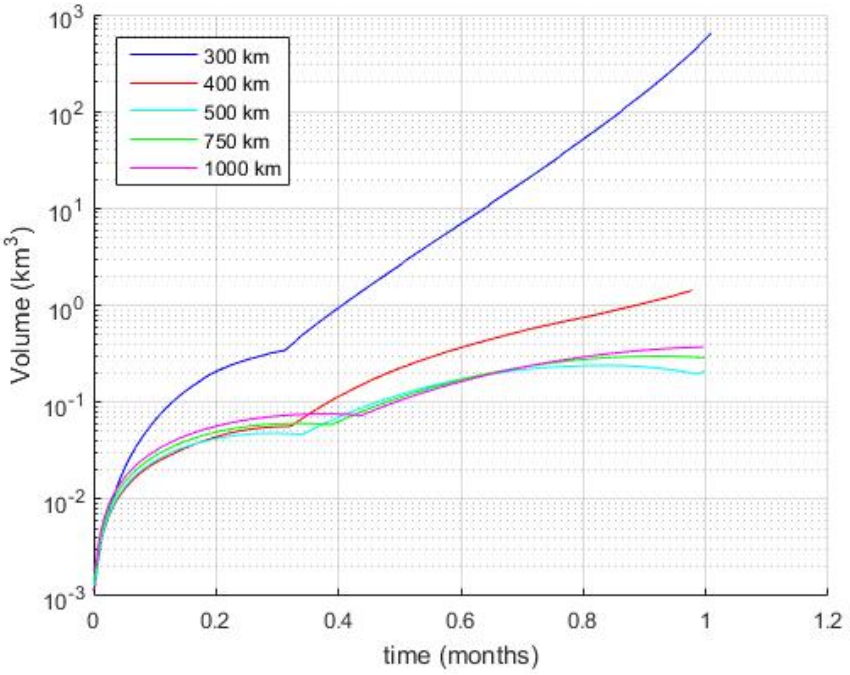

Figure 66: Maximum Volume Enclosing Constellation (1 Month) (SV = 1 m/s & Offset = 0°) (Altitude Comparison)

Figure 67 is a plot of the maximum volume of the constellation over 3 years. The plots for 300 and 400 km terminate once the first satellite in the constellation re-enters Earth's atmosphere. Though it is not readily apparent as it is for other dispersal patterns, the fact that the plots for maximum volume are continuously growing for all altitudes means that the satellites in these constellations never fully populate the orbit plane.

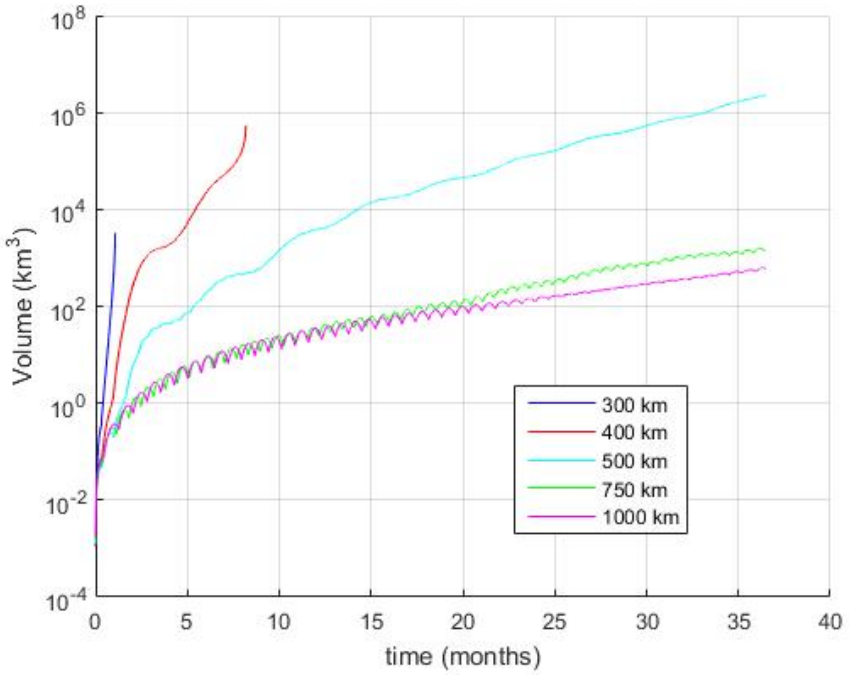

Figure 67: Maximum Volume Enclosing Constellation (Lifetime) (SV = 1 m/s & Offset = 0°) (Altitude Comparison)

To properly compare how the maximum volume of a constellation varies with altitude, an analysis similar to the one explained above is also conducted for a dispersal pattern with a separation velocity of 1 m/s and an offset of 45°. Figure 68 through Figure 70 show how the maximum volume varies with respect to altitude for this dispersal pattern for 1 day, 1 month, and 3 years, respectively.

Figure 68 shows the same starting pattern as Figure 65, though the maximum volume of the constellations at lower altitudes does not initially overtake the maximum volume of the constellations at higher altitudes. This is caused by the component of the separation velocity that can be projected onto the control satellite's velocity vector. This component will create an apogee or perigee point, depending on the direction of the separation velocity, which will change the orbital period of the satellites within the constellation. This will result in the satellites spreading out along the orbit path. This

motion is the dominant factor affecting the maximum volume of the constellation, which is why, though still present, the greater effect of aerodynamic drag is not readily observable over the same time period for deployment parameters of 1 m/s and 0° for separation velocity and deployment plane offset.

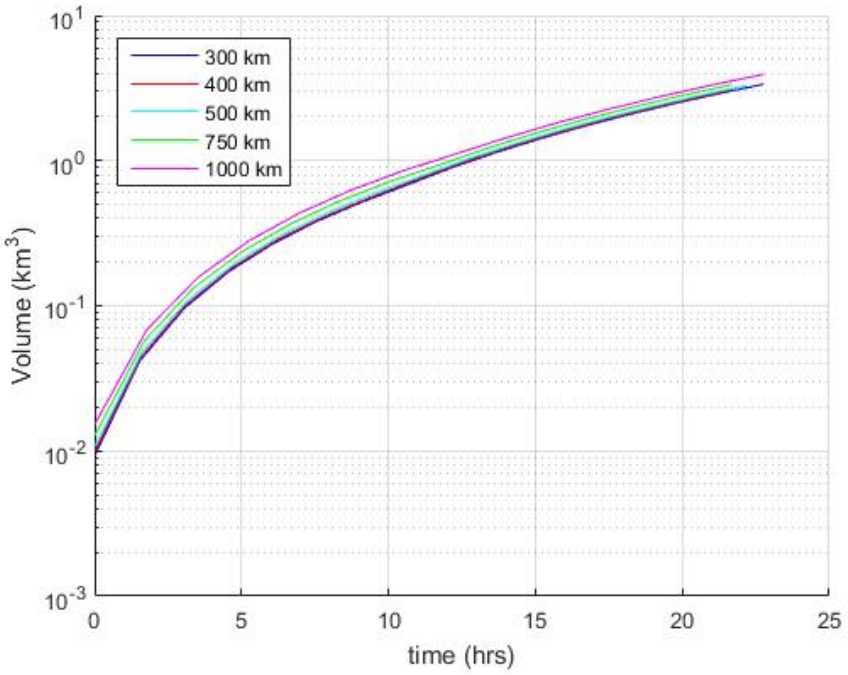

Figure 68: Maximum Volume Enclosing Constellation (1 Day) (SV = 1 m/s & Offset = 45°) (Altitude Comparison)

In Figure 69 the increased aerodynamic drag present at 300 km and 400 km can be seen as it acts on the constellation by the fact that the volumes of the constellations at those two altitudes grow more quickly when compared to the constellations at higher altitudes.

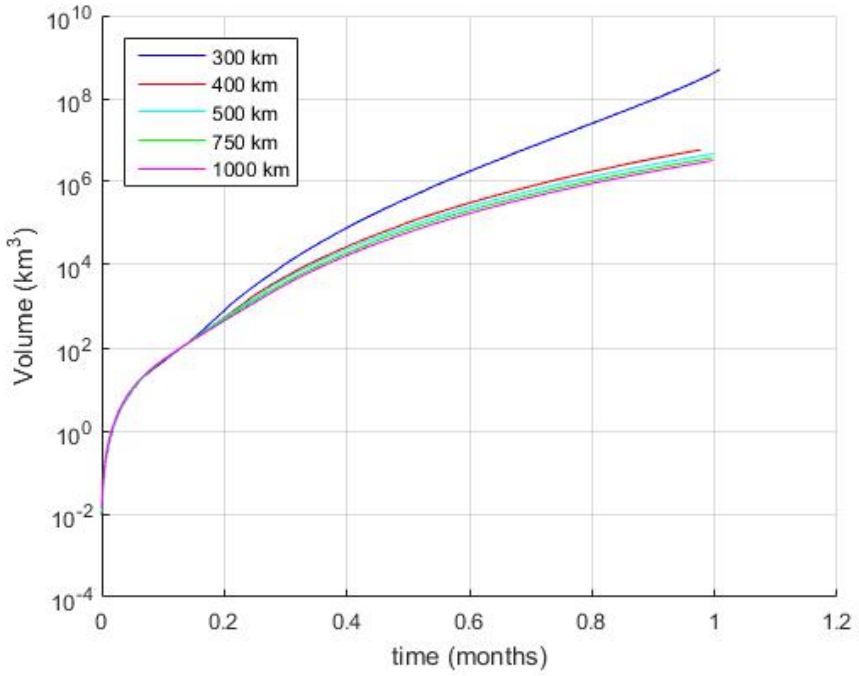

Figure 69: Maximum Volume Enclosing Constellation (1 Month) (SV = 1 m/s & Offset = 45°) (Altitude Comparison)

Figure 70 displays the maximum volume of constellations deployed with an offset of 45° and a separation velocity of 1 m/s for the constellation's lifetime, or the first 3 years, whichever is shorter. The plots for 300 km and 400 km both end short of the 3-year limit because the constellations at those altitudes reenter the atmosphere shortly after 1 month for the 300 km case, and about 8 months for the 400 km case. While the constellation at 300 km did not last long enough to fully populate the orbit, the other four altitudes are able to, which can be seen by the leveling off of the maximum volume plots. The downward dips observed after the plot of the maximum volume levels off occur when part of the orbit is not populated by the constellation, which can be more clearly seen later in Figure 76.

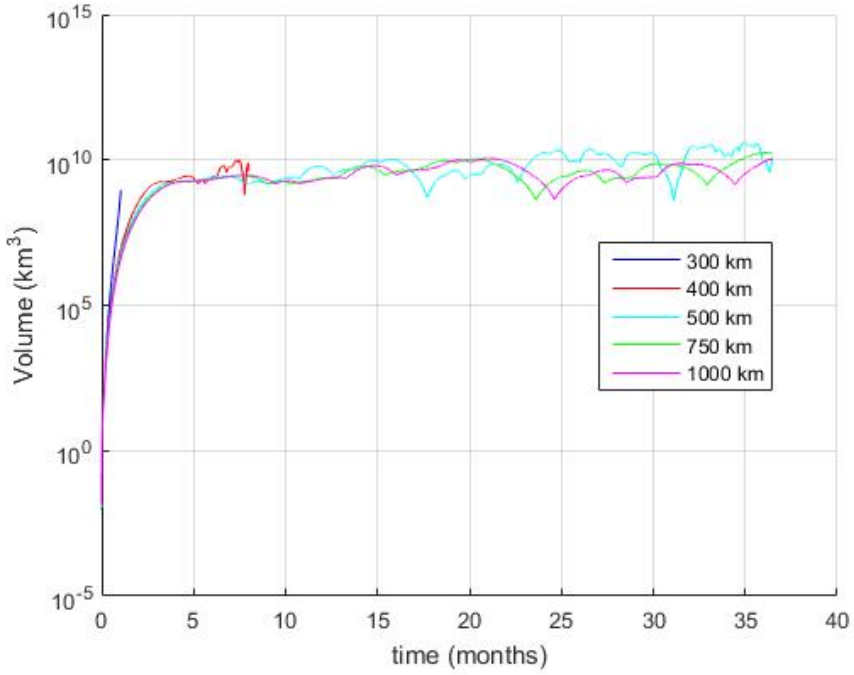

Figure 70: Maximum Volume Enclosing Constellation (Lifetime) (SV = 1 m/s & Offset = 45°) (Altitude Comparison)

4.3.2 Altitude Maximum Distance Trends

Figure 71 shows, for a deployment plane with a normal vector in the same direction as the velocity vector of the control satellite, the potential difficulties involving conjunctions within, the tracking and identification of, and communication with individual satellites within the constellation are present for all the altitudes tested between 300 km and 1,000 km. At least once per orbit, for all tested altitudes, the maximum distance between any two satellites in the constellation is below 500 m for the first 24 hours after deployment. If the largest separation is 500 m, that means, over that specific time period, every other satellite pair in the constellation is at most 500 m apart, which represents a very compact constellation.

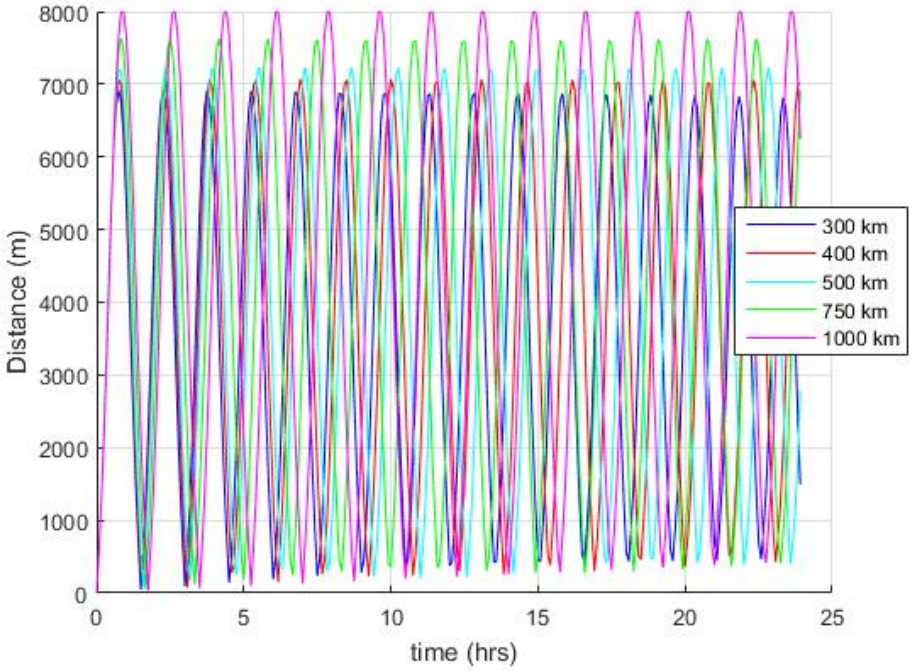

Figure 71: Maximum Distance Between Any Two Satellites (1 Day) (SV = 1 m/s & Offset = 0°) (Altitude Comparison)

Figure 72 confirms previous insights from the analysis of the maximum volume trends, showing the maximum distance for the constellations at 300 km and 400 km growing quicker that those at higher altitudes. From this plot, it is also clearly noticeable that the rate at which the maximum distance plot increases grows faster over time as the altitude of the constellation decreases. This effect is being caused by the increased atmospheric drag and its greater effect on decreasing the semi-major axis of the individual satellites.

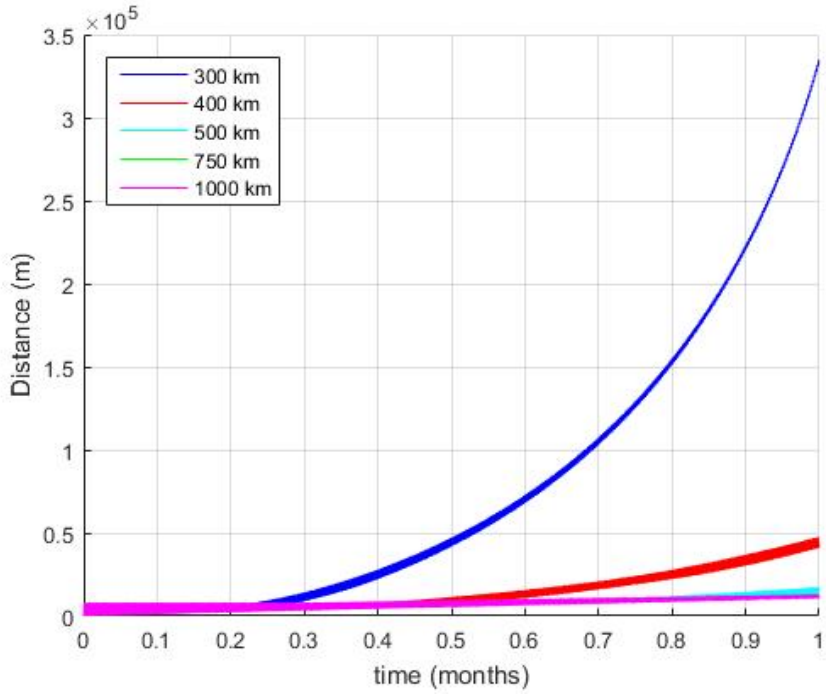

Figure 72: Maximum Distance Between Any Two Satellites (1 Month) (SV = 1 m/s & Offset = 0°) (Altitude Comparison)

The plot, over the first 3 years, of maximum distance between any two satellites in the constellation when the offset of the deployment plane is 0°, illustrated in Figure 73, is an interesting plot. Due to the lack of phasing caused by the initial deployment, other forces affecting the satellites can be observed. The overall trend, with respect to altitude, is that the lower the satellite is, the more quickly the maximum distance increases. A second observation is that, although constellations at low altitudes spread out more quickly, the longer lifetime of the constellations at higher altitudes will eventually allow them to achieve a higher maximum distance between a satellite pair.

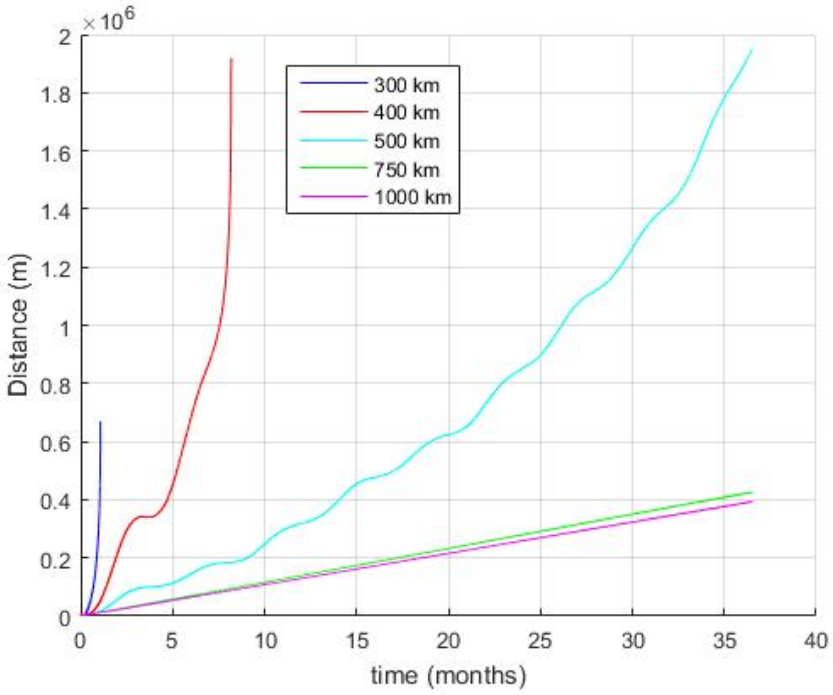

Figure 73: Maximum Distance Between Any Two Satellites (Lifetime) (SV = 1 m/s & Offset = 0°) (Altitude Comparison)

Figure 74 and Figure 75 displays the behavior of the maximum distance within the constellation when the offset of the deployment plane is equal to 45°. Similar to Figure 68, Figure 74 does not show much difference over the first day because this measurement is dominated by the relative phasing of the satellites within the constellation. Figure 75 does show the maximum distance within the constellation growing quicker for 300 km and 400 km, which is the expected behavior from the analysis of the maximum volume. In the constellation deployed at 300 km, a satellite pair does end up on opposite sides of the orbit after 28 days, indicated by the peak occurring at this point.

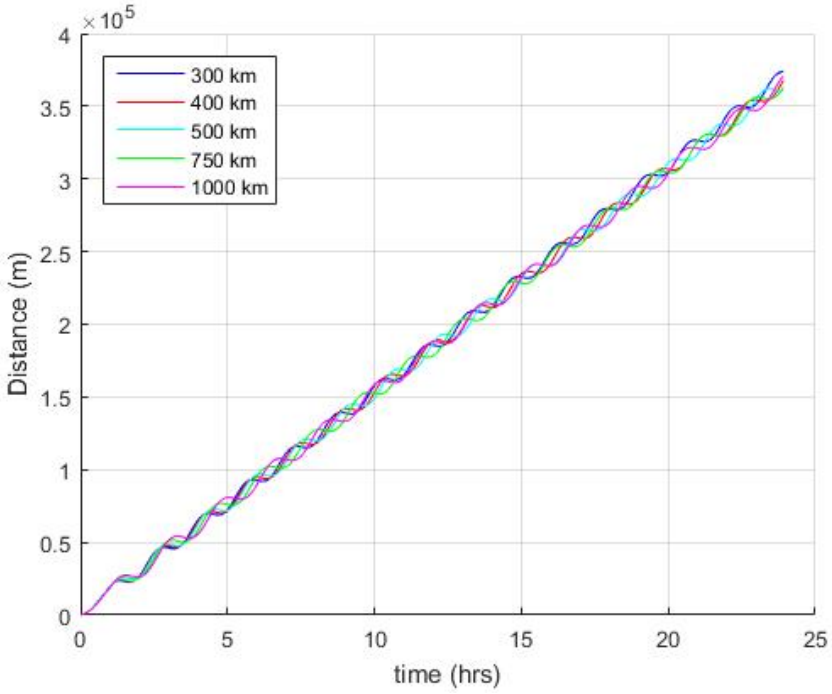

Figure 74: Maximum Distance Between Any Two Satellites (1 Day) (SV = 1 m/s & Offset = 45°) (Altitude Comparison)

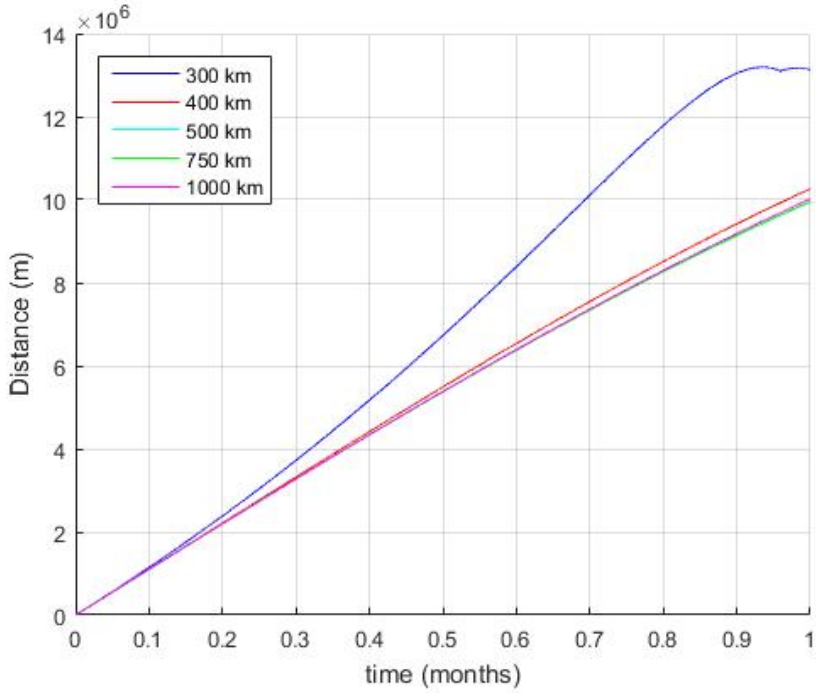

Figure 75: Maximum Distance Between Any Two Satellites (1 Month) (SV = 1 m/s & Offset = 45°) (Altitude Comparison)

Set over the same time period as Figure 70, the data displayed in Figure 76 can be linked to some of the observed behaviors. In Figure 70, the dips in the maximum volume of the constellation corresponded to potential gaps in coverage. The dips in Figure 70 coincide with the more pronounced dips in Figure 76. Once the peak of the maximum distance plot has been achieved, dips signify that no satellite pair in the constellation is on opposite sides of the orbit: the larger the dip, the larger the gap between satellites in the orbit plane. A second useful piece of information can be observed in Figure 76, and that is the altitude of the constellation. At any given point in time, for a circular orbit, the maximum distance between any two satellites on orbits that are nearly the same is when they are on opposite sides of the orbit. If the orbit is circular, this is also the diameter of the orbit the satellites are on and, as the diameter of the orbit decreases, so does the maximum possible distance between any two satellites that are on that orbit. The 500 km initial deployment altitude in Figure 76 shows the diameter of the orbit decreasing as time goes on. Note that this behavior is present in all of the plots above 300 km contained within Figure 76. The 500 km case is just used to illustrate the concept.

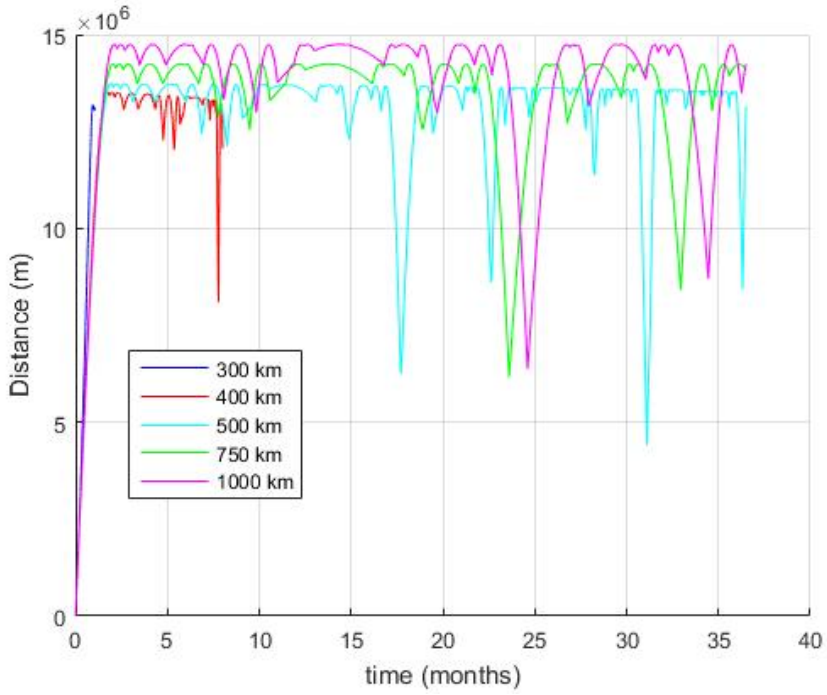

Figure 76: Maximum Distance Between Any Two Satellites (Lifetime) (SV = 1 m/s & Offset = 45°) (Altitude Comparison)

4.4 Inclination Trends

To conduct the inclination trend analysis, the data is parsed into eight sets. For all of the sets, the altitude, RAAN, and argument of latitude are set to 300 km, 0°, and 0° respectively. The data is then separated into the eight sets to compare tests cases with the same separation velocity (1 m/s or 2 m/s) and dispersal plane offset (0°, 45°, 90°, or 135°) for circular orbits with inclinations of 0°, 15°, 30°, 45°, 60°, 75°, and 90°.

4.4.1 Inclination Maximum Volume Trends

Figure 77 shows the behavior of maximum volume of a constellation of satellites with a separation velocity of 1 m/s and deployment plane offset of 0° over the lifetime of the respective constellations. Over the first two weeks, there is not a noticeable trend, but after that period in time, trends in the data start to become evident. There are two trends

in the data presented on the plots within Figure 77. One trend is that, with the exception of the orbits with inclinations of 90°, the higher the inclination, the longer the lifetime of the satellite. The second trend is the rate of increase of the maximum volume. For the inclinations below 60°, the trend is that the rate of increase of the maximum volume decreases as inclination increases. For inclinations greater than 60° the rate of increase of the maximum volume begins to increase as inclination increases, suggesting that a minimum is present near an inclination of 60°.

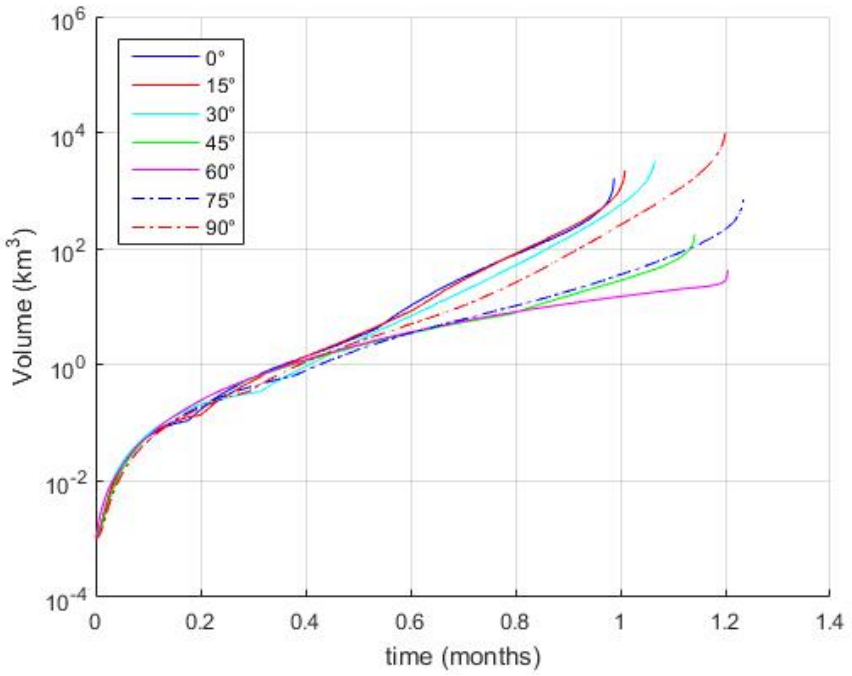

Figure 77: Maximum Volume Enclosing Constellation (Lifetime) (SV = 1 m/s & Offset = 0°) (Inclination Comparison)

Figure 78 displays the maximum volume of the constellation for a separation velocity of 1 m/s and a deployment plane offset of 45°. The general behavior is that the lower the inclination, the higher the maximum volume is of the constellation. The maximum volume of the constellation for orbits with an inclination of 0° does not follow this trend and consistently does not follow this trend with different separation velocities

and offsets. Figure 79 is comparable to Figure 78 but for a separation velocity of 2 m/s, and the maximum volume of the 0° inclination is the minimum of both plots.

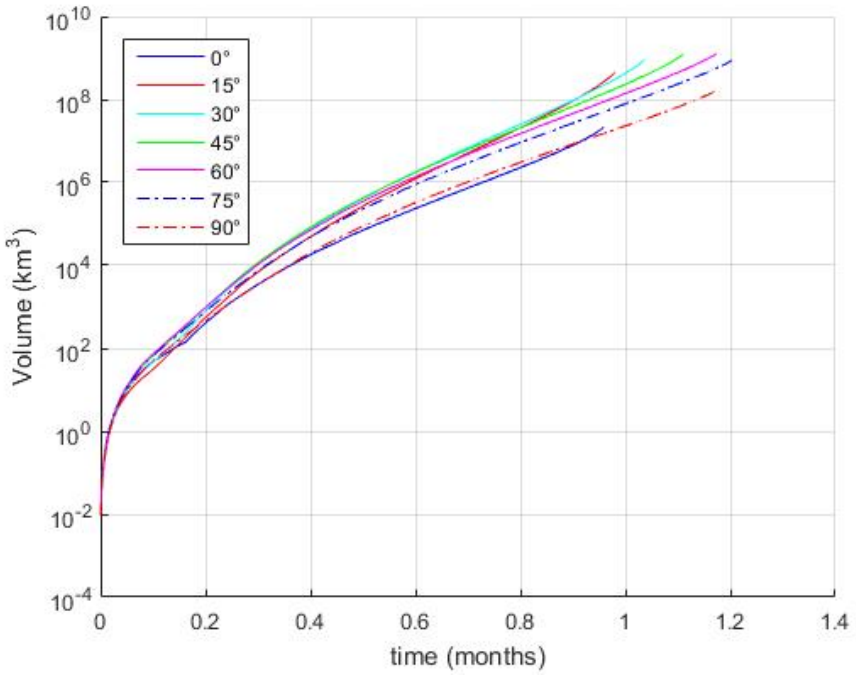

Figure 78: Maximum Volume Enclosing Constellation (Lifetime) (SV = 1 m/s & Offset = 45°) (Inclination Comparison)

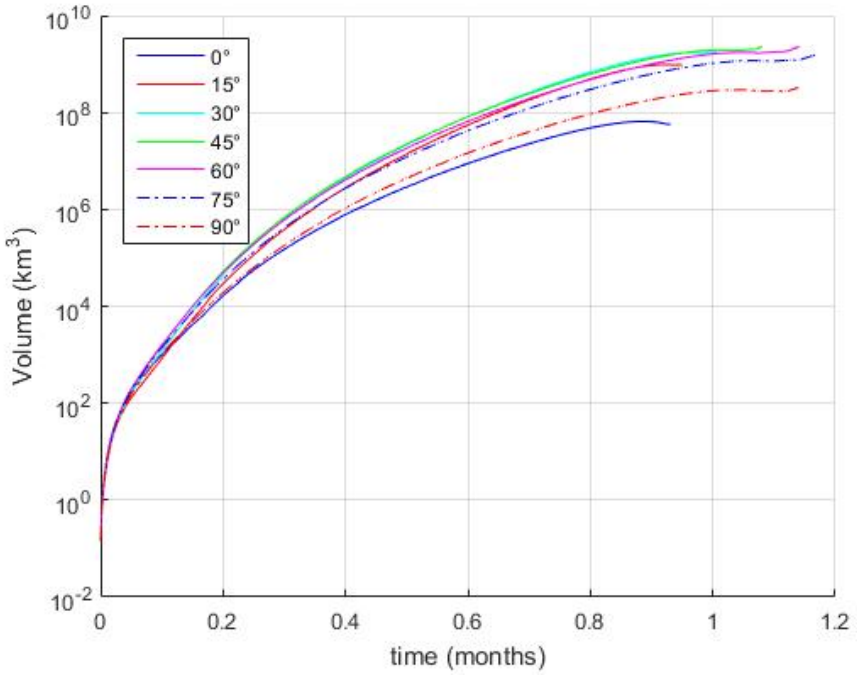

Figure 79: Maximum Volume Enclosing Constellation (Lifetime) (SV = 2 m/s & Offset = 45°) (Inclination Comparison)

4.4.2 Inclination Maximum Distance Trends

Figure 80 and Figure 81 are plots showing the maximum distance between any two satellites in the constellation with an initial separation velocity of 1 m/s. The plots differ from one another with respect to the offset of the deployment plane. Figure 80 has a deployment plane offset of 0°, while Figure 81 has a deployment plane offset of 45°. From these two figures, it is apparent that, over the first 24 hours after deployment, the inclination of an orbit has very little effect on initial dispersal of the satellites. From this, one can make the logical conclusion that a deployment scheme, for an altitude of 300 km, that has been set up to meet certain criteria over the first 24 hours, can be applied to multiple inclinations with little effect on the performance of the deployment scheme.

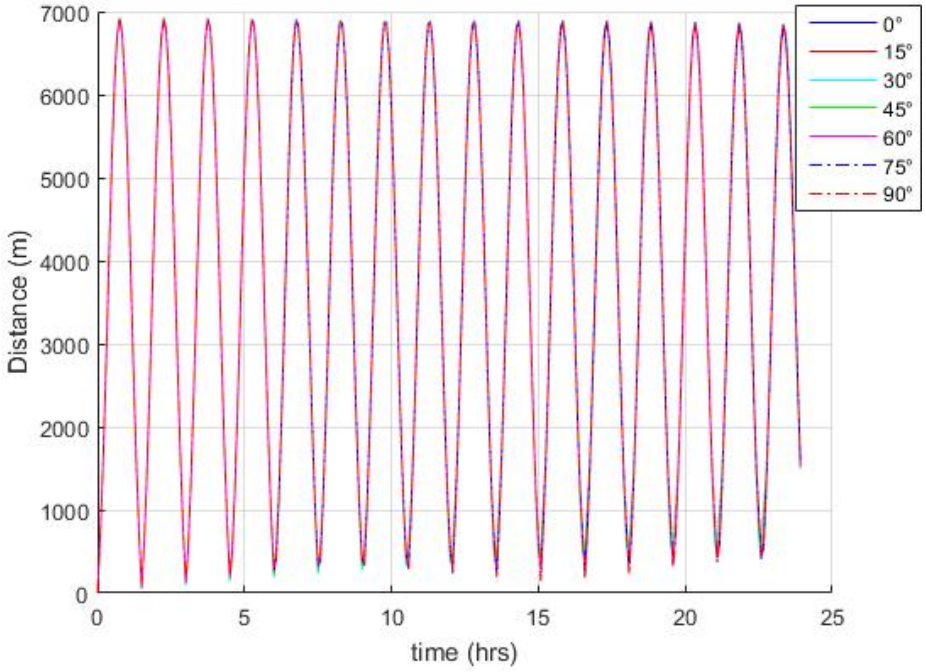

Figure 80: Maximum Distance Between Any Two Satellites (1 Day) (SV = 1 m/s & Offset = 0°) (Inclination Comparison)

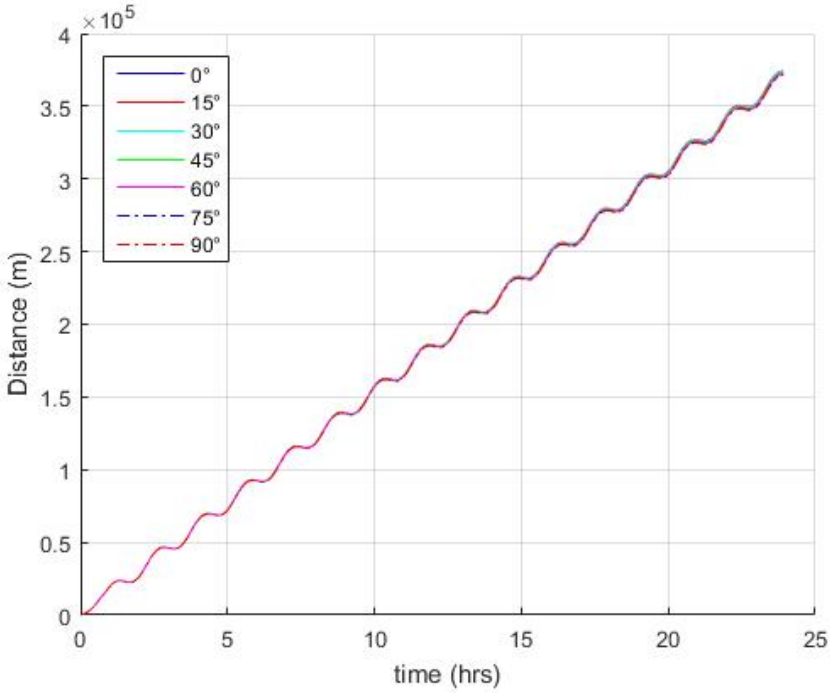

Figure 81: Maximum Distance Between Any Two Satellites (1 Day) (SV = 1 m/s & Offset = 45°) (Inclination Comparison)

Figure 82 displays, for the lifetime of the constellations, the maximum distance between any two satellites in the constellation when deployed with a separation velocity of 1 m/s and a deployment plane offset of 0°. Similar to Figure 77, there is a noticeable trend with respect to the lifetime of the constellation, with polar orbits being the outlier. Figure 82 also shows that the lowest maximum distance at the time of reentry is around 60°.

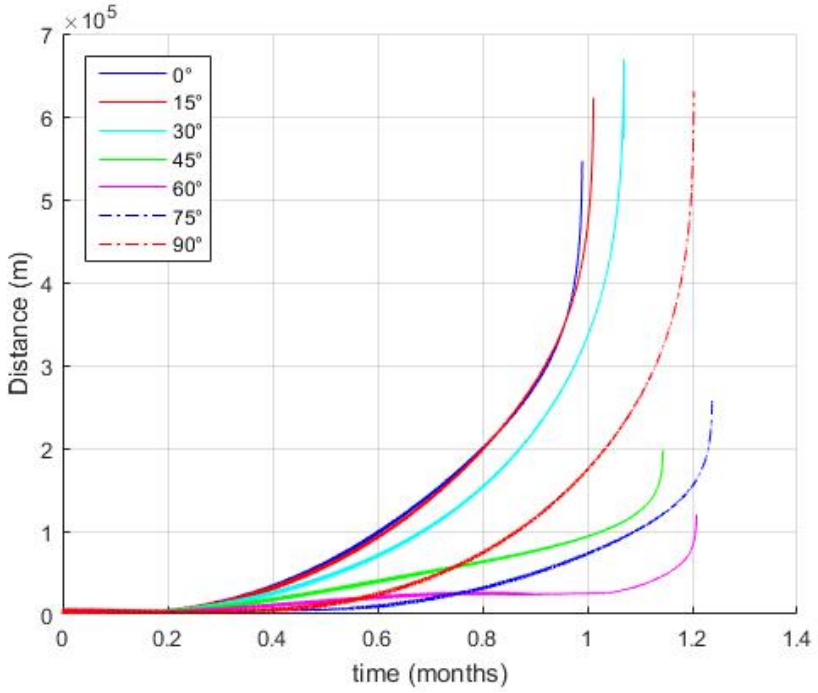

Figure 82: Maximum Distance Between Any Two Satellites (Lifetime) (SV = 1 m/s & Offset = 0°) (Inclination Comparison)

Figure 83 shows the maximum distance between any satellite pair within the constellation, over the lifetime of the constellation, for a separation velocity of 1 m/s and an offset of 45°. While there is very little separation due to different inclinations over the first week, after that, it becomes noticeable that the rate of increase of the maximum distance within the constellation increases faster for lower inclinations.

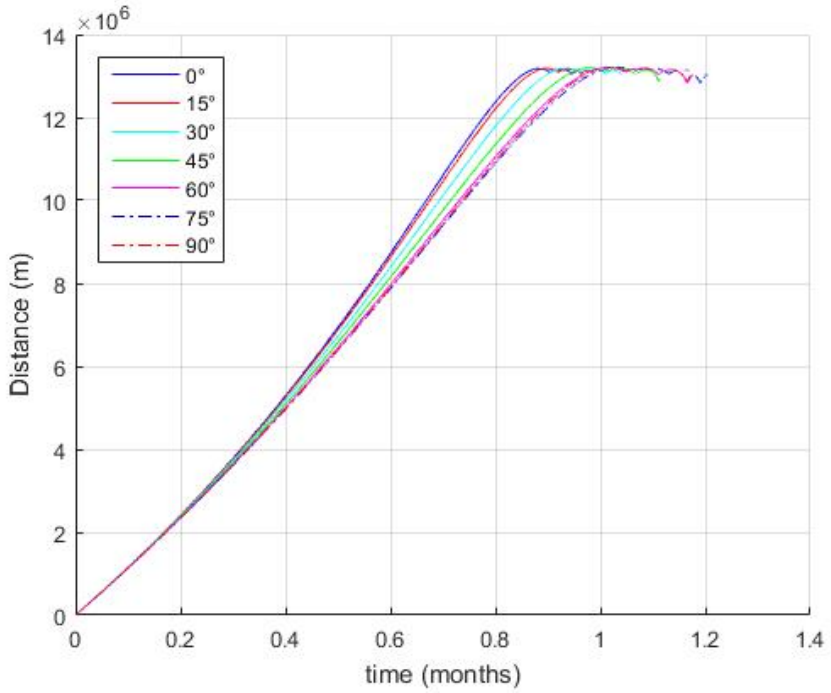

Figure 83: Maximum Distance Between Any Two Satellites (Lifetime) (SV = 1 m/s & Offset = 45°) (Inclination Comparison)

4.5 Geometry Trends

To conduct the geometry trend analysis, the data is parsed into 23 sets. For all of the sets, the RAAN and argument of latitude are both set to 0°. The data is then separated into the 23 sets to compare tests cases with the same separation velocity, altitude, and inclinations for circular orbits with deployment plane offsets of 0°, 45°, 90°, and 135°. For an altitude of 300 km and an inclination of 30°, separation velocities of 1 m/s, 1.5 m/s, and 2 m/s are tested and are each their own set. For all other altitudes and inclinations, only separation velocities of 1 m/s and 2 m/s are tested. For an altitude of 300 km, inclinations from 0° to 90° with steps of 15° are tested. For all other altitudes (400 km, 500 km, 750 km, and 1,000 km), only an inclination of 30° is tested.

4.5.1 Geometry Maximum Volume Trends

The maximum volume enclosing the constellation of satellites deployed into an orbit with an altitude and inclination of 300 km and 30°, respectively, with a separation velocity of 1 m/s, is shown in Figure 84. Figure 84 shows, for the first 24 hours after deployment, two initial groupings with respect to maximum volume. In the upper group, the two constellations deployed with offsets of 45° and 135° behave in a similar fashion over the first 24 hours. In the lower group, the two constellations deployed with offsets of 0° and 90° differ from one another immediately. This difference is caused by the increased phasing observed in the constellation with a deployment plane offset of 90°. The fact that an offset of 0° results in a constellation that does not spread out quickly with time has been highlighted multiple times so far in this investigation.

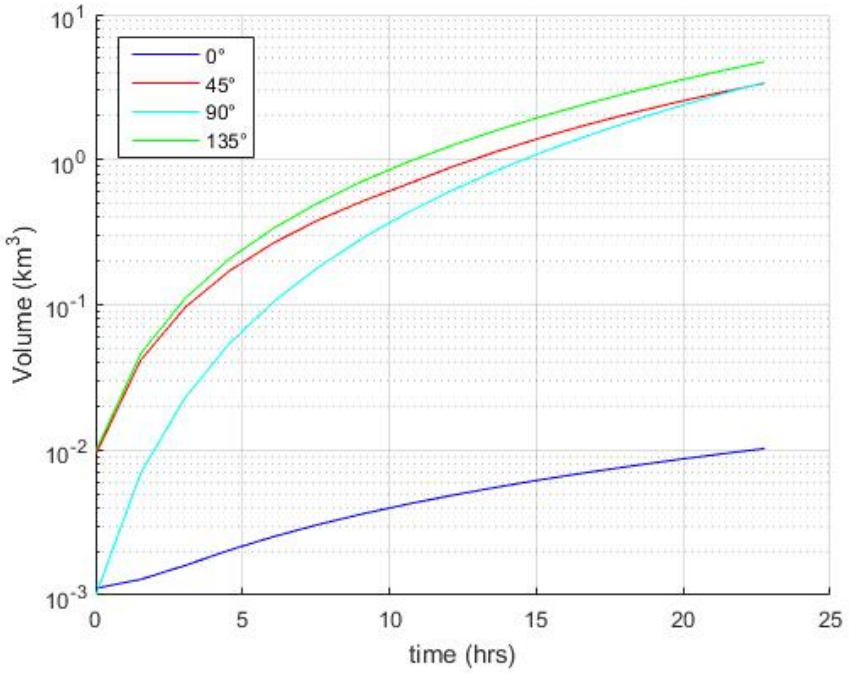

Figure 84: Maximum Volume Enclosing Constellation (1 Day) (DV = 1 m/s - Alt = 300 km - Inc = 30°) (Geometry Comparison)

Figure 85 displays the same data as Figure 84, with the difference being that Figure 85 covers the entire lifetime of the constellations. From Figure 85, it can be seen that geometry does have an effect on the lifetime of the constellation. The constellation deployed with an offset of 0° has the longest lifetime, followed by the constellations with 45° and 135°, with the constellation deployed with an offset of 90° experiencing the shortest lifetime. Notice that the plots for 45° and 135° hardly deviate from one another in Figure 85. Since the maximum volume is still increasing when the constellations reenter the atmosphere, the orbit that the constellation is occupying is not fully populated before reentry.

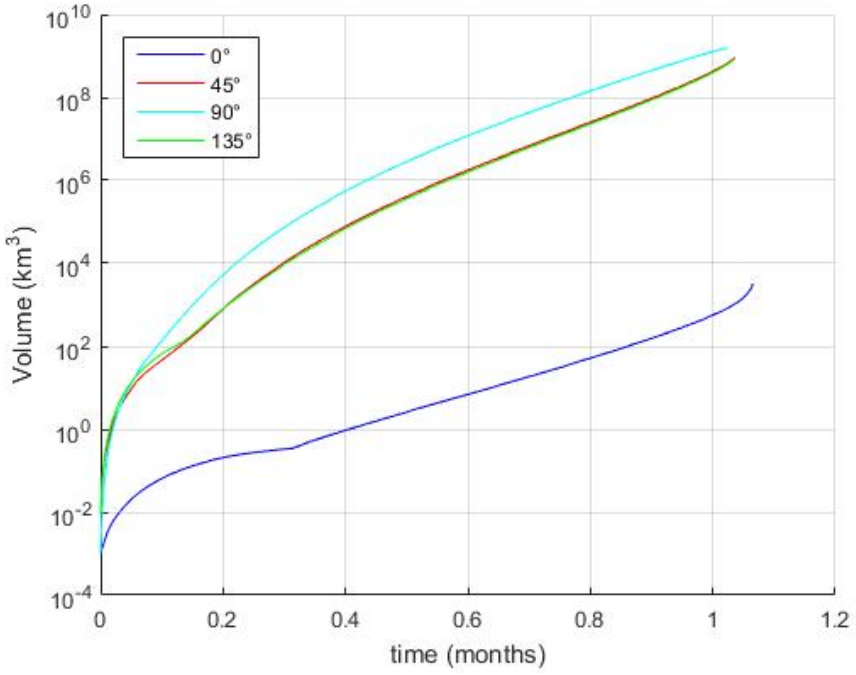

Figure 85: Maximum Volume Enclosing Constellation (Lifetime) (DV = 1 m/s - Alt = 300 km - Inc = 30°) (Geometry Comparison)

4.5.2 Geometry Maximum Distance Trends

The maximum distance between any two satellites within the constellation over the first 24 hours of deployment is shown in Figure 86. This plot simply shows that the increased phasing present when the offset is not 0° dominates the behavior of this metric over the first 24 hours after deployment.

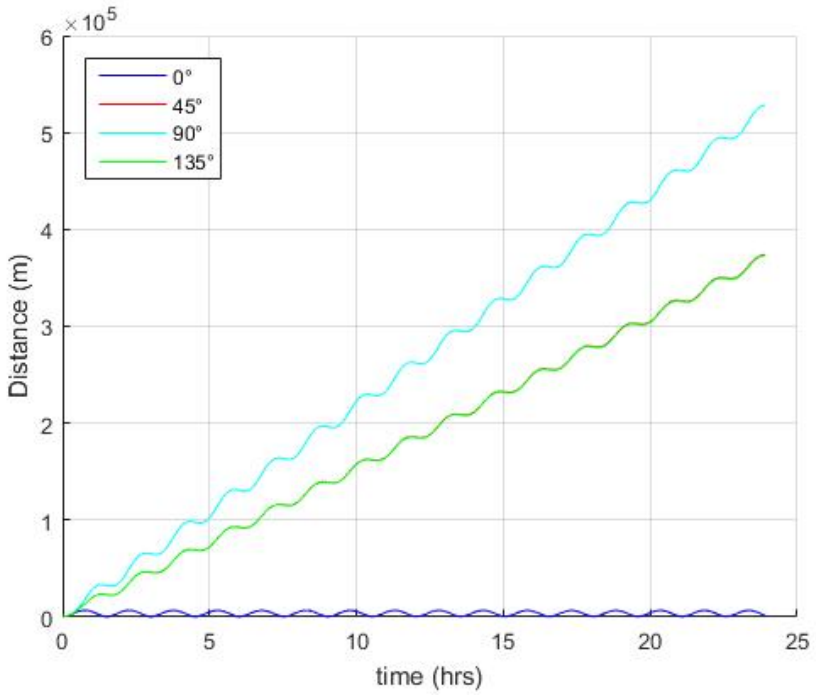

Figure 86: Maximum Distance Between Any Two Satellites (1 Day) (DV = 1 m/s - Alt = 300 km - Inc = 30°) (Geometry Comparison)

Figure 87 shows that for offsets of 45°, 90°, and 135°, at least one pair of satellites within the constellation is on opposite sides of the orbit before reentry. This, combined with Figure 85, can give insight into the layout of the constellation. An offset of 90° is also shown to be able to distribute a constellation across half of an orbit faster than deployments utilizing offsets of 0°, 45°, and 135°. This is not a very illuminating insight, as it could have been logically concluded without conducting the investigation, but

logical insights, and their later validation within a simulation, help to analyze the overall validity of the results.

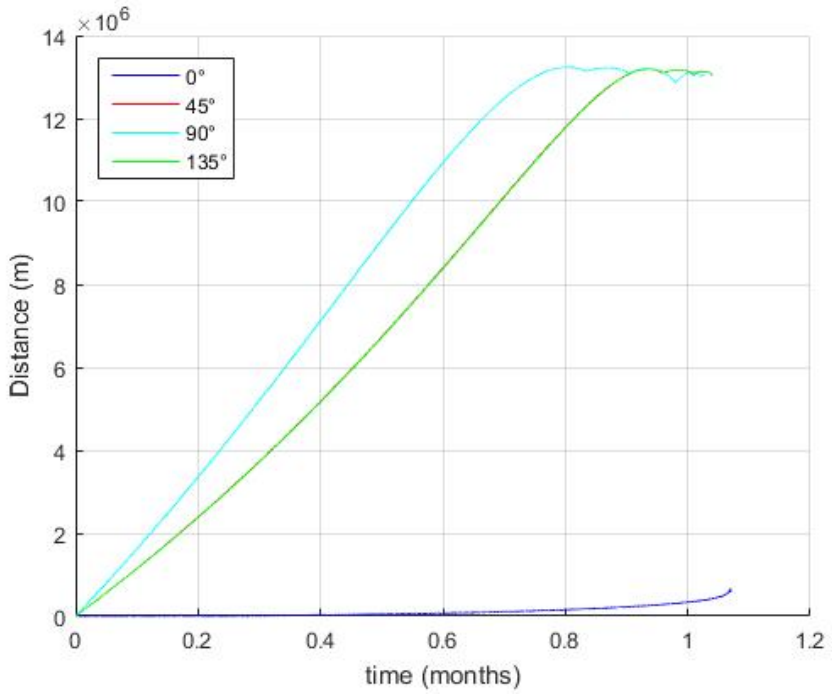

Figure 87: Maximum Distance Between Any Two Satellites (Lifetime) (DV = 1 m/s - Alt = 300 km - Inc = 30°) (Geometry Comparison)

4.6 Separation Velocity Trends

To conduct the separation velocity trend analysis, the data is parsed into 44 sets. For all of the sets, the RAAN and argument of latitude are both set to 0°. The data is then separated into the 44 sets to compare tests cases with the same deployment plane offset, altitude, and inclinations for circular orbits with separation velocities of 1 m/s, 1.5 m/s (when applicable – this value is not tested for all sets), and 2 m/s. For an altitude of 300 km, inclinations from 0° to 90° with steps of 15° are tested. For all other altitudes (400 km, 500 km, 750 km, and 1,000 km), only an inclination of 30° is tested. Deployment

plane offsets of 0°, 45°, 90°, and 135° are tested for all altitude and inclination combinations mentioned.

4.6.1 Separation Velocity Maximum Volume Trends

The maximum volume enclosing the constellation of satellites deployed into an orbit with an altitude and inclination of 300 km and 30°, respectively, with a deployment plane offset of 45°, is shown in Figure 88. Over the range in which CubeSats are typically deployed, the greater the velocity in which the satellites are deployed, the higher the maximum volume occupied by the constellation is over the first 24 hours.

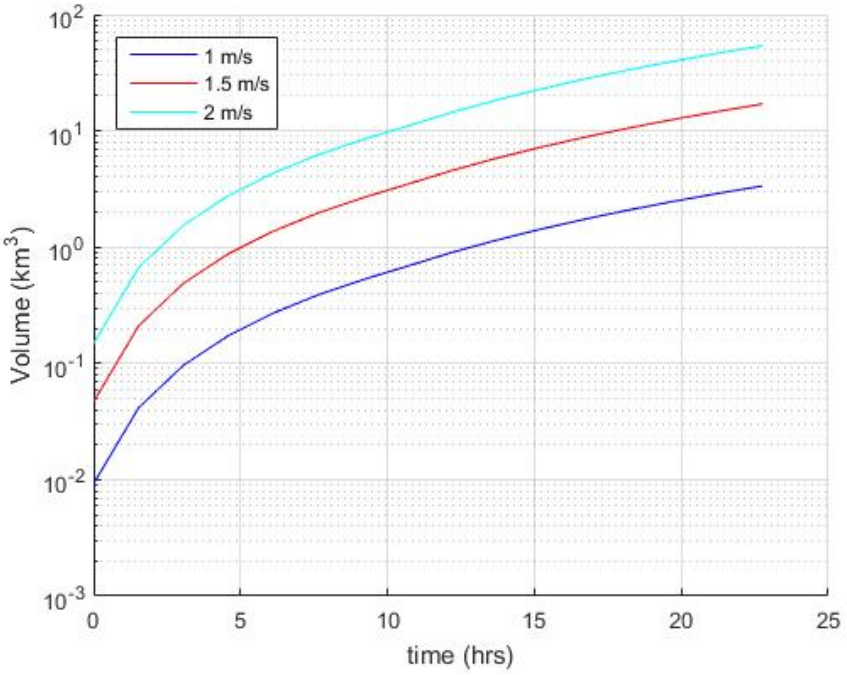

Figure 88: Maximum Volume Enclosing Constellation (1 Day) (Alt = 300 km - Inc = 30° - Offset = 45°) (Separation Velocity Comparison)

Figure 89 is a continuation of Figure 88, showing the maximum volume enclosing the constellation over the lifetime of the constellation. The trend from the first 24 hours

continues for the majority of the lifetime of the constellation. After 1 month, the maximum volume of the case utilizing a separation velocity of 2 m/s starts to decrease. This shows that, for a deployment plane offset of 45° and a separation velocity of 2 m/s, the satellites move around the orbit until some of the satellites pass by each other. The lifetime of the constellation is shown to have a small dependence on the separation velocity. A separation velocity of 2 m/s corresponds to the shortest lifetime, and a separation velocity of 1 m/s corresponds to the longest, out of the three separation velocities compared.

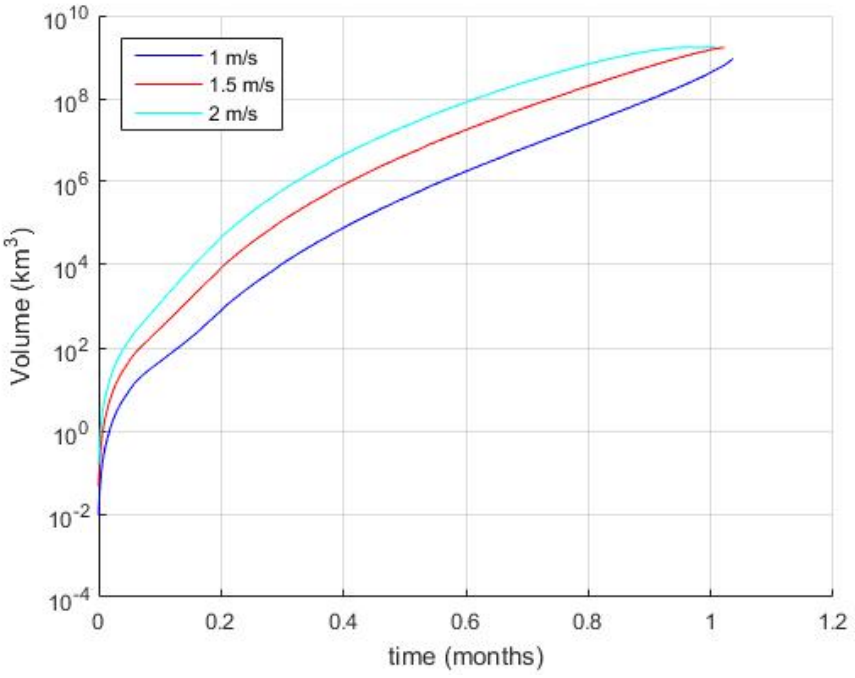

Figure 89: Maximum Volume Enclosing Constellation (Lifetime) (Alt = 300 km - Inc = 30° - Offset = 45°) (Separation Velocity Comparison)

4.6.2 Separation Velocity Maximum Distance Trends

Figure 90 displays the maximum distance between any two satellites in the constellation for the first 24 hours after a deployment into an orbit with an altitude of 300

km and an inclination of 30°, utilizing a deployment plane offset of 45°. The relationship between separation velocity and maximum distance is straightforward for these initial conditions. The relationship is that the higher the separation velocity, the faster the maximum distance between any two satellites within the constellation increases.

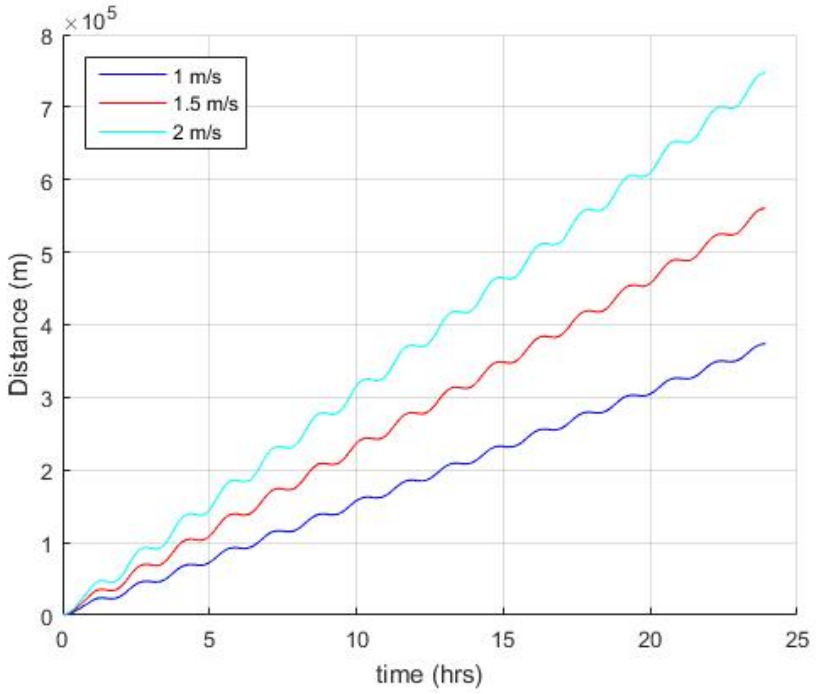

Figure 90: Maximum Distance Between Any Two Satellites (1 Day) (Alt = 300 km - Inc = 30° - Offset = 45°) (Separation Velocity Comparison)

Figure 91 is a continuation of Figure 90, showing the maximum distance between any two satellites in the constellation over the lifetime of the constellation. The trends observed in Figure 90 continue, showing the maximum distance within the constellation increases quicker for faster separation velocities. A separation velocity of 2 m/s, for an orbit with an altitude of 300 km, an inclination of 30° and a deployment plane offset of 45°, takes around 2.5 weeks until two of the satellites are on opposite sides of the orbit

with respect to one another. For separation velocities of 1.5 m/s and 1 m/s, the time required to achieve this is close to 3 weeks and 3.5 weeks, respectively.

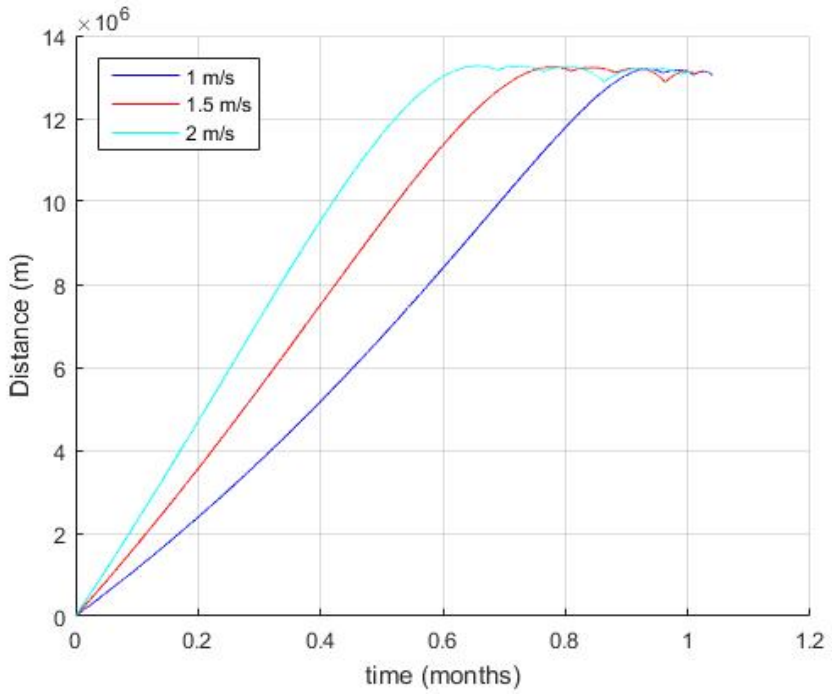

Figure 91: Maximum Distance Between Any Two Satellites (Lifetime) (Alt = 300 km - Inc = 30° - Offset = 45°) (Separation Velocity Comparison)

4.7 Argument of Latitude Trends

Unlike the other trend analyses that have been completed up to this point, only one set is used to conduct the argument of latitude trend analysis. For this analysis, the altitude and inclination are set to 300 km and 30°, while the separation velocity and deployment plane offset are set to 1 m/s and 0°. The values of argument of latitude that are implemented in order to complete a trend analysis are: 0°, 30°, 60°, 90°, 120°, 150°, 180°, 210°, 240°, 270°, 300°, and 330°.

4.7.1 Argument of Latitude Maximum Volume Trends

Figure 92 shows that the behavior of the maximum volume of the constellation over the first 24 hours has a distinct pattern. There are clearly four bands present in Figure 92, with launches occurring at 30°, 150°, 210°, and 330° making up the top band. Launches occurring at an argument of latitude of 60°, 120°, 240°, and 300° form the second band. The third band is comprised of launches occurring at 0° and 180° and the bottom most band are the plots for launches occurring at 90° and 270°. The values of the argument of latitudes makes the bands have a symmetrical quality to where they fall on the graph. This will be explained in more detail momentarily.

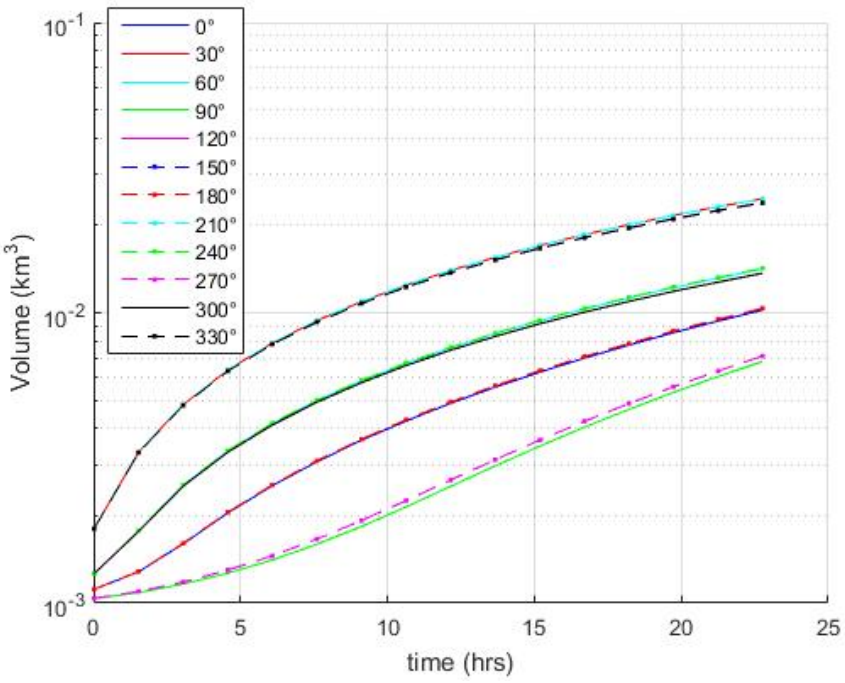

Figure 92: Maximum Volume Enclosing Constellation (1 Day) (Alt = 300 km - Inc = 30° - Offset = 0°) (Argument of Latitude Comparison)

From Figure 93, it is evident that the maximum volume stops behaving strictly according to the bands after the first week on orbit, but the maximum volume of launches

occurring a 0° and 180°, the ascending and descending node, respectively, and launches occurring at 90° and 270° track one another closely for the duration of the lifetime of the constellation.

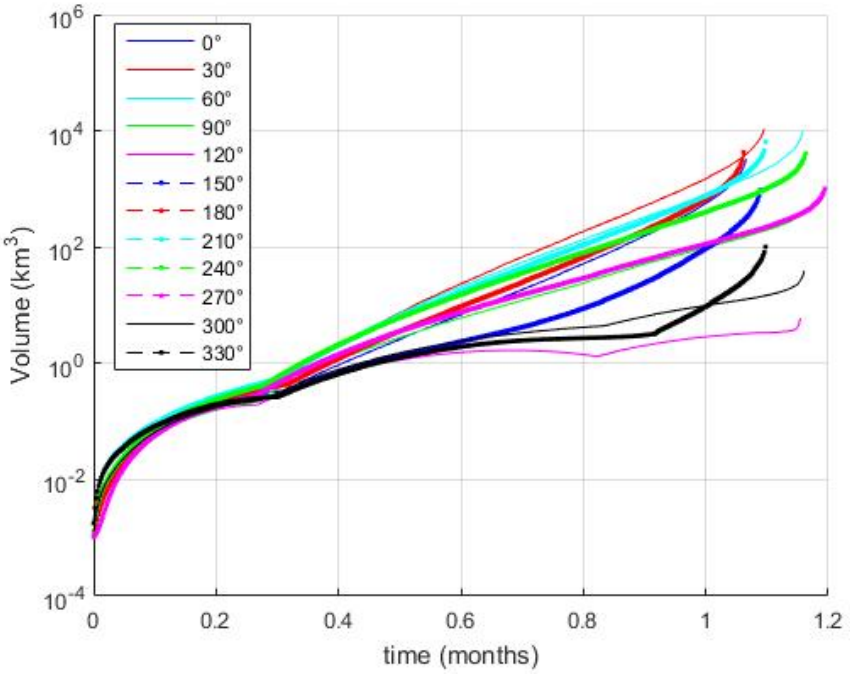

Figure 93: Maximum Volume Enclosing Constellation (Lifetime) (Alt = 300 km - Inc = 30° - Offset = 0°) (Argument of Latitude Comparison)

4.7.2 Argument of Latitude Maximum Distance Trends

Figure 94 displays the maximum distance between any two satellites in the constellation over the first 24 hours after deployment. From the plots shown, changing the argument of latitude has little effect on the maximum distance between any two satellites within the constellation over this time period.

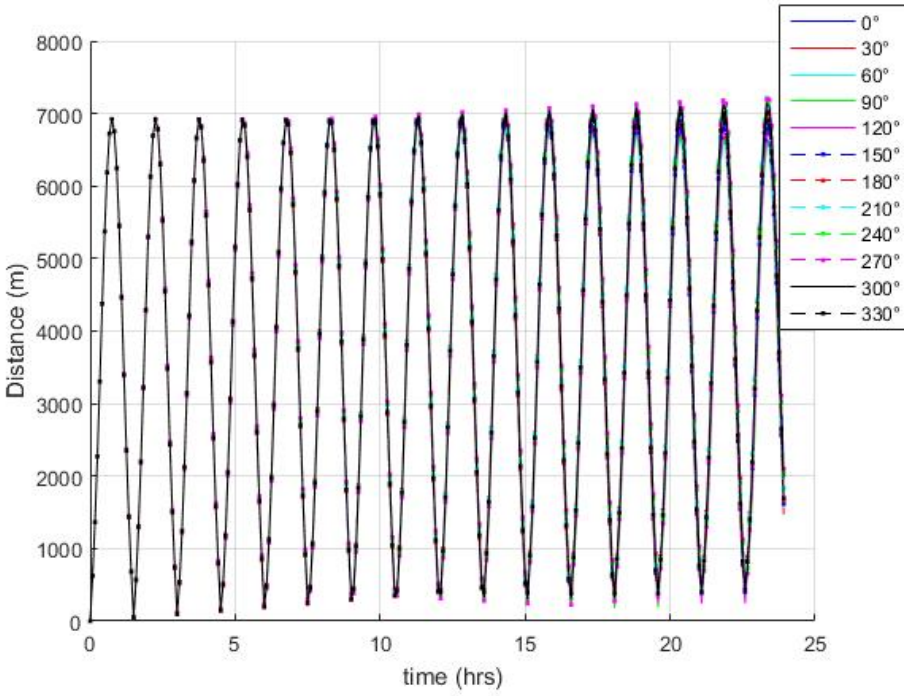

Figure 94: Maximum Distance Between Any Two Satellites (1 Day) (Alt = 300 km - Inc = 30° - Offset = 0°) (Argument of Latitude Comparison)

Figure 95 is a continuation of Figure 94, showing the maximum distance between any two satellites in the constellation over the lifetime of the constellation. It is in this plot that some interesting connections can be made. While it is clear there is a connection between the behavior of constellations deployed with an initial argument of latitude of 0° and 180°as well as 90° and 270°, it is from Figure 95 that the other linked pairs become more apparent, with a linked pair just meaning that the behavior of the deployed constellations display similar tendencies. Twelve different arguments of latitude are tested, leading to six linked pairs. The pairs are linked by degrees past node. For example, 30° and 210° are a linked pair, because both constellations are deployed 30° past a node. The other three pairs are 60° and 240°, 120° and 300°, and 150° and 330°. The six linked pairs all share similar expected lifetimes, with the 0°-180° pair

experiencing the shortest lifetime and the 90°-270° pair experiencing the longest lifetime. Two of the linked pairs, 0°-180° and 90°-270°, shows very similar behavior with respect to maximum distance within the constellation. Three of the four remaining pairs show that the constellation launched over the northern hemisphere experienced more separation than the constellation of its linked pair. The 120°-300° linked pair is the outlier for this observation.

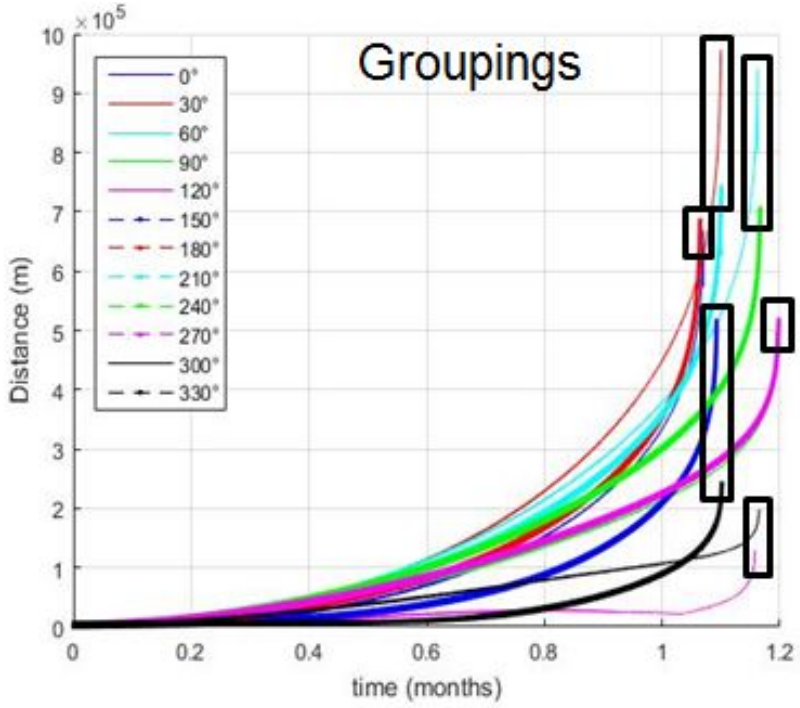

Figure 95: Maximum Distance Between Any Two Satellites (Lifetime) (Alt = 300 km - Inc = 30° - Offset = 0°) (Argument of Latitude Comparison)

4.8 Delayed Deployment Trends

In order to develop a trend analysis of how delaying the deployment of part of the constellation affects the behavior of the constellation, four deployment scenarios are created. How the individual deployment scenarios are built is discussed in Chapter 3. The four deployment scenarios that are tested fall into two categories, the first of which is

‘Sequence’. In a ‘Sequence’ deployment scenario, satellite 1 is deployed at time zero, a set period of time passes, and then satellites 2 is deployed. The satellite numbering scheme is presented in Figure 17. This process is repeated until all eight satellites have been deployed. Two ‘Sequence’ type deployment scenarios are tested, one with a delay time between deployments of 1 minute, and a second with a delay time between deployments of 5 minutes. The second category that a deployment scenario can be classified as is ‘Half & Half’. In a ‘Half & Half’ deployment scenario, satellites 1 through 4 are deployed at time zero, a set time period passes, and then satellites 5 through 8 are deployed. Two ‘Half & Half’ deployment scenarios are tested, one with a delay time of 5 minutes, and a second with a delay time of 45 minutes. A visual representation of the delayed deployment schemes is shown in Figure 96. Figure 96(a) shows the initial dispersal pattern of a constellation utilizing a ‘Sequence’ deployment scenario. Figure 96(b) and Figure 96(c) show the initial dispersal pattern of a constellation utilizing a ‘Half & Half’ deployment scenario. Figure 96(b) depicts the initial dispersal after one minute, when only the first half of the constellation has been deployed, while Figure 96(c) depicts the initial dispersal after six minutes, when the entire constellation has been deployed.

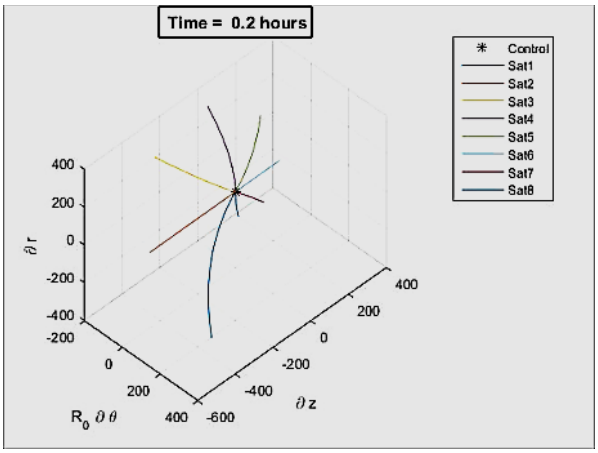

(a)

Sequence

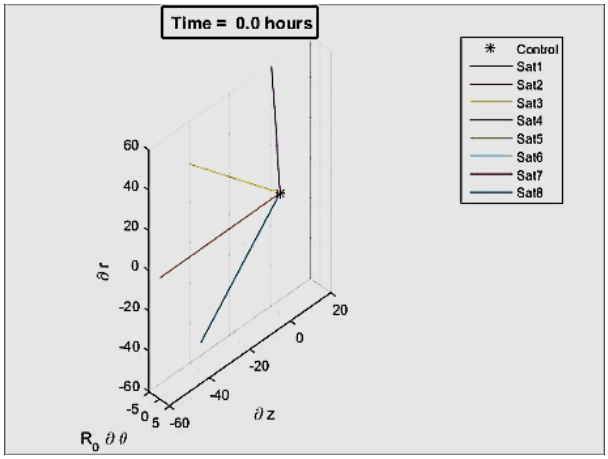

(b)

Half & Half – Time = 1 min

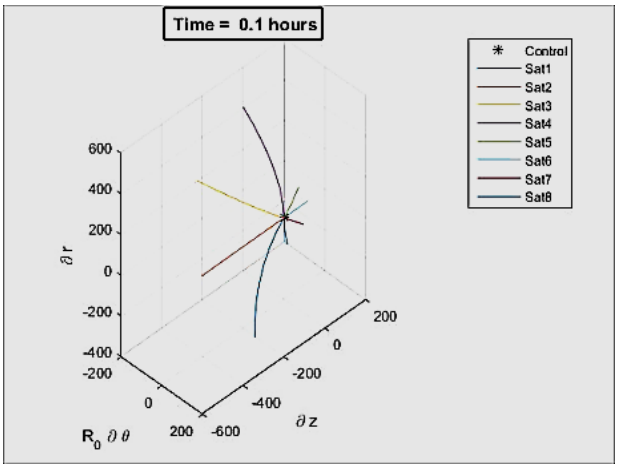

(c)

Half & Half – Time = 6 min

Figure 96: Visual Representation of Delayed Deployment Schemes

For this analysis, the altitude and inclination are set to 300 km and 30°, while the separation velocity and deployment plane offset are set to 1 m/s and 0°. This is used as the 'Default' measurement that is present in Figure 97 through Figure 100. Note the time zero for Figure 97 through Figure 100 is the moment the last satellite is deployed for each individual constellation.

4.8.1 Delayed Deployment Maximum Volume Trends

Figure 97 shows that the initial maximum volume metrics for constellations containing satellites whose deployments are delayed with respect to one another start much higher when compared to a constellation whose satellites are all deployed simultaneously. The deployment scenarios with the largest time gaps between deployments have the largest maximum volume over the first 24 hours.

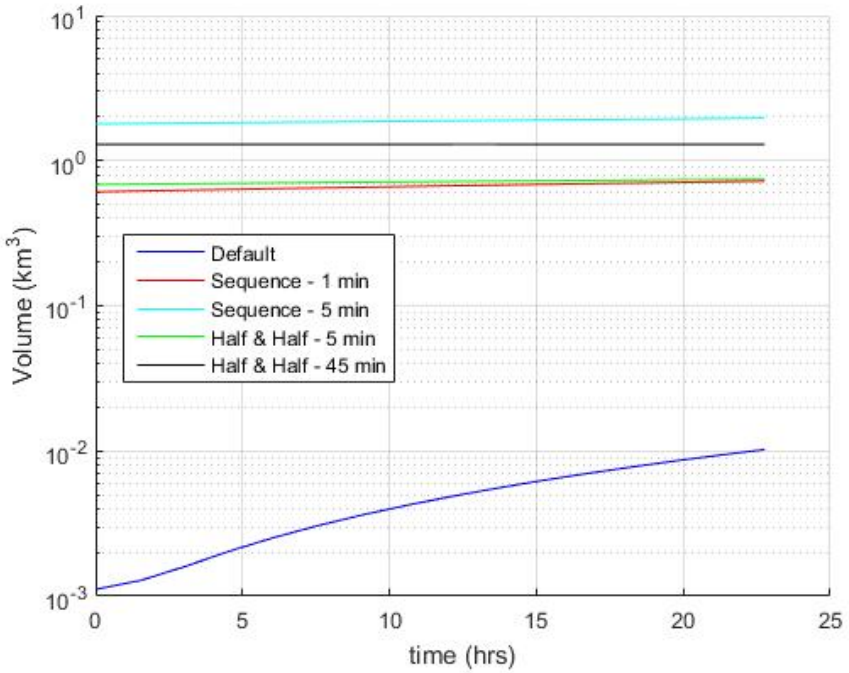

Figure 97: Maximum Volume Enclosing Constellation (1 Day) (Alt = 300 km - Inc = 30° - Offset = 0°) (Delayed Deployment Comparison)

Figure 98 displays how the maximum volume enclosing the constellation behaves over the lifetime of the constellation. The ‘Sequence’ deployment with a delay time of 5 minutes still represents the constellation with the largest maximum volume. It is interesting that the two deployment scenarios with the shorter delay times start with a maximum volume much higher than the default scenario, but actually reenter with a smaller maximum volume than the default scenario that had no delay between deployments. Of the four scenarios, the ‘Half & Half’ deployment scenario with a delay time of 45 minutes shows the most interesting behavior. The volume of this constellation shrinks over the first week after deployment and then reenters the Earth’s atmosphere at the end of its life with the smallest maximum volume.

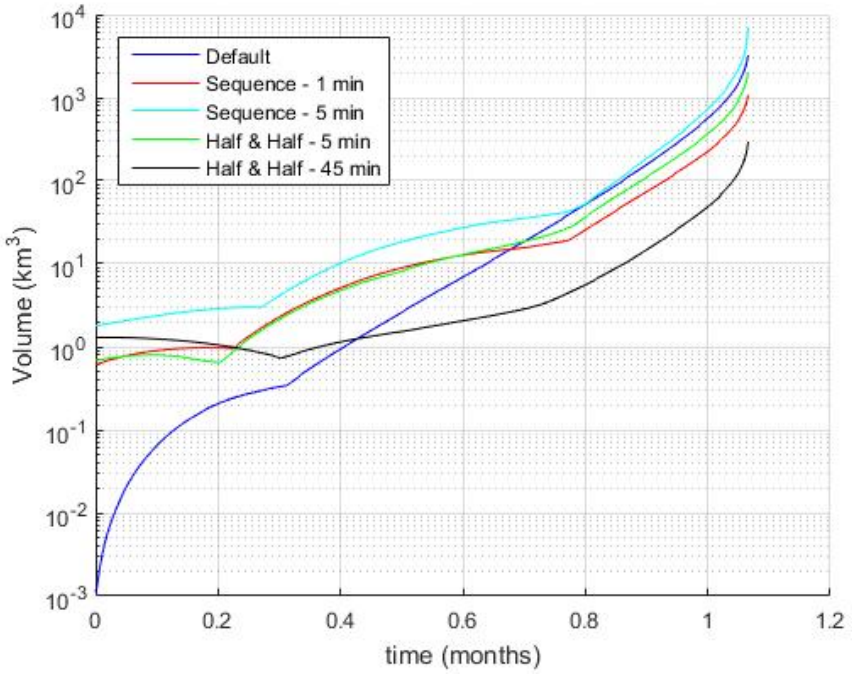

Figure 98: Maximum Volume Enclosing Constellation (Lifetime) (Alt = 300 km - Inc = 30° - Offset = 0°) (Delayed Deployment Comparison)

4.8.2 Delayed Deployment Maximum Distance Trends

Figure 99 shows how spreading the deployment of some of the satellites within the constellation out over 35 (Sequence – 5-minute delay) to 45 minutes (Half & Half – 45-minute delay) can help facilitate the initial tracking and identification of a freshly deployed constellation. The minimum of the maximum distance between any two satellites over the first 24 hours for the ‘Sequence-5’ deployment scenario is over 1.5 km while the minimum of the maximum distance for the ‘Half & Half-45’ deployment scenario is over 3.5 km.

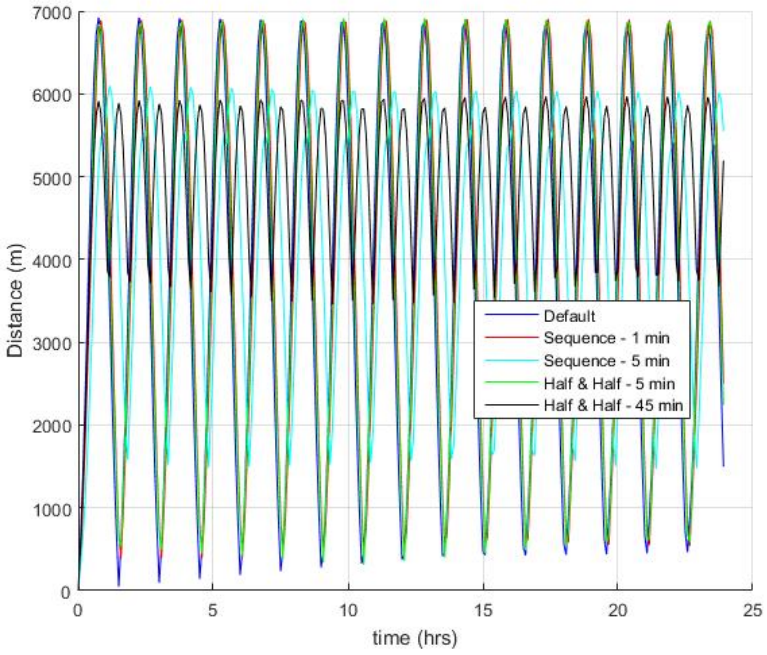

Figure 99: Maximum Distance Between Any Two Satellites (1 Day) (Alt = 300 km - Inc = 30° - Offset = 0°) (Delayed Deployment Comparison)

Figure 100 is a continuation of Figure 99, showing the maximum distance between any two satellites in the constellation over the lifetime of the constellation. From Figure 100, it is observed that the delayed deployment scenarios tested had very little effect on the overall lifetime of the constellation. Three of the four delayed deployment scenarios actually recorded values smaller for the maximum distance between any two satellites within the constellation than the default test scenario that is plotted for comparison purposes. The only delayed deployment scenario that returned a larger maximum distance values is the 'Sequence' deployment scenario that used a delay of 5 minutes between deployments.

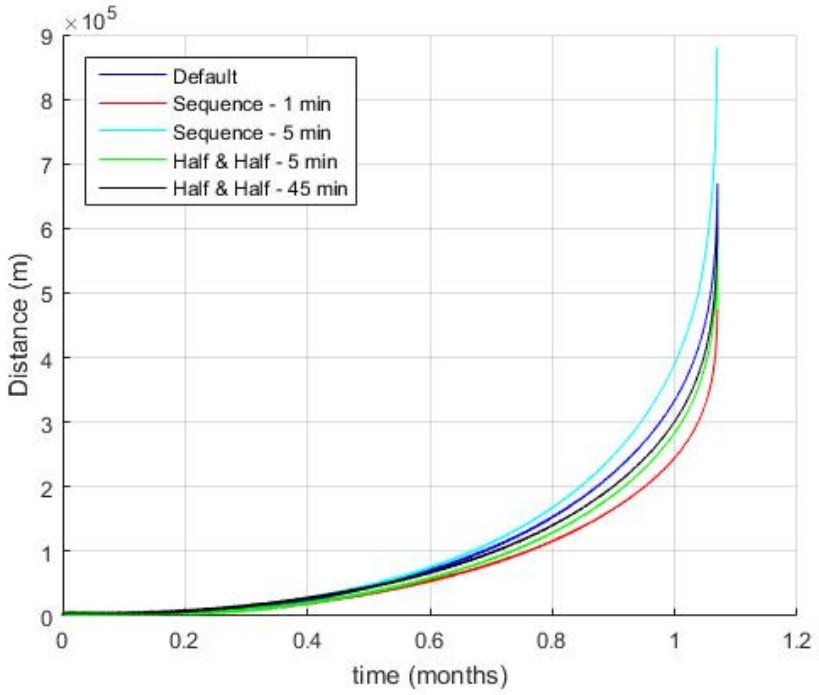

Figure 100: Maximum Distance Between Any Two Satellites (Lifetime) (Alt = 300 km - Inc = 30° - Offset = 0°) (Delayed Deployment Comparison)

4.9 Discussion

4.9.1 Comparisons to Previous Work

Puig-Suari, Zohar, and Leveque initially attempted to deploy a constellation along the anti-velocity vector separated by time, which resulted in minimal dispersal of the satellites. No direct correlation to this deployment scheme is accomplished in this current investigation, but none of the analysis that is conducted disagrees with Puig-Suari's conclusion. Puig-Suari's work is explained in Chapter 2, but is repeated here to aide with the comparison. Puig-Suari then decided to vary the magnitude of the different deployment velocities along the deployment path. To accomplish this while still maintaining a constant ejection velocity from the deployer, a radial semi-circular

deployment was implemented by Puig-Suari. A radial semi-circular deployment scenario ejects the first satellite along the velocity vector and the last satellite along the anti-velocity vector.[26] In Puig-Suari's work, all of the remaining satellites were ejected into the upper half of the plane containing both the velocity vector and radial vector. Eight 3U CubeSats were ejected using two versions of this deployment scenario. The first version deploys the satellites with a constant angle between deployments, while the second version varies the angle of the satellite deployments to create a constant differential between the magnitudes of the component of the separation velocity along the velocity vector of the deployer. Puig-Suari concluded that both versions populated the constellation in the same amount of time, but the deployment scenario that utilized a constant differential in in-track separation velocity resulted in a more even distribution along the orbit path.[26]

A modified version of the constant angle deployment scheme is tested in the current investigation, while no version of the constant differential separation velocity is implemented. The difference between the scheme utilized by Puig-Suari and the scheme used in this current investigation is that Puig-Suari deployed eight CubeSats into the upper-half of the deployment plane, while the comparable deployment scheme used in this current investigation ejects eight CubeSats into the entire deployment plane. Both Puig-Suari's investigation and this current investigation's conclusions agree that this deployment scheme disperses the CubeSats better than dispersing along the anti-velocity vector, though the constellation will not be evenly dispersed along the orbit path. The final conclusion from Puig-Suari's work that is comparable to the results of the analysis that is conducted in this current investigation focuses on the behavior of a constellation

with respect to altitude. Puig-Suari's work concluded that the lower the altitude of the initial deployment, the faster the constellation disperses along the orbit path. This current investigation results in the same conclusion.

Kilic, Scholz, and Asma implemented a specific orbit for their analysis. The initial orbit used in Kilic's work has an altitude of 320 km, an inclination of 79°, an eccentricity of 0, a RAAN of 40°, and a true anomaly (argument of latitude) of 155°.[27] Kilic's investigation resulted in multiple conclusions regarding how to avoid collisions immediately after deployment. Those conclusions are that CubeSats should be ejected from minimum 'ballistic coefficient' to maximum 'ballistic coefficient' (lightest satellite to heaviest satellite based on Kilic's definition), that ejection of satellites perpendicular to the velocity vector leads to an elevated risk of collisions, and that the safest deployment scenario is in the anti-velocity direction.[27] The present investigation assumes a constant ballistic coefficient for all of the deployed satellites, so this current investigation offers no comparison for this finding. Kilic also described the safest deployment vector as being in the anti-velocity direction. Both Puig-Suari's investigation and this current investigation concluded that deploying all of the satellites in the anti-velocity direction leads to minimal dispersal of the constellation, but for collision risk analysis between the deployer and a deployed CubeSat, this current investigation agrees that deployment along the anti-velocity vector minimizes the risk of conjunction. It should be noted that this present investigation finds minimal difference in collision risk analysis between deployments along the velocity vector and the anti-velocity vector. Kilic's finding of the anti-velocity vector being the safest deployment vector is most likely linked to the specific deployer dynamics that are accounted for in Kilic's work. The final conclusion from Kilic's work

that is comparable to the results of the analysis that is conducted in this current investigation is that ejection of satellites perpendicular to the velocity vector leads to an elevated risk of collisions. This current investigation results in the same conclusion.

4.9.2 Mission Specific Analysis

4.9.2.1 Recent CubeSat Missions

The SENSE mission is presented in Chapter 2 as an example of how deploying a large number of CubeSats during a single launch can lead to difficulties with the tracking and identification of, and communicating with, the individual CubeSats comprising the constellation. The present investigation resulted in a few key takeaways that can be utilized in the future to facilitate the tracking and identification of, and communication with, a newly deployed constellation. The first key takeaway is that one should ensure that no CubeSats are deployed in to the plane normal to the velocity vector of the deployer. Ensuring that at least some component of the separation velocity is in either the velocity or anti-velocity direction aides in the dispersal of the constellation. The next finding is to delay the deployment of satellites in the same dispenser with respect to one another. Deploying satellites along the same vector with minimal differences in separation velocity keeps at least part of the constellation in close proximity to one another, hindering tracking, identification, and communication. The final key takeaway that will promote the initial dispersal of a constellation is that, if satellites must be launched over a short period of time, one should have the respective deployment vectors be separated by 180°. This, combined with avoiding ejection into the plane normal to the velocity vector of the deployer, will promote the growth of the constellation, which will

facilitate the tracking and identification of, and communication with, the deployed constellation.

While the SENSE mission would have benefited from a constellation that prioritized initial dispersal, other missions involving CubeSats may prioritize some individual satellites staying close to one another. One example of this is the CanX-4 and CanX-5 formation flying mission, which was also detailed in Chapter 2. This mission would have benefited from a deployment scheme that resulted in these two CubeSats staying relatively close to one another until at least one satellite could be brought online. One option, which this mission was not able to utilize, is to load both CubeSats into the same dispenser and separate the deployment of each satellite by a few minutes. The second option, resulting from the analysis conducted in this investigation, is to deploy both satellites into the same deployment plane, with close to the same magnitude of separation velocity in the radial, transverse, and normal directions, but with opposite signs in the radial direction (This corresponds to the satellite 1-3 or satellite 5-7 pair for a deployment with an offset of either 45°, 90° or 135°). Separating the deployments by a few minutes will reduce the chance of conjunctions occurring while keeping the satellites close to one another while the individual CubeSats are being brought online.

The one time period that is examined in this investigation that has not been discussed in this section so far is the operational phase. How the individual satellites move with respect to one another over the operational lifetime is of importance if the individual satellites are part of the same constellation. This investigation finds that deploying constellations into planes with an offset of 45°, 90°, or 135° will eventually populate the entire orbit path if the initial deployment altitude is high enough. The

methodology of having a fixed angle of 45° between every deployment vector in plane does not lend itself to a uniform dispersal. While not tested in this investigation, Puig-Suari's deployment scenario that varies the angle of the satellite deployments to create a constant differential between the magnitudes of the component of the separation velocity along the velocity vector of the deployer does provide a more uniform dispersal of the satellites within the constellation.[26] This will be useful if the mission required optimal ground coverage under the orbit path, though it should be noted that some type of propulsion will be necessary to stop the relative drift that is induced by initial deployment once the individual satellites reach their assigned slots along the orbit path.

4.9.2.2 Mission Specific Deployment Strategies

To associate the results of the analysis of this investigation to specific types of missions, four general types of missions will be used. The four types of missions are imagery, communication, formation flying, and general. For the purposes of this discussion, imagery satellites are associated with sun-synchronous orbits, communication satellites with Molniya orbits, and formation flying missions with satellites operating in LEO. A general mission is defined as operating in LEO, where the initial dispersal of the constellation is a priority, but how the satellites behave relative to one another after that is not a concern. This would be the case for a launch in which the individual satellites are stand-alone systems that are not designed to operate jointly with the other deployed satellites. In reality, any combination of the above is possible.

In order to apply the results of this investigation to a particular type of mission, the priorities of that mission type must be established. For all of the mission types, it is

desired to have the deployed satellites dispersed in such a way as to aide with tracking, identification, and communication, but, for a formation flying mission, for example, it is desired to minimize the relative drift of the individual satellites, where for an imagery and communication mission, it is desired to disperse along the orbit path to increase the ground coverage of the constellation.

The analysis of how to prevent the problems experienced by the SENSE mission listed above can be applied to all four mission types. This is possible because the priorities of the four mission types over the first 24 hours are the same. All four mission types want to avoid conjunctions and aide in the initial tracking and identification of, and communication with, the individual satellites comprising the constellation. This means: to facilitate the initial dispersal of the constellation, avoid deploying into the plane normal to the velocity vector, and avoid launching multiple satellites from the same deployment mechanism simultaneously. The final key takeaway from the SENSE mission analysis, that can be applied to the initial dispersal of these four mission types, that will promote the initial dispersal of a constellation is, if satellites must be launched over a short period in time, one should have the respective deployment vectors be separated by 180°. Applying these three practices will promote the growth of the constellation, which will facilitate the tracking and identification of, and communication with, the deployed satellites. It should be noted that the much longer periods of Molniya orbits increase the maximum separation between the individual satellites during a single orbit (see Section 4.2.3 for more details), which helps the initial tracking and identification of the satellites contained within the constellation.

It is during the system checkout phase, and into the operational phase, that the priorities of the four mission types start to differ from one another. A constellation designed for an imagery or communication mission will want to disperse their satellites along the orbit path, while a formation flying mission will want to keep the constellation relatively close together during this time period. After the initial dispersal, a general mission will not be concerned with how the satellites move with respect to one another, as the individual satellites are all designated for their own missions.

For imagery and communication missions, ensuring that some portion of the separation velocity vector is in the same direction as either the velocity, or anti-velocity, vector of the deployer will promote dispersal along the orbit path. Varying the magnitude of this component will ensure relative drift between the individual satellites. This investigation utilized constant angle separation, which will work, but Puig-Suari's deployment scenario that varies the angle of the satellite deployments to create a constant differential between the magnitudes of the component of the separation velocity along the velocity vector of the deployer does provide a more uniform dispersal of the satellites within the constellation.[26]

The analysis applicable to the system checkout phase of a formation flying mission is presented earlier in Section 4.9.2.1 during the analysis of the CanX-4 and CanX-5 formation flying mission. A formation flying mission will benefit from a deployment scheme that results in some CubeSats staying relatively close to one another until at least one satellite could be brought online. One option is to load multiple CubeSats into the same dispenser and separate the deployment of each satellite by a few minutes. The second option, resulting from the analysis conducted in this investigation, is

to deploy the satellites into the same deployment plane, with close to the same magnitude of separation velocity in the radial, transverse, and normal directions, but with opposite signs in the radial direction (This corresponds to the satellite 1-3 or satellite 5-7 pair for a deployment with an offset of either 45°, 90° or 135°). Separating the deployments by a few minutes will reduce the chance of conjunctions occurring while keeping the satellites close to one another while the individual CubeSats are being brought online.

4.10 Chapter Summary

This chapter contains two different types of the analysis. The first type of analysis focuses on deployment scenarios for low Earth, sun synchronous, and Molniya orbits. For this analysis, the three phases of interest are discussed. Those three phases are: (1) the first 24 hours after deployment, (2) the first few weeks after deployment in which the initial identification and tracking of the individual satellites is being conducted, and (3) during the operational lifetime of the satellite, which, for the purposes of this investigation, is 3 years, unless the satellite deorbits before that period of time. To analyze the behavior of a constellation, the distance from any single satellite within the constellation to any other satellite is tracked. From those distances, the minimum and maximum spacing between any two satellites within the constellation is determined. The last metric that is calculated is the volume of a polygon that would encompass the constellation.

The second type of analysis that is examined is an overall trend analysis on how varying the type of orbit (altitude and inclination) and the four deployment variables

(geometry, delayed deployment, location within the orbit, and separation velocity) affect the distance and volume metrics that are calculated from the individual test case analyses.

The final section of this chapter contains a discussion of how the results of this investigation compare to previous research that is being conducting on the deployment of CubeSats. The final section also contains a discussion of how the results of this investigation can be used to resolve problems that have been experienced by past missions that have been caused by the deployment of CubeSats. Also included in this section is a discussion of how the results of this investigation can be applied to specific types of missions.

V. Conclusions and Recommendations

5.1 Chapter Overview

In this chapter, the overall conclusions of this investigation are discussed, along with how those conclusions apply to specific mission types. Accompanying the discussion of the conclusions are recommendations on how these conclusions can be applied to an operational environment. The strengths, weaknesses, and limitations of this investigation are presented and explained. This chapter concludes with recommendations of how this investigation can be expanded with the application of future work.

5.1 Conclusions of Investigation

1. The use of a single dispenser to deploy multiple CubeSats simultaneously can lead to difficulties with the tracking and identification of, and the communication with, the satellites being dispersed. If the same dispenser is being used to launch multiple satellites, the dispenser should not disperse satellites into the plane normal to the velocity vector of the deployment vehicle, and, if possible, a mechanism should be implemented that will at least separate the deployments in time or separation velocity, preferably both.
2. A deployment into the plane with a normal vector in the same direction as the velocity vector of the control satellite (offset = 0°) does not promote the dispersal of a constellation over the first 24 hours. Furthermore, constellations deployed with an offset of 0° disperse much slower over their lifetime than constellations deployed with nonzero offsets. Deployment of satellites into this plane should be avoided if possible.

3. The overall trend, with respect to altitude, is that the lower the satellite is, the more quickly the maximum distance between any two satellites in the constellation increases. A second observation is that, although constellations at low altitudes spread out more quickly, the longer lifetime of the constellations at higher altitudes will eventually allow them to achieve a higher maximum distance between a satellite pair, which correlates to a larger volume. This highlights a tradeoff between deployment time and operational lifetime. A constellation with the same deployment scenario, at a lower altitude, will naturally populate the orbit path quicker than one at a higher altitude, but the constellation will also have a shorter lifetime as a result.
4. For deployments occurring at an altitude of 300 km, the inclination of the deployment orbit has a minor effect on constellation dispersal over the first 24 hours, and a deployment scheme that has been set up to meet certain criteria over the first 24 hours may be applied to multiple inclinations for that altitude with the expectation of little effect on the performance of that specific deployment scheme. A potential use of this is the development of general deployment patterns that could then be slightly modified to meet the specific needs of an individual launch. In contrast, the lifetime of the constellation increases as the inclination of deployment increases from 0° to 75°, with a slight reduction occurring between 75° and 90°.
5. The delayed deployment of part of the constellation can greatly increase the maximum volume of a constellation immediately after deployment while varying the long-term effects. This could allow for the development of

deployment schemes that provide adequate initial separation to facilitate tracking and identification, while tailoring the behavior of the constellation over the next few weeks after deployment.

6. Argument of latitude trends indicate behavior linked to degrees past the ascending node. The behavior of constellations utilizing nodal and polar deployment locations match each other quite well. The maximum separation in the constellations not deployed on a node or over a pole depends on the hemisphere over which the constellation is deployed. It should be noted that the start time of the simulation (28 Jan 15) and the altitude of the deployment (300 km) may be strongly linked to this result.
7. 180° of separation between the deployment vectors, for deployment vectors that do not lie in the plane normal to the velocity vector of the control satellite (offset = 0°), will cause initial separation between the satellites, avoiding inadvertent conjunctions.
8. 90° of separation between the deployment vectors does NOT always result in satellite separation. The separation between the satellites with 90° of separation between deployment vectors is dependent on both the offset of the deployment plane and which specific vectors in the deployment plane are used to deploy the individual satellites. Some of these satellite pairs indicate minimal satellite separation.

5.2 Mission Specific Conclusions

Results show that to facilitate the initial dispersal of the constellation, it is advisable to avoid deploying into the plane normal to the velocity vector of the deployer, and to also avoid launching multiple satellites from the same deployment mechanism simultaneously, and to have the respective deployment vectors be separated by 180°. Applying these three practices will promote the growth of the constellation over the first 24 hours after deployment, which will facilitate the tracking and identification of, and communication with, the deployed satellites. This finding is applicable to multiple mission types because problems with conjunctions, tracking, identification, and communication are present in most deployments, regardless of mission type.

For imagery and communication missions, ensuring that some portion of the separation velocity vector is in the same direction as either the velocity or anti-velocity vector of the deployer will promote dispersal along the orbit path. Varying the magnitude of this component will ensure relative drift between the individual satellites. This investigation utilized constant angle separation, which will disperse the satellites along the orbit path. Puig-Suari's deployment scenario that varies the angle of the satellite deployments to create a constant differential between the magnitudes of the component of the separation velocity along the velocity vector of the deployer does provide a more uniform dispersal of the satellites within the constellation; yet, to lock this constellation in place, some form of propulsion will need to be available on individual satellites.[26]

A formation flying mission will benefit from a deployment scheme that results in some CubeSats staying relatively close to one another until at least one satellite could be brought online. One option is to load multiple CubeSats into the same dispenser and

separate the deployment of each satellite by a few minutes. The second option, resulting from the analysis conducted in this investigation, is to deploy the satellites into the same deployment plane, with close to the same magnitude of separation velocity in the radial, transverse, and normal directions, but with opposite signs in the radial direction (This corresponds to the satellite 1-3 or satellite 5-7 pair for a deployment with an offset of either 45°, 90° or 135°). Separating the deployments by a few minutes will reduce the chance of conjunctions occurring while keeping the satellites close to one another while the individual CubeSats are being brought online.

5.3 Significance and Limitations of the Present Investigation

The use of small satellites in both the private and public sectors is increasing every year. A by-product of this growth is the deployment of many satellites from a single launch platform. This investigation highlights an area of growing concern, offers a few best-practice solutions that can be implemented to mitigate some of the problems that arise from deploying multiple satellites over a short period in time, and lays the foundation for future work that can be implemented to address these problems well before a constellation of CubeSats ever leaves the ground.

While this investigation has many strengths, there are some limitations present. This investigation utilized a few overarching assumptions. The first assumption is that there are no propulsion systems on the CubeSats. This assumption limited the user control of the behavior of the constellation to the initial deployment. This was by design, so that change in the behavior of the constellation when the deployment variables are adjusted could be studied, but this assumption also limits the ability of the constellation

to stop the relative motion along the orbit path once an optimum dispersal has been achieved. The second assumption used in this investigation is that the ballistic coefficient of the individual satellites is fixed throughout time. This implies that both the satellites mass and attitude are fixed throughout the simulation. This is also by design, so the behavior of the constellation is not affected by differential drag acting upon the individual satellites, but this is ultimately an unrealistic assumption. Previous investigations have focused on the use of differential drag to control a formation of satellites[37,38] and expanding on this current investigation utilizing more realistic parameters, possibly combining this current investigation with the use of differential drag formation control, is a promising area of future study.

Other assumptions that are used in this investigation concern the perturbing forces acting on the individual satellites. Third body gravity is not taken into account for any satellite operating with an altitude at or below 1,000 km. Solar radiation pressure was also similarly neglected. The last assumption concerning perturbing forces acting on the satellite comes from the gravity model used. Since a 2x2 gravity model is used in this investigation, all of the Earth's deviations from a spherical object other than the Earth's oblateness, major continents, and the Atlantic and Pacific Oceans are ignored. While this does decrease the accuracy of the model with respect to the actual model, the purpose of this investigation is to study the relative motion of the satellites, and a 2x2 model was chosen because it will accurately model the gravitational forces, namely the secular effects of J_2, that this investigation was designed to focus on.

One of the two remaining limitations of this investigation is the number of satellites in a constellation, which is limited to eight throughout the investigation. This is

part of the initial methodology but does impose a limitation on the number of deployment vectors per plane that can be studied. The last limitation of this study is the limit of three years imposed on the individual constellations. For this analysis the limit is practical, but one cannot definitely say what the behavior of the constellations implemented in this investigation will be after three years, because it was never simulated and analyzed.

5.4 Recommendations for Future Work

The area of this investigation that shows the most potential involves the creation of deployment scenarios utilizing previously simulated data. The utilization of stored deployment data to create and optimize deployment scenarios to meet specific criteria can potentially be used apply this analysis to real world satellite deployments by developing deployment schemes tailored to the needs of a specific launch. Applying this methodology to a real world example, which utilizes more realistic mission parameters (e.g., different deployer characteristics, no deployment plane restriction, dissimilar satellites) to show proof of concept of its utility to real world operators is where this investigation can make the greatest contribution.

A natural starting point to apply the above concept is the creation and testing of different delayed deployment scenarios. The trend analysis completed in this investigation concerning delayed deployment schemes offers a solid foundation for future work to build on. The sheer number of different combinations possible means that the future work can be structured around work that has already been completed, while still allowing the researcher the freedom to explore ideas of their own creation.

The next recommendation for future work is the continuation of the investigation by increasing the number of test cases to test a wider (or finer) range of values for the given deployment variables. In this investigation, four different deployment variables are utilized to analyze how they affect the behavior of the constellation. To isolate the effect of one variable, the others are held constant. For example, the argument of latitude trend analysis is conducted in an orbit with an altitude of 300 km and an inclination of 30°. This same analysis can be completed for other combinations of altitude and inclination to test to see what the effects of changing argument of latitude is for different orbits, including different times. Of the six trend analyses completed, the argument of latitude trend analysis is the most likely linked to the start date of the simulation.

The final recommendation for future work is to increase the number of satellites ejected into the deployment plane to more than eight. This will allow for a more complete analysis on if there exist three (or more) deployment vectors within the same plane that can be used either simultaneously, or near simultaneously, and still result in initial satellite separation between all deployed satellites. Having eight deployment vectors in a deployment plane did not yield any definitive results for any combination greater than two. Having more deployment vectors in a deployment plane will allow for more combinations to be explored.

5.5 Chapter Summary

In this chapter, the conclusions of this investigation are presented and explained. The main takeaways are:

- Do not deploy CubeSats into the plane normal to the velocity vector of the deployment vehicle. This can lead to problems with conjunctions, tracking, identification, and communication over the first 24 hours, which are the exact problems that one is trying to avoid over this period in time.
- For deployments occurring at an altitude of 300 km, the inclination of the deployment orbit has a small effect on constellation dispersal over the first 24 hours, and a deployment scheme that has been set up to meet certain criteria over the first 24 hours may be applied to multiple inclinations for that altitude with the expectation of little effect on the performance of that specific deployment scheme.
- Separating the deployment vectors of individual satellites by 180° (and avoiding the plane normal to the deployment vehicles' velocity vector) will result in initial satellite separation. This can be used to design the placement of the deployment mechanisms that are attached to the launch vehicle to mitigate risk of conjunctions and reduce the likelihood of difficulties with the tracking and identification of, and communication with, the individual satellites in the constellation.

The four recommendations for future work are to create deployment scenarios utilizing previously simulated data, to apply this concept in the creation and testing of different delayed deployment scenarios, to increase the number of test cases to test a wider (or finer) range of values for the given deployment variables, and to change the number of satellites deployed per plane to more than eight. This last recommendation is focused on finding out if three relative deployment vectors can consistently provide

satellite separation despite orientation. While this investigation does have its own weaknesses, it highlights an area of growing concern, offers a few best-practice solutions that can be implemented quickly to mitigate some of the problems that arise from deploying multiple satellites over a short period in time, and lays the foundation for future work that can be implemented to address these problems well before a constellation of CubeSats ever leaves the ground.

Appendix

Test Case	# of Satellites per Ring	Timing of Deployments (sec)	# of Deployments	Altitude (km)	Inclination (°)	Angle of Deployment Plane (°)	Ejection Velocity (m/s)	Argument of Latitude (°)
1.01	8	0	1	300	30	0	1	0
1.02	8	0	1	300	30	0	1.5	0
1.03	8	0	1	300	30	0	2	0
1.04	8	0	1	300	30	45	1	0
1.05	8	0	1	300	30	45	1.5	0
1.06	8	0	1	300	30	45	2	0
1.07	8	0	1	300	30	90	1	0
1.08	8	0	1	300	30	90	1.5	0
1.09	8	0	1	300	30	90	2	0
1.1	8	0	1	300	30	135	1	0
1.11	8	0	1	300	30	135	1.5	0
1.12	8	0	1	300	30	135	2	0
1.13	8	0	1	300	15	0	1	0
1.14	8	0	1	300	15	0	2	0
1.15	8	0	1	300	15	45	1	0
1.16	8	0	1	300	15	45	2	0
1.17	8	0	1	300	15	90	1	0
1.18	8	0	1	300	15	90	2	0
1.19	8	0	1	300	15	135	1	0
1.2	8	0	1	300	15	135	2	0
1.21	8	0	1	300	0	0	1	0
1.22	8	0	1	300	0	0	2	0
1.23	8	0	1	300	0	45	1	0
1.24	8	0	1	300	0	45	2	0

1.25	8	0	1	300	0	90	1	0
1.26	8	0	1	300	0	90	2	0
1.27	8	0	1	300	0	135	1	0
1.28	8	0	1	300	0	135	2	0
1.29	8	0	1	300	45	0	1	0
1.3	8	0	1	300	45	0	2	0
1.31	8	0	1	300	45	45	1	0
1.32	8	0	1	300	45	45	2	0
1.33	8	0	1	300	45	90	1	0
1.34	8	0	1	300	45	90	2	0
1.35	8	0	1	300	45	135	1	0
1.36	8	0	1	300	45	135	2	0
1.37	8	0	1	300	60	0	1	0
1.38	8	0	1	300	60	0	2	0
1.39	8	0	1	300	60	45	1	0
1.4	8	0	1	300	60	45	2	0
1.41	8	0	1	300	60	90	1	0
1.42	8	0	1	300	60	90	2	0
1.43	8	0	1	300	60	135	1	0
1.44	8	0	1	300	60	135	2	0
1.45	8	0	1	300	75	0	1	0
1.46	8	0	1	300	75	0	2	0
1.47	8	0	1	300	75	45	1	0
1.48	8	0	1	300	75	45	2	0
1.49	8	0	1	300	75	90	1	0
1.5	8	0	1	300	75	90	2	0
1.51	8	0	1	300	75	135	1	0
1.52	8	0	1	300	75	135	2	0

1.53	8	0	1	300	90	0	1	0
1.54	8	0	1	300	90	0	2	0
1.55	8	0	1	300	90	45	1	0
1.56	8	0	1	300	90	45	2	0
1.57	8	0	1	300	90	90	1	0
1.58	8	0	1	300	90	90	2	0
1.59	8	0	1	300	90	135	1	0
1.6	8	0	1	300	90	135	2	0
1.61	8	0	1	400	30	0	1	0
1.62	8	0	1	400	30	0	2	0
1.63	8	0	1	400	30	45	1	0
1.64	8	0	1	400	30	45	2	0
1.65	8	0	1	400	30	90	1	0
1.66	8	0	1	400	30	90	2	0
1.67	8	0	1	400	30	135	1	0
1.68	8	0	1	400	30	135	2	0
1.69	8	0	1	500	30	0	1	0
1.7	8	0	1	500	30	0	2	0
1.71	8	0	1	500	30	45	1	0
1.72	8	0	1	500	30	45	2	0
1.73	8	0	1	500	30	90	1	0
1.74	8	0	1	500	30	90	2	0
1.75	8	0	1	500	30	135	1	0
1.76	8	0	1	500	30	135	2	0
1.77	8	0	1	750	30	0	1	0
1.78	8	0	1	750	30	0	2	0
1.79	8	0	1	750	30	45	1	0
1.8	8	0	1	750	30	45	2	0

1.81	8	0	1	750	30	90	1	0
1.82	8	0	1	750	30	90	2	0
1.83	8	0	1	750	30	135	1	0
1.84	8	0	1	750	30	135	2	0
1.85	8	0	1	1000	30	0	1	0
1.86	8	0	1	1000	30	0	2	0
1.87	8	0	1	1000	30	45	1	0
1.88	8	0	1	1000	30	45	2	0
1.89	8	0	1	1000	30	90	1	0
1.9	8	0	1	1000	30	90	2	0
1.91	8	0	1	1000	30	135	1	0
1.92	8	0	1	1000	30	135	2	0
1.93	8	60	4(1)	300	30	0	1	0
1.94	8	60	4(2)	300	30	0	1	0
1.95	8	60	4(3)	300	30	0	1	0
1.96	8	60	4(4)	300	30	0	1	0
1.97	8	300	2(1)	300	30	0	1	0
1.98	8	300	2(2)	300	30	0	1	0
1.99	8	900	1(3)	300	30	0	1	0
2.00	8	900	2(3)	300	30	0	1	0
2.01	8	900	3(3)	300	30	0	1	0
2.02	8	0	1	300	96.7425	0	1	0
2.03	8	0	1	400	97.1006	0	1	0
2.04	8	0	1	500	97.4089	0	1	0
2.05	8	0	1	750	98.4009	0	1	0
2.06	8	0	1	1000	99.5503	0	1	0
2.07	8	0	1	300 (perigee)	63.3213	0	1	-
2.08	8	0	1	400 (perigee)	63.3213	0	1	-

2.09	8	0	1	500 (perigee)	63.3213	0	1	-
2.10	8	0	1	750 (perigee)	63.3213	0	1	-
2.11	8	0	1	1000 (perigee)	63.3213	0	1	-
2.12	8	-	6 min after	300	30	0	1	0
2.13	8	-	7 min after	300	30	0	1	0
2.14	8	-	8 min after	300	30	0	1	0
2.15	8	-	20 min after	300	30	0	1	0
2.16	8	-	25 min after	300	30	0	1	0
2.17	8	-	35 min after	300	30	0	1	0
2.18	8	-	40 min after	300	30	0	1	0
3.01	8	0	1	300	30	0	1	0
5.01	8	60	1	300	30	0	1	0
5.02	8	120	1	300	30	0	1	0
5.03	8	180	1	300	30	0	1	0
5.04	8	240	1	300	30	0	1	0
5.05	8	300	1	300	30	0	1	0
5.06	8	360	1	300	30	0	1	0
5.07	8	420	1	300	30	0	1	0
5.1	8	600	1	300	30	0	1	0
5.15	8	900	1	300	30	0	1	0
5.2	8	1200	1	300	30	0	1	0
5.25	8	1500	1	300	30	0	1	0
5.3	8	1800	1	300	30	0	1	0
5.35	8	2100	1	300	30	0	1	0
5.4	8	2400	1	300	30	0	1	0
5.45	8	2700	1	300	30	0	1	0
8.02	8	0	1	300	30	0	1	30

8.03	8	0	1	300	30	0	1	60
8.04	8	0	1	300	30	0	1	90
8.05	8	0	1	300	30	0	1	120
8.06	8	0	1	300	30	0	1	150
8.07	8	0	1	300	30	0	1	180
8.08	8	0	1	300	30	0	1	210
8.09	8	0	1	300	30	0	1	240
8.1	8	0	1	300	30	0	1	270
8.11	8	0	1	300	30	0	1	300
8.12	8	0	1	300	30	0	1	330

Bibliography

1 Buchen, E., "SSC15-VII-7 Small Satellite Market Observations," AIAA/USU Conference on Small Satellites, 2015, pp. 1–5.

2 Richardson, G., Schmitt, K., Covert, M., and Rogers, C., "Small Satellite Trends 2009-2013," Proceedings of the AIAA/USU Conference on Small Satellites, 2015.

3 Systems Tool Kit® (STK), Exton, PA: Analytical Graphics, Inc, 2015, Version: 10.

4 Chin, A., Coelho, R., Nugent, R., Munakata, R., and Puig-Suari, J., "CubeSat: The Pico-Satellite Standard for Research and Education," AIAA SPACE 2008 Conference & Exposition, 2008, pp. 1–11.

5 California Polytechnic State University, "Cubesat design specification," The CubeSat Program, California Polytechnic State University, 2009.

6 Abramowitz, L., and Avrett, C. J., "SSC15-V-1 SENSE: Lessons Learned through Acquisition and On-Orbit Operations," 2015.

7 Wertz, James R.; Everett, David F.; Puschell, J. J., ed., Space Mission Engineering: The New SMAD, Hawthorne, CA: Microcosm Press, 2011.

8 Newman, J., Sakoda, D., and Panholzer, R., "CubeSat Launchers, ESPA-rings, and Education at the Naval Postgraduate School," 2007, pp. 1–6.

9 Dell'Elce, L., Arnst, M., and Kerschen, G., "Probabilistic Assessment of the Lifetime of Low-Earth-Orbit Spacecraft: Uncertainty Characterization," Journal of Guidance, Control, and Dynamics, vol. 38, 2015, pp. 900–912.

10 Springmann, J. C., Bertino-Reibstein, A., and Cutler, J. W., "Investigation of the on-orbit conjunction between the MCubed and HRBE CubeSats," IEEE Aerospace Conference Proceedings, 2013, pp. 1–8.

11 Wiesel, W., Spaceflight Dynamics, 3rd Edition, Beavercreek, OH, Aphelion Press, 2010.

12 de Selding, P., "OneWeb Taps Airbus To Build 900 Internet Smallsats," Spacenews Available: http://spacenews.com/airbus-wins-oneweb-contract/, Date accessed: 2015-10-13.

13 de Selding, P., "SpaceX To Build 4,000 Broadband Satellites in Seattle," Spacenews Available: http://spacenews.com/spacex-opening-seattle-plant-to-build-4000-broadband-satellites/, Date accessed: 2015-10-13.

14 Snow, A., Buchen, E., and Olds, J., "Global Launch Vehicle Market Assessment," SpaceWorks Available: http://images.spaceref.com/docs/2014/2013_Global_Launch_Vehicle_Market_Assessment_July2014.pdf, Date accessed: 2015-8-14.

15 Bradford, J., “2015 Small Satellite Market Observations,” SpaceWorks Available: http://spaceworksforecast.com/docs/SpaceWorks_Small_Satellite_Market_Observations_2015.pdf, Date accessed: 2015-8-14.

16 Platzer, P., Wake, C., and Gould, L., “Smaller Satellites, Smarter Forecasts: GPS-RO Goes Mainstream,” AIAA/USU Conference on Small Satellites, 2015, pp. 1–5.

17 Davis, T. M., “SSC15-VII-4 Operationally Responsive Space – The Way Forward,” 2015.

18 Newman, J., and Zee, R. E., “No Drift Recovery and Station Keeping Results for the Historic CanX-4/CanX-5 Formation Flying Mission,” Proceedings of the 29th Annual AIAA/USU Conference on Small Satellites, 2015.

19 Rivers, T. D., Heskett, J., and Villa, M., “RILDOS: A Beaconing Standard for Small Satellite Identification and Situational Awareness,” 2015.

20 David A. Vallado, Fundamentals of Astrodynamics and Applications, 3rd Edition, Hawthorne, CA: Microcosm Press, 2007.

21 Szebehely, V., “The History and Background of Astrodynamics,” Acta Astronautica, vol. 20, 1989, pp. 79–81.

22 Federal Aviation Administration, “Describing Orbits,” Available: http://www.faa.gov/other_visit/aviation_industry/designees_delegations/designee_types/ame/media/section iii.4.1.4 describing orbits.pdf, Date accessed: 2016-2-12

23 Clohessy, R. S., and Wiltshire, “The Clohessy-Wiltshire Equations of Relative Motion,” Journal of Aerospace Sciences, vol. 27, 1960, pp. 653–658.

24 Hill, G. W., “Researches in the Lunar Theory,” American Journal of Mathematics, vol. 1, 1878, pp. 5–26.

25 Wiesel, W., Modern Astrodynamics, 2nd Edition, Beavercreek, OH: Aphelion Press, 2010.

26 Puig-Suari, J., Zohar, G., and Leveque, K., “Deployment of CubeSat Constellations Utilizing Current Launch Opportunities,” 27th Annual AIAA/USU Conference on Small Satellites, 2013, pp. 1–7.

27 Kilic, C., Scholz, T., and Asma, C., “Deployment strategy study of QB50 network of CubeSats,” RAST 2013 - Proceedings of 6th International Conference on Recent Advances in Space Technologies, 2013, pp. 935–939.

28 MATLAB®, Natick, MA: The MathWorks, Inc., 2015, Version: R2015b.

29 McNeil, L., Spatial Temporal Information Systems: An Ontological Approach Using STK®, Boca Raton, FL: CRC Press, 2014.

30 National Geospatial-Intelligence Agency, “Office of Geomatics: World Geodetic System 1984 (WGS 84),” Available: http://earth-info.nga.mil/GandG/wgs84/, Date accessed: 2016-2-12.

31 NASA, N., “EGM96 The NASA GSFC and NIMA Joint Geopotential Model,” Available: http://cddis.nasa.gov/926/egm96/egm96.html, Date accessed: 2016-2-12.

32 Delaunay, B., “Sur la forme des courbes,” Journal de Physique et le Radium, vol. 12, 1939, pp. 793–800.

33 de Berg, M. et al., Computational Geometry, Berlin: Springer, 2008.

34 MathWorks, “Delaunay Triangulation” Available: http://www.mathworks.com/help/matlab/ref/delaunaytriangulation-class.html, Date accessed: 2016-1-16.

35 Zurita, A., *Minimum Fuel Trajectory Design in Multiple Dynamical Environments Utilizing Direct Transcription Methods and Particle Swarm Optimization*, Master's Thesis, Air Force Institute of Technology, Wright-Patterson Air Force Base, Ohio, 2016, Draft.

36 Simmons, R., "MECH532: Introduction to Spaceflight Dynamics," Graduate Course, Air Force Institute of Technology, Wright-Patterson Air Force Base, Ohio, 2015.

37 Wedekind, J., *Characterizing and Controlling the Effects of Differential Drag on Satellite Formations*, Master's Thesis, Air Force Institute of Technology, Wright-Patterson Air Force Base, Ohio, 2006.

38 Hajovsky, B., *Satellite Formation Control Using Atmospheric Drag*, Master's Thesis, Air Force Institute of Technology, Wright-Patterson Air Force Base, Ohio, 2007.

REPORT DOCUMENTATION PAGE

Form Approved
OMB No. 074-0188

1. REPORT DATE *(DD-MM-YYYY)*	2. REPORT TYPE	3. DATES COVERED *(From – To)*
24-03-2016	Master's Thesis	Aug 2014 – Mar 2016

TITLE AND SUBTITLE
Multi-CubeSat Deployment Strategies: How Different Satellite Deployment Schemes Affect Satellite Separation and Detection for Various Types of Constellations and Missions

5a. CONTRACT NUMBER

5b. GRANT NUMBER

5c. PROGRAM ELEMENT NUMBER

6. AUTHOR(S)

Biehl, Scott A., Jr., 1st Lt, USAF

5d. PROJECT NUMBER

5e. TASK NUMBER

5f. WORK UNIT NUMBER

7. PERFORMING ORGANIZATION NAMES(S) AND ADDRESS(S)
Air Force Institute of Technology
Graduate School of Engineering and Management (AFIT/ENY)
2950 Hobson Way, Building 640
WPAFB OH 45433-8865

8. PERFORMING ORGANIZATION REPORT NUMBER

AFIT-ENY-MS-16-M-198

9. SPONSORING/MONITORING AGENCY NAME(S) AND ADDRESS(ES)

AFRL Space Vehicles Directorate
3550 Aberdeen Avenue SE
Kirtland AFB NM 87117-5776
POC: N/A

Principal DoD Space Advisor Staff
1670 Air Force Pentagon
Washington DC 20330-1670C
703-693-5799
POC: Maj Stuart A. Stanton

10. SPONSOR/MONITOR'S ACRONYM(S)

AFRL/RV

11. SPONSOR/MONITOR'S REPORT NUMBER(S)

12. DISTRIBUTION/AVAILABILITY STATEMENT
DISTRUBTION STATEMENT A. APPROVED FOR PUBLIC RELEASE; DISTRIBUTION UNLIMITED.

13. SUPPLEMENTARY NOTES

14. ABSTRACT
As economics drive an increased demand for small satellites and, consequently, an increase in the number of satellites deployed per launch, different deployment schemes and their effects on satellite dynamics must be well understood. While there are advantages to deploying multiple satellites at once, users may have trouble with tracking, identifying, and communicating with their satellites. This investigation examines the deployment of eight 3U CubeSats, and the resulting relative motion within a constellation. Both the distance between any two satellites within a constellation and the volume of a polygon encompassing a constellation are used to analyze the satellite dynamics within a constellation. Deployment schemes differ from one another by varying the deployment geometry, by delaying the ejection of specific CubeSats relative to one another, the deployment location, and the separation velocity imparted upon the CubeSats for various mission types. This investigation presents several conclusions. Delaying the deployment of part of a constellation increases the maximum volume of the constellation over the first 24 hours while varying long term effects. Deployments into the plane normal to the velocity vector of the deployer result in minimal dispersal of a constellation. Finally, lower constellation deployment altitudes disperse a constellation faster.

15. SUBJECT TERMS
CubeSat, satellite deployment strategies, satellite constellation dispersal, Systems Took Kit (STK), small satellites, orbital mechanics

16. SECURITY CLASSIFICATION OF:			17. LIMITATION OF ABSTRACT	18. NUMBER OF PAGES	19a. NAME OF RESPONSIBLE PERSON
a. REPORT	b. ABSTRACT	c. THIS PAGE			Maj Christopher D. Geisel, Ph.D., AFIT/ENY
U	U	U	UU	192	19b. TELEPHONE NUMBER *(Include area code)* (937) 785-3636, ext 4237 Christopher.Geisel@afit.edu

Standard Form 298 (Rev. 8-98)
Prescribed by ANSI Std. Z39-18